Shahid Chamran
University of Ahwaz

2

Journal of

Hydraulic Structures

Scientific Professional Quarterly



انجمن
هیدرولیک
ایران

Spring 2013
Volume 1
Issue 2

JORNAL OF
HYDRAULIC STRUCTURES
SHAHID CHAMRAN UNIVERSITY oF AHVAZ

Manager
Prof. Hamid R.Ghafouri

Editor-in-chief
Prof.Hossein M. V.Samani
Civil Engeering Department
ShahidChamran University, Ahwaz, Iran

Members
Prof. Hamid R. Ghafouri
Civil Engeering Department
ShahidChamran University, Ahwaz, Iran
Prof. Mohammad M. Shooshtari
Civil Engeering Department
ShahidChamran University, Ahwaz, Iran
Prof. Mahmood S. Bajestan
Hydraulic Structures Department
ShahidChamran University, Ahwaz, Iran
Prof. Saeed R. S. Yazdi
Civil Engineering Department
K.N.Toosi University of Technology, Tehran, Iran
Prof. Ahmadreza M. Gharabaghi
Civil Engineering Faculty
Sahand University of Technology, Tabriz, Iran
Prof. Behzad Ataie Ashtiani
Civil Engineering Department
Sharif University of Technology, Tehran, Iran
Prof. Masoud Ghodsian
Faculty of Civil & Environmental Engineering
TarbiatModarres University, Tehran, Iran
Prof. Mahmood Javan
School of Agriculture
Shiraz University, Shiraz, Iran
Prof. Javad Farhoudi
Department of Irrigation & Reclamation Eng
University of Tehran, Tehran, Iran
Prof. Mohammad R. Jaefarzadeh
Department of Civil Engineering
Ferdowsi University, Mashhad, Iran
Prof. Nasser Talebbeydokhti
Department of Civil Engineering
Shiraz University, Shiraz, Iran
Dr. Mohammad S. Pakbaz
Civil Engeering Department
ShahidChamran University, Ahwaz, Iran
Dr. Massoud Oulapour
Civil Engeering Department
ShahidChamran University, Ahwaz, Iran
Dr. Arash Adib
Civil Engeering Department
ShahidChamran University, Ahwaz, Iran
Dr. Ali Haghighi
Civil Engeering Department
ShahidChamran University, Ahwaz, Iran
Dr. Mojtaba Labibzadeh
Civil Engeering Department
ShahidChamran University, Ahwaz, Iran

Shahid Chamran
Univeristy of Ahvaz

انجمن هیدرولیک ایران

CONTENTS

VOL I NO II SPRING 2013

II AIMS AND SCOPE

01 A Discrete Singular Convolution Method for the Seepage Analysis in Porous Media with Irregular Geometry
Zayeri Baghlani Nejad, M. Shokrollahi

10 A Case Study of Water Quality Modeling of the Gargar River, Iran
M. Rafiee, A. M. Akhond Ali, H. Moazed, S. W. Lyon, N. Jaafarzadeh, B. Zahraie

23 Discharge Coefficient in Vertical Intakes with Additional Plates
V. Naderi, D. Farsadizadeh, A. Hossein Zadeh Dalir, H. Arvanaghi

33 Evaluation of Hydraulic Sensitivity Indicators for Baffle Modules (Case Study: Varamin Irrigation and Drainage Network)
M. Seyedjavad, M. Mashaal, A. A. Montazar

44 A New Two Dimensional Model for Pollutant Transport in Ajichai River
H. Derakhshan, M. Zarei Bistkonj

53 Theoretical Criterion for Stability of Free Hydraulic Jump on Adverse Stilling Basins
H. Khalili Shayan, J. Farhoudi

Aims and Scope

The Journal publishes high-quality peer-reviewed articles addressing the **latest developments and applied methods in Hydraulic Structures.** This includes the following:

- ✓ Dams and associated structures
- ✓ River Structures
- ✓ Offshore and Onshore Structures
- ✓ Irrigation and Drainage Channel Networks
- ✓ Bridges
- ✓ Water Storage and Conveyance Structures
- ✓ Pipelines and Pump Stations
- ✓ Sewerage Systems
- ✓ Water and Wastewater Treatment Plants
- ✓ Historical Water Structures

The Journal aims at providing an efficient route to fast-track publication, **within 10-12 weeks after manuscript submission**.

Manuscripts in the following categories will be considered for publication: **research articles**, **technical notes**, **case reports** and **discussions**. The general areas covered by the Journal include:

- ✓ Technical and methodological advances in application, design/selection, production, modification of construction materials.
- ✓ Advances in numerical and analytical methods.
- ✓ Application of Nanotechnology in Hydraulic Structures
- ✓ Hydro informatics
- ✓ Geomechanics of Hydraulic Structures
- ✓ Hydraulic aspects of Hydraulic Structures
- ✓ Optimization techniques
- ✓ Damage detection techniques

General Information

Title: Journal of Hydraulic Structures
Subject: Hydraulics and water resources engineering
Coverage area: International
Journal Type: Scientific and technical
License Holder: Shahid Chamran University
Editor-in-Chief: Prof. Hossein M. V. Samani
Manager: Prof. Hamid R. Ghafouri
Editorial coordinator: Dr. Ali Haghighi

Language Editors:
Majid SadollahKhani
Soroosh Kamali
Address: Engineering Faculty Shahid Chamran University of Ahvaz
Phone #: +986113330010-20 (5610 & 5603)
Fax #: +986113337010
Language: English
Email: jhs@scu.ac.ir
Website: jhs.scu.ac.ir

A Discrete Singular Convolution Method for the Seepage Analysis in Porous Media with Irregular Geometry

Amir Zayeri Baghlani Nejad[1], *Mohammad Shokrollahi*[1]
[1]Engineering Department, Jundi-Shapur University of Technology, Dezful, Iran

Abstract

A novel discrete singular convolution (DSC) formulation is presented for the seepage analysis in irregular geometric porous media. The DSC is a new promising numerical approach which has been recently applied to solve several engineering problems. For a medium with regular geometry, realizing of the DSC for the seepage analysis is straight forward. But DSC implementation for a medium with irregular geometry encounters some challenging issues. To overcome the difficulty, a novel DSC scheme for seepage analysis in irregular geometric porous media is proposed. There is no general analytical solution for the seepage analysis in irregular geometries; thus, the validation of the proposed algorithm is carried out by comparing the results with those from available numerical methods. Good agreement between the results shows that the proposed algorithm can be utilized in solving seepage analysis as a new approach.

Keywords: Discrete Singular Convolution, Seepage, Numerical Analysis, Irregular Geometric Medium

1. Introduction

One of the important problems in water resource management discipline is the seepage analysis in porous media. Water leakage in the body of the soil dams, seepage from the body of the channel and foundation of the concrete dams and water movement in aquifers are some of the practical examples in this branch. Apart from a few cases with special boundary conditions, governing equations on water seepage have no analytical solutions. Regarding this matter, numerical approaches can be utilized as proper instruments for solving the equations. Recently, one of the novel approaches which is used to solve the problems is discrete singular convolution (DSC). This method was invented to solve the differential equations by Wei (1999). After then, this method was implemented to solve a wide variety of engineering problems. Firstly, Wei enlisted the DSC to solve vibration problems in the field of solid mechanics (2001c). Then Civalek developed the method in 3D problems (2007). Navier-Stokes equations were analyzed using the DSC by Wan and Wei (2000). Xin et-al. analyzed nonlinear circuits in the field of electromagnetic (2004). Solving the quantum equations (Wei 2000) and edge detecting (Hou and Wei 2002), are other applications of the DSC. More recently, the authors of this paper developed the DSC algorithm for non-Darcian seepage analysis in the coarse porous media (Zayeri Baghlani Nejad and Shokrollahi 2011). A wide number of reviews about the DSC works can be found in Reference Shokrollahiand Zayeri Baghlani Nejad (2014).

DSC formulation which is presented in reference (Zayeri Baghlani Nejad and Shokrollahi 2011) is limited to media with rectangular geometries. However, in a great number of real problems, such as ground water movement, water seepage from the body of the soil dams and similar problems, the solution domain doesn't have rectangular geometry. The objective of this paper is developing the DSC formulation for seepage analysis in the media with arbitrary irregular geometries. To this end, the method which was enlisted by Charles and Moinuddin for developing differential

quadrature method in analyzing vibration of the non-rectangular plates is applied (1996).

In continue details of the DSC method will be discussed firstly. Then, formulation of the mentioned approach will be presented in the irregular domains. After that, discretization and solution of the governing equations of the water movement in porous media will be implemented. A computer program will be written for modeling some problems. Finally, the DSC results will be compared with those of the finite element method to validate the algorithm.

2. DSC method

Discrete singular convolution (DSC) method is a relatively new numerical technique in applied mechanics which was originally introduced by Wei (1999). Since then, the DSC method applied to various science and engineering problems. Accurate results and exact convergence have demonstrated that the DSC is a reliable and convenient numerical approach. The mathematical foundation of the DSC algorithm is the theory of distributions and wavelet analysis. Like some other numerical methods, the DSC method discretizes the spatial derivatives and, therefore, reduces the given partial differential equations into a system of linear algebraic equations. So, in the DSC algorithm, any function $f(x)$ and its derivatives with respect to a coordinate at a grid point x are approximated by a linear sum of the functional values in the narrow domain $[x\text{-}x_{\text{-M}},\ x\text{+}x_{\text{M}}]$ in that coordinate direction. This expression can be written as follows (Wei 1999):

$$f^{(n)}(x) \approx \sum_{i=-M}^{M} \delta_{\Delta,\sigma}^{(n)}(x - x_i) f(x_i) \tag{1}$$

where superscript n (n = 0, 1, 2...) denotes the nth-order derivative with respect to x. The 2M +1 is the computational bandwidth which is usually smaller than the whole computational domain. Therefore, the resulting approximation matrix has a banded structure, which makes the DSC method more efficient than normal global methods and is particularly valuable with respect to large scale computations. $\{x_i\}$ is an appropriate set of discrete points on which the DSC of Eq. (1) is well-defined and δ is a singular kernel. The DSC algorithm can be realized by using many approximation kernels (Wei et al. 2002b). However, it was shown (Wei 2001b; Wei et al. 2002a; Wei 2000; Wei 2001a) that for many problems, the use of the Regularized Shannon Kernel (RSK) is very efficient. The RSK is given by (Wei 1999):

$$\delta_{\Delta,\sigma}(x - x_k) = \frac{\sin\left(\frac{\pi}{\Delta}(x - x_k)\right)}{\frac{\pi}{\Delta}(x - x_k)} \exp\left(-\frac{(x - x_k)^2}{2\sigma^2}\right) \tag{2}$$

In these equations, $\Delta = L/(N-1)$ is the grid spacing and N is the number of grid points. The parameter σ determines the width of the Gaussian envelope and often varies in association with the grid spacing, i.e., $\sigma = r.\Delta$, here r is a parameter chosen in computations.

First and second derivative of RSK with respect to x is defined as below:

$$\delta_{\Delta,\sigma}^{(1)}(x_m - x_k) = \frac{\cos\frac{\pi}{\Delta}(x - x_k)}{(x - x_k)} \exp\left(\frac{-(x - x_k)^2}{2\sigma^2}\right) - \frac{\sin\frac{\pi}{\Delta}(x - x_k)}{\frac{\pi}{\Delta}(x - x_k)^2} \exp\left(\frac{-(x - x_k)^2}{2\sigma^2}\right) \tag{3}$$

$$\delta_{\Delta,\sigma}^{(2)}(x_m - x_k) = -\frac{(\frac{\pi}{\Delta})\sin\frac{\pi}{\Delta}(x-x_k)}{(x-x_k)}\exp\left(\frac{-(x-x_k)^2}{2\sigma^2}\right) - 2\frac{\cos\frac{\pi}{\Delta}(x-x_k)}{(x-x_k)^2}\exp\left(\frac{-(x-x_k)^2}{2\sigma^2}\right)$$
$$-2\frac{\cos(\frac{\pi}{\Delta})(x-x_k)}{\sigma^2}\exp\left(\frac{-(x-x_k)^2}{2\sigma^2}\right) + 2\frac{\sin\frac{\pi}{\Delta}(x-x_k)}{\frac{\pi}{\Delta}(x-x_k)^3}\exp\left(\frac{-(x-x_k)^2}{2\sigma^2}\right) \quad (4)$$
$$+\frac{\sin\frac{\pi}{\Delta}(x-x_k)}{\frac{\pi}{\Delta}(x-x_k)\sigma^2}\exp\left(\frac{-(x-x_k)^2}{2\sigma^2}\right) + \frac{\sin\frac{\pi}{\Delta}(x-x_k)}{\frac{\pi}{\Delta}\sigma^4}(x-x_k)\exp\left(\frac{-(x-x_k)^2}{2\sigma^2}\right)$$

$$\delta_{\Delta,\sigma}^{(1)}(0) = 0 \quad (5)$$

$$\delta_{\Delta,\sigma}^{(2)}(0) = -\frac{1}{\sigma^2} - \frac{\pi^2}{3\Delta^2} \quad (6)$$

As the DSC kernel is symmetric, the DSC computation requires a total of M fictitious grid points (FPs) outside each edge. Furthermore, the solution carries out for the grids inside the domain, so FPs must be eliminated. More precisely, it requires function values on these FPs which could be determined from those inside the domain by applying the boundary condition equations. Some attempts have been carried out for applying boundary conditions by researchers. Wei et al. (2001), Wei et al. (2002b), Zhao and Wei (2002), proposed a practical method to incorporate the boundary conditions. After that, Zhao et al. (2005) applied the iteratively matched boundary method to impose the free boundary conditions for Euler beams. More recently, Wang and Xu (2010) present a method for applying boundary conditions using the Taylor's series expansion. For gaining more details about the DSC method, interested readers may refer to the works of Wei et al. (2002a), Wei et al. (2002b); Wei (2001c), Xiang et al. (2002), Wei (2000), Wei (2001a) and Civalek (2008).

3. Formulation of the DSC in irregular geometric media

If the calculation in a domain with irregular geometry is to be considered in a global cartesian coordinate (Fig. 1-a), with a mapping this in a natural coordinate system ξ and η (Fig. 1-b), the calculation will be simplified. Relations between the points in two domains define as follows (Charles and Moinuddin 1996):

$$x = \sum_{k=1}^{N_s} S_i(\xi,\eta)x_i \qquad y = \sum_{k=1}^{N_s} S_i(\xi,\eta)y_i \quad (7)$$

where x_i and y_i $(i = 1,2,...,N_s)$ are the coordinates of boundary nodes and $S_i(\xi,\eta)$ are interpolation functions. The mapping of an irregular medium is shown in Fig. 1 by use of 12 node transformation.

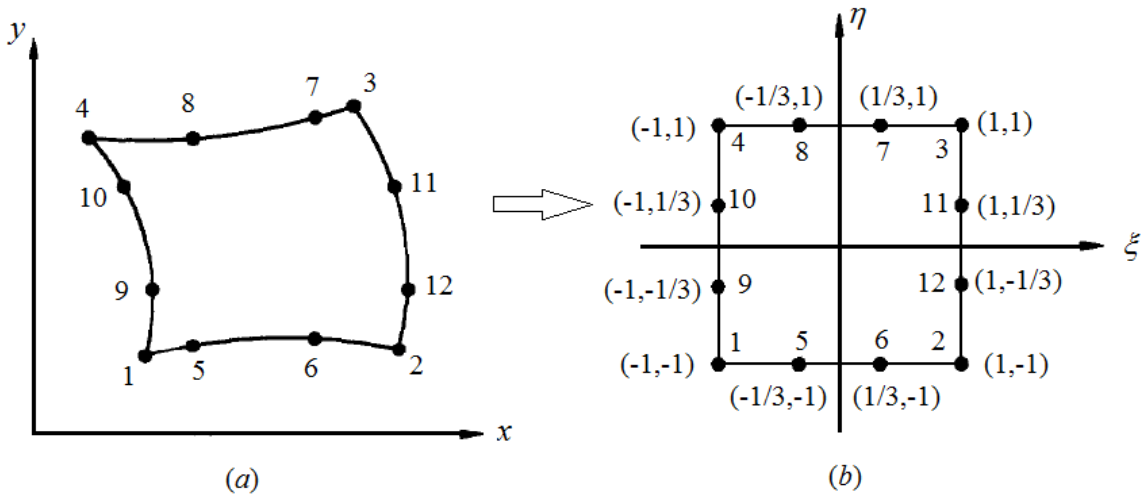


Fig. 1 12 node transformation mapping of a medium with irregular geometry

The S_i function must be defined in a way that its value will be considered as unit at the *i*th node and zero in the other $(N_s - 1)$ nodes. For example, if we use eight nodes for mapping of the geometry of the medium, it is convenient to use of the following functions (Han and Liew 1997):

$$\begin{aligned} S_i(\xi,\eta) &= \frac{1}{4}(1+\xi\xi_i)(1+\eta\eta_i)(\xi\xi_i+\eta\eta_i-1) && i=1,3,5,7; \\ S_i(\xi,\eta) &= \frac{1}{2}(1-\xi^2)(1+\eta\eta_i) && i=2,6; \\ S_i(\xi,\eta) &= \frac{1}{2}(1+\xi\xi_i)(1-\eta^2) && i=4,8 \end{aligned} \tag{8}$$

where ξ_i and η_i are the coordinates of the *i*th node in the $\xi-\eta$ coordinate system.

Based on the chain rule of the derivative, the relation between first and second derivatives in the two coordinate systems can be written as follows (Han and Liew 1997):

$$\begin{Bmatrix} \partial f/\partial x \\ \partial f/\partial y \end{Bmatrix} = J_0^{-1} \begin{Bmatrix} \partial f/\partial \xi \\ \partial f/\partial \eta \end{Bmatrix}$$
$$\begin{Bmatrix} \partial^2 f/\partial x^2 \\ \partial^2 f/\partial y^2 \\ 2\partial^2 f/\partial x\partial y \end{Bmatrix} = J_2^{-1} \begin{Bmatrix} \partial^2 f/\partial \xi^2 \\ \partial^2 f/\partial \eta^2 \\ \partial^2 f/\partial \xi\partial \eta \end{Bmatrix} - J_2^{-1} J_1 J_0^{-1} \begin{Bmatrix} \partial f/\partial \xi \\ \partial f/\partial \eta \end{Bmatrix} \tag{9}$$

where J_0 , J_1 and J_2 matrixes are:

$$J_0=\begin{bmatrix}\partial x/\partial\xi & \partial y/\partial\xi\\ \partial x/\partial\eta & \partial y/\partial\eta\end{bmatrix} \qquad J_1=\begin{bmatrix}\partial^2 x/\partial\xi^2 & \partial^2 y/\partial\xi^2\\ \partial^2 x/\partial\eta^2 & \partial^2 y/\partial\eta^2\\ \partial^2 x/\partial\xi\partial\eta & \partial^2 y/\partial\xi\partial\eta\end{bmatrix}$$

$$J_2=\begin{bmatrix}(\partial x/\partial\xi)^2 & (\partial y/\partial\xi)^2 & (\partial x/\partial\xi)(\partial y/\partial\xi)\\ (\partial x/\partial\eta)^2 & (\partial y/\partial\eta)^2 & (\partial x/\partial\eta)(\partial y/\partial\eta)\\ (\partial x/\partial\xi)(\partial x/\partial\eta) & (\partial y/\partial\xi)(\partial y/\partial\eta) & \frac{1}{2}((\partial x/\partial\xi)(\partial y/\partial\eta)+(\partial x/\partial\eta)(\partial y/\partial\xi))\end{bmatrix} \tag{10}$$

The following matrixes can be defined for simplification:

$$A=J_0^{-1}=\left[a_{ij}\right]_{2\times2} \qquad B=J_2^{-1}=\left[b_{ij}\right]_{3\times3} \qquad T=J_2^{-1}J_1J_0^{-1}=\left[t_{ij}\right]_{3\times2} \tag{11}$$

Approximation of the *n*th-order derivative of the *f* function (equation 4) can be mapped from $x-y$ coordinate system to the $\xi-\eta$ coordinate system, using equations (7) to (10). For instance, the first order derivative of the f function using new DSC formulation in the $\xi-\eta$ coordinate system is as follows:

$$\left.\frac{\partial f}{\partial x}\right|_{x=x_i}=a_{11}\sum_{k=-m}^{m}\delta_{\Delta,\sigma}^{(1)}(k\Delta\xi)\,f(\xi_k)+a_{12}\sum_{k=-m}^{m}\delta_{\Delta,\sigma}^{(1)}(k\Delta\eta)\,f(\eta_k) \tag{12}$$

4. Governing equations

The governing equation of water movement in porous media is the Richards equation (Richards 1931):

$$\frac{\partial(\rho_w V_x)}{\partial x}+\frac{\partial(\rho_w V_y)}{\partial y}+\frac{\partial(\rho_w V_z)}{\partial z}+\frac{\partial(\rho_w n S_w)}{\partial t}=0 \tag{13}$$

In the above equation *V* is the current velocity, ρ_w is the mass density of water, *n* is the void ratio of soil, S_w is the saturation of soil and *t* is the time parameter.

Despite the fact that all the physical systems are 3D, as the water movement in parallelogram vertical planes are similar, the Z coordinate is eliminated from the calculation for simplicity (Harr 1962). So, assuming the saturated medium and steady stream, the continuity equation will be as follows:

$$\frac{\partial V_x}{\partial x}+\frac{\partial V_y}{\partial y}=0 \tag{14}$$

The combination of Darcy's law and continuity equation will due to the following equation for modeling of seepage in homogenous porous media.

$$k_x\frac{\partial^2 h}{\partial x^2}+k_y\frac{\partial^2 h}{\partial y^2}=0 \tag{15}$$

where *h* is piezometric head and k_x and k_y are hydraulic conductivities in *x* and *y* directions, respectively.

For solving the seepage analysis in a porous medium, the solution domain must be mapped to a regular medium and then it must be meshed. After that, N_ξ and N_η are the number of equidistant nodes in both directions of new coordinate system. The distance between the nodes are Δ_ξ and Δ_η. The governing equation (15) will be descretized at these nodes.

The discrete form of the governing equation (15) in the natural coordinate system for every arbitrary node (ξ_i,η_j) could be shown as follows:

$$(k_x b_{11}+k_y b_{21})_{ij}\sum_{k=-m}^{m}\delta^{(2)}_{\Delta,\sigma}(k\Delta\xi)h_{i+k,j}+(k_x b_{12}+k_y b_{22})_{ij}\sum_{k=-m}^{m}\delta^{(2)}_{\Delta,\sigma}(k\Delta\eta)h_{i,j+k}+$$
$$(k_x b_{13}+k_y b_{23})_{ij}\sum_{k=-m}^{m}\delta^{(1)}_{\Delta,\sigma}(k\Delta\xi)\times\sum_{k=-m}^{m}\delta^{(1)}_{\Delta,\sigma}(k\Delta\eta)h_{i,j+k}-(k_x t_{11}+k_y t_{21})_{ij}\times \quad (16)$$
$$\sum_{k=-m}^{m}\delta^{(1)}_{\Delta,\sigma}(k\Delta\xi)h_{i+k,j}-(k_x t_{12}+k_y t_{22})_{ij}\sum_{k=-m}^{m}\delta^{(2)}_{\Delta,\sigma}(k\Delta\eta)h_{i,j+k}=0$$

The equations of the boundary conditions depend on the problem. Boundary conditions could be carried out after writing these equations in the new coordinate system and descretizing them. For example, the boundary condition at a boundary parallel with y direction is:

$$\frac{\partial h}{\partial x}=0 \quad (17)$$

The discrete form of the equation (17) in the transformed coordinate system is:

$$a_{11}\sum_{k=-m}^{m}\delta^{(1)}_{\Delta,\sigma}(k\Delta\xi)h_{i+k,j}+a_{12}\sum_{k=-m}^{m}\delta^{(1)}_{\Delta,\sigma}(k\Delta\eta)h_{i,j+k}=0 \quad (18)$$

The boundary condition could be easily participated in the calculation by use of the equation (18).

Implementing the equation (16) for every node over the solution domain and applying the boundary conditions due to construction an equation system that its matrix form is as follows:

$$[\boldsymbol{C}]\{h\}=\{d\} \quad (19)$$

where $\{h\}=\{h_{1,1},h_{1,2},.....,h_{N\xi\times N\eta}\}$. Solving equations (19) produces water head at each node.

5. Results

To confirm the analysis and validate the proposed algorithm, an example is solved using the modified DSC. The obtained results are compared with those of the conventionally finite element method. Details of the problem and procedure of solution are illustrated below:

Example: plan of a farm which has a pool for fish growing on its center is shown in Fig. 2. The water head of the pool with respect to the base level is considered as 7 m. There are two irrigation channels in north and south sides which their water head is 10 m with respect to the base level. The objective is to calculate the water head at points of the field. In this example we consider that $k_x=k_y$, so paying attention to the equation (16), these coefficients will be eliminated from the solution.

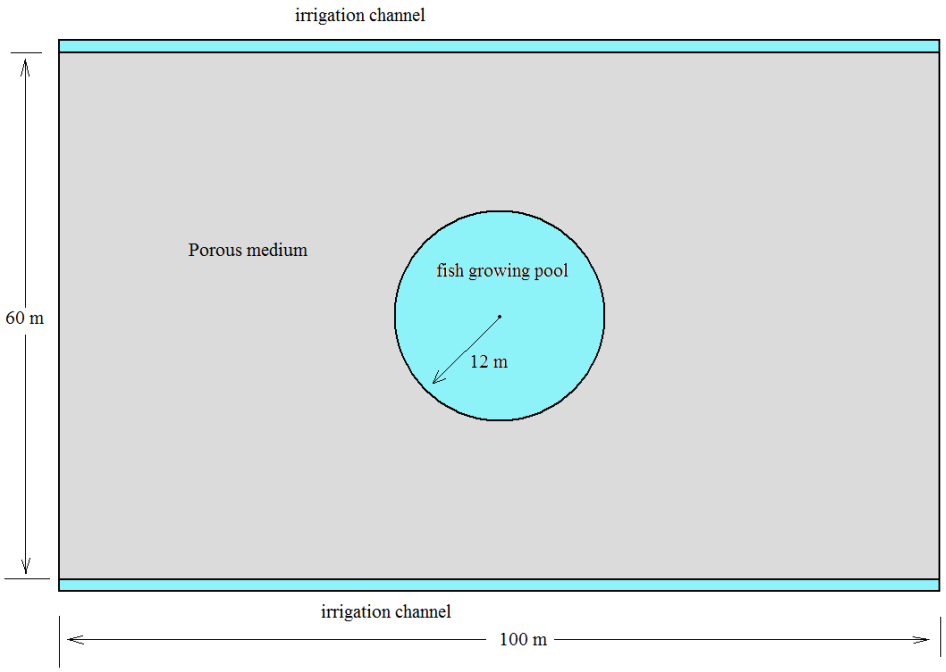


Fig. 2 Geometric specifications of the example

As the shape and the boundary conditions of the problem are symmetric, we can carry out the calculations for a quarter of the solution domain (Fig. 3). For solving the problem using the modified DSC, 8-node transform is employed. Fig. 3 shows the boundary conditions and boundary nodes for mapping the solution domain.

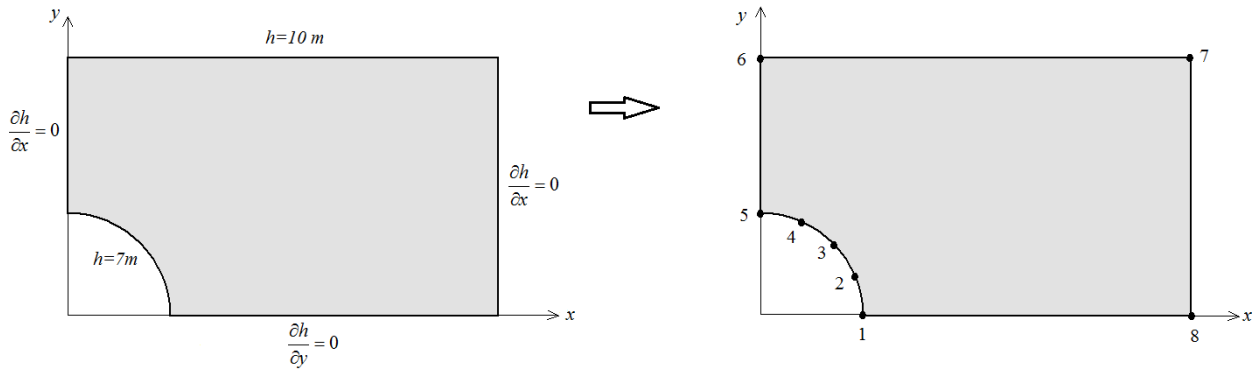


Fig. 3 Boundary conditions and locations of the transformation nodes for mapping of a quarter of the solution domain

Using the written computer program, *h* values are calculated at various nodes of the domain. Fig. 4 shows the equipotential lines obtained from the new numerical model. Comparison between the results with those of finit element method is utilized for validation. For achieving to this end, the water head obtained from two methods is exhibited for some chosen point in table (1). The coordinates of points in this table are those that devoted to the Fig. 4. As it is seen, there is a good agreement between the results of proposed algorithm and finite element method. This matter shows the accuracy of the new DSC algorithm.

Table1 Comparison of the water heads obtained from the DSC and finite element methods at some nodes in (x, y) coordinate system.

ERROR	h_{DSC} (m)	h_{FEM} (m)	Y (m)	X (m)
3.13E-05	9.5947	9.5944	8.02	16.04
1.06E-05	9.4092	9.4093	12.04	16.10
1.08E-05	9.2441	9.2440	16.09	16.23
2.20E-05	9.1070	9.1068	20.15	16.46
0.00E+00	9.0041	9.0041	24.24	16.80
2.10E-05	9.5332	9.5330	8.00	20.01
3.41E-05	8.8053	8.8050	19.08	24.49
1.16E-05	8.6460	8.6459	22.31	24.98
1.19E-05	8.4187	8.4186	24.67	27.15
2.13E-05	9.3728	9.3726	7.84	27.95
0.00E+00	9.0832	9.0832	11.65	27.99
0.00E+00	8.8161	8.8161	15.38	28.09
5.90E-05	8.4705	8.4700	21.33	28.14
1.17E-05	8.5796	8.5795	18.73	28.61
2.46E-05	8.1354	8.1352	23.77	30.72
0.00E+00	8.7230	8.7230	11.99	35.48
2.19E-05	9.1257	9.1255	8.05	36.01
0.00E+00	8.1892	8.1892	16.22	36.59
1.30E-05	7.7195	7.7194	20.12	37.19
3.61E-05	8.3104	8.3101	13.65	39.60
1.13E-05	8.8805	8.8804	9.01	40.16
3.95E-04	7.6020	7.5990	17.73	41.25

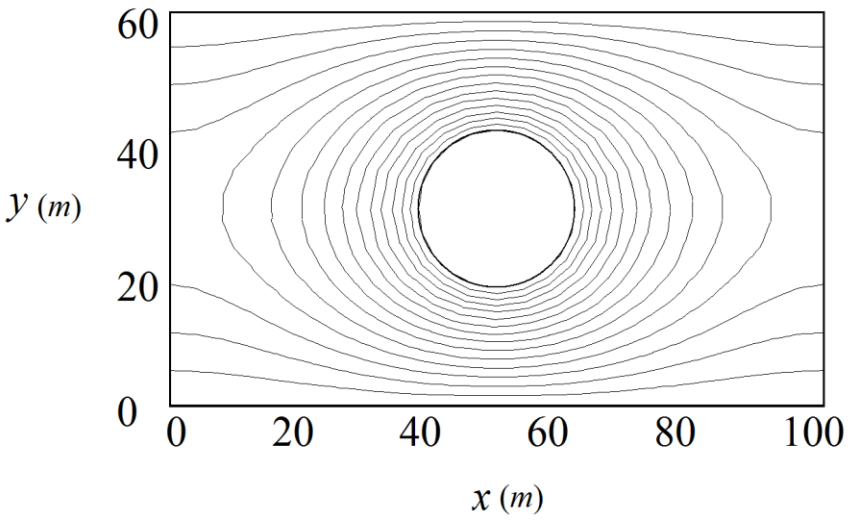


Fig. 4 Equipotential lines obtained from the DSC method in the entire of the solution domain

6. Conclusion

In this paper a novel formulation of the DSC is presented for seepage analysis in media with irregular geometry. The governing equations and boundary conditions are discretized using the proposed approach and a computer program is produced for solving some examples. A problem with irregular geometry solved by use of a new algorithm and the results are compared with those of finite element method. Good agreement between the results demonstrated that the proposed algorithm could be utilized as a promising approach to solve the seepage through porous media.

References

1 Charles, W. Bert and Moinuddin, Malik (1996). The differential quadrature method for irregular domains and application to plate vibration, International Journal of Mechanical Sciences, 38, 589-606.

2 Civalek, O. (2007). Three-dimensional vibration, buckling and bending analyses of thick rectangular plates based on discrete singular convolution method, International Journal of Mechanical Sciences, Vol. 49, pp. 752-765.

3 Civalek, O. (2008). Vibration analysis of conical panels using the method of discrete singular convolution. Communications in Numerical Methods in Engineering, 24(3),169–181.

4 Han J. B. and Liew, K.M. (1997). An eight-node curvilinear differential quadrature formulation for Reissner/Mindlin plates, Computer Methods in Applied Mechanics and Engineering, 141, 265–280.

5 Harr, M. E., (1962). Groundwater and Seepage, McGraw-Hill, New York.

6 Hou, Z.J. and Wei, G.W. (2002). A new approach to edge detection, J. Pattern Recognition Society, 35, 1559–1570.

7 Shokrollahi,M., Zayeri baghlani nejad,A. (2014). Numerical analysis of free longitudinal vibration of non-uniform rods; Discrete singular convolution (DSC) approach, Engineering mechanics, Accepted.

8 Richards, L. A. (1931). Capillary conduction of liquids through porous mediums, Physics, 1, 318-333.

9 Wan, D. C., and Wei, G.W. (2000). Numerical study of Euler and Navier-Stokes Equations by Efficient Discrete Singular Convolution Method, ACTA MECHANICA SINICA, 16(3), 223-239.

10 Wang, X., Xu, S. (2010). Free vibration analysis of beams and rectangular plates with free edges by the discrete singular convolution. Journal of Sound and Vibration, 329(10), 1780–1792.

11 Wei, G.W. (2001a). A new algorithm for solving some mechanical problems. Computer Methods in Applied Mechanics and Engineering, 190(15), 2017–2030.

12 Wei, G.W. (1999). Discrete singular convolution for the Fokker-Planck equation, J. Chem. Phys. 110(18), 8930-8942.
13 Wei, G.W. (2001b).Discrete singular convolution for beam analysis. Engineering Structures, 23(9) 1045–1053.
14 Wei, G.W. (2000). Solving quantum eigenvalue problems by discrete singular convolution. Journal of Physics B: Atomic, Molecular and Optical Physics, 33 (3), 343–352.
15 Wei, G.W. (2001c).Vibration analysis by discrete singular convolution. Journal of Sound and Vibration, 244(3), 535–553.
16 Wei, G.W., Zhao, Y.B., Xiang, Y. (2002a). A novel approach for the analysis of high-frequency vibrations. Journal of Sound and Vibration, 257 (2), 207– 246.
17 Wei, G.W., Zhao, Y.B., Xiang, Y. (2002b). Discrete singular convolution and its application to the analysis of plates with internal supports: part 1. Theory and algorithm. International Journal for Numerical Methods in Engineering, 55(8), 913–946.
18 Wei, G.W., Zhao, Y.B, Xiang, Y. (2001). The determination of natural frequencies of rectangular plates with mixed boundary conditions by discrete singular convolution, International Journal of Mechanical Sciences, 43(8), 1731–1746.
19 Xiang, Y., Zhao, Y.B., Wei, G.W. (2002). Discrete singular convolution and its application to the analysis of plates with internal supports: part 2. Applications. International Journal for Numerical Methods in Engineering, 55(8), 947–971.
20 Xin Zhou, Dian Zhou, Jin Liu, Ruiming Li, Xuan Zeng and Charles Chiang. (2004). Steady-State Analysis of Nonlinear Circuits Using Discrete Singular Convolution Method, Proceedings of the Design, Automation and Test in Europe Conference and Exhibition, IEEE Computer Society.
21 Zayeri Baghlani Nejad, A. and, Shkrollahi, M. (2011). Numerical Solution of Turbulent leakage problem by using new algorithms DSC, Irrigation and water engineering, 2, 36-42, (In Persian).
22 Zhao Y.B., Wei G.W. (2002). DSC analysis of rectangular plates with non-uniform boundary conditions, Journal of Sound and Vibration, 255 (2), 203–228.
23 Zhao, S., Wei, G.W., Xiang, Y. (2005). DSC analysis of free-edged beams by an iteratively matched boundary method, Journal of Sound and Vibration, 284(1-2), 487–493.

A Case Study of Water Quality Modeling of the Gargar River, Iran

Mojtaba Rafiee[1], Ali Mohammad Akhond Ali[1], Hadi Moazed[1], Steve W. Lyon[2], Nemat Jaafarzadeh[3], Banafsheh Zahraie[4]
[1]Faculty of Water Science and Engineering, Shahid Chamran University, Ahvaz, Iran
[2]Faculty of Physical Geography and Quaternary Geology, Stockholm University, Stockholm, Sweden
[3]Faculty of Environmental Health, Ahvaz Jondishapour University of Medical Science, Ahvaz, Iran
[4]School of Civil Engineering, College of Engineering, University of Tehran, Tehran, Iran

Abstract

Human activities in the recent years have considerably increased the rate of water pollution in many regions of the world. In this case study, the main sources of wastewater discharging into the Gargar River were identified. Using river and point source flow rates and water quality parameters measured along the river, the river water quality was simulated using a commonly used, one-dimensional water quality model, the QUAL2K model. Simulated values of DO, CBOD, NH_4-N and NO_3-N demonstrated the accuracy of the model and despite a significant data shortage in the study area, QUAL2K model was found to be an acceptable tool for the assessment of water quality. Still, for this case study, it was found that the model was most sensitive to river and point source flows and moderate to fast CBOD oxidation, and nitrification rates.

Keywords: Water Quality, QUAL2K, Modeling, Wastewater Discharge, Whole-System Water Management

1. Introduction

Continuously increasing human activities have considerably increased global rates of water pollution in recent decades. Agricultural, municipal, and industrial activities typically lead to discharge of significant amounts of nutrients and organic materials into rivers and streams. Discharge of degradable wastewaters into flowing waters can impair water quality. For example they can result in a decrease of dissolved oxygen (DO) concentrations due to assimilation of pollutants by microorganisms, chemical oxidations of reduced pollutants, and respiration of plants, algae and phytoplankton (Drolc and Konkan, 1996). The problems associated with low DO levels are even more critical during low flow periods. Low DO concentrations or, in an extreme situation, anaerobic conditions create unbalanced ecosystems with fish mortality, odors and aesthetic nuisances (Cox, 2003). Since fish typically cannot survive when DO content is less than 3mg/L (Novotny, 2002), DO content is therefore often considered a barometer of the ecological health of a stream and is one of the most important water quality parameters to maintain for protecting fish (Chang, 2005). To ensure good overall river health, however, water quality must also meet threshold levels of several other key parameters including carbonaceous biochemical oxygen demand (CBOD), total nitrogen (TN), total phosphorus (TP), temperature and pH (Kannel et al., 2007). For example, the permissible range of pH is 6.5–8.5 for fisheries (EMECS, 2001) and 6.5–9.2 for drinking water quality according to the Iranian drinking water standard (IPBO, 1992). Considering BOD levels in rivers, even though there are currently no regulations or recommended limits according to Iranian standards, other international guidelines (e.g., the European Union directives) indicate a permissible range for BOD between 3 and 6 mg/L for various types of fisheries (EEC, 1978).

In order to achieve such targets of water quality, planning and management are needed along an entire river to ensure that the assimilative capacity remains sufficient along the entire river (Campolo et al., 2002). To address this, the complex relationships between waste loads from different sources and the resulting water quality of the receiving waters need to be characterized. These relationships are best described with mathematical models (Deksissa et al., 2004). A widely used mathematical model for assessing

conventional pollutant impact is QUAL2E (Brown and Barnwell, 1987; Drolc and Konkan, 1996). One of the major inadequacies of this model, however, is its lack of provisions for conversion of algal death to carbonaceous biochemical oxygen demand (Ambrose et al., 1987, 1988; Park and Uchrin, 1996, 1997). As such, Park and Lee (2002) developed QUAL2K, a one-dimensional, steady flow model, which includes the simulation of new water quality interactions such as conversion of algal death to BOD, denitrification process, and DO change caused by plants. To date, applications of the freely available QUAL2K model (see http://www.ecy.wa.gov/) for water quality strategies are numerous and varied. Kannel et. al (2006) confirmed the usefulness of QUAL2K in data-shortage conditions. Fan et al. (2009) applied a HEC-RAS-assisted QUAL2K to simulate water quality and the QUAL2K model proved to be an effective tool in evaluation of potential water quality improvement programs in a tidal river. Cho et al. (2010) calibrated the QUAL2K input parameters in the Gangneung Namdaecheon River on the Korean peninsula using an optimization technique. Their calibration results showed good correspondence for most of the water quality variables considered with the exception of DO and Chl-a that showed relatively large errors in some parts of the river. Zhang et al. (2012) simulated the water quality in Hongqi River, a polluted river in China, and could evaluate the reduction rates of BOD, NH_3-N, TN and TP along the river.

In the real situation of a river, unsteady and two- or three-dimensional models are typically considered more appropriate for representing interactions between waste loads and the receiving waters; however, these types of models typically require large amounts of data that are unavailable in many systems. For example, in the Gargar River, where this current study focuses, there is a data deficiency with regards to water quality monitoring. To work around this shortcoming, QUAL2K, a steady-state model, was chosen and tested as a framework appropriate for a modest water quality modeling. Moreover, when the flow and pollution transport are dominated by longitudinal changes (such as in Gargar River) and the river is long with respect to the mixing length relative to the cross-section, the central QUAL2K assumption of one-dimensional processes is typically valid. In the current study, QUAL2K model was applied in a data-limited setting along the Gargar River, Iran. The discharges of municipal wastewater and fisheries along the river were identified and analyzed. This case study is novel as, in addition to identifying wastewater discharge into the river, it simulates Gargar River water quality for the first time and tests the applicability of the simplifying assumptions (i.e., one-dimensional flows and transports) behind QUAL2K. This gathering of observed water quality data and a case study simulation model provides a solid basis for future work into model development and optimization strategies relevant for river-scale water quality management.

2. Material and methods

2.1. Study area

The Gargar River (Gargar Canal) is a historical, man-made branch of the Karoon River, which is separated from the main channel north of Shoushtar City. The Gargar River's monthly average flow varies between 10 and 31 m^3/s based on data measured in the last ten years. Water is diverted to Gargar River by an ancient dam known as Band-e Mizan. It flows about 82 km before re-joining the Karoon main river in a place called Band-e-ghir. The Gargar River is a part of Shoushtar historical hydraulic system and was registered as an UNESCO world heritage site in 2009 (UNESCO, 2009). There are a number of canals, historical dams and watermills of the Shoushtar historical hydraulic system located adjacent to the Gargar River. The upstream section of the Gargar River has been dug in a solid rock and in the downstream section it enters a soft-soil plane (ICHHTO, 2008).

The Gargar River is highly polluted because many fish farms discharge their wastewater into the river. Further, due to the world heritage status and associated protection issues and some water intakes preparing water for municipal and agricultural purposes along the river, the investigation of water quality management is very important in this region. The high temperatures in the region, with average monthly temperatures that vary between 14.7 and 37.5 ^oC in the coolest and warmest months, respectively, lead to higher chemical/biological reaction rates in the river than would be expected in temperate regions. Altogether, these factors make the Gargar

River a good and interesting candidate for a case study application of QUAL2K to test the model's utility as a water quality model in a data limited situation.

2.2. Monitoring sites and available data

The monitoring stations used in this study (Figure 1) consist of five stations: Band-e mizan (S1), Pol-e Koshtargah (S2), Dar Khazineh (S3), Seyd Hasan (S4) and Band-e ghir (S5). Data were gathered at these stations and from several wastewater dischargers (Table 1) in dry and wet seasons. For the wet season, observations were conducted on 3 May 2011. For the dry season, observations were conducted on 13 October 2010. Since it was only possible to collect two observations at each station, there is a lack of data relative to typical applications of QUAL2K (e.g., Kannel et al., 2006). The parameters measured at each station included discharge, water temperature, pH, 5-day biochemical oxygen demand as O_2 (BOD_5), dissolved oxygen (DO), ammonium (NH_4-N), nitrate (NO_3-N) and nitrite (NO_2-N). It should be noted, however, that the nitrite concentrations were negligible in the river. Water samples from the river and wastewater samples from the dischargers were collected, transported and analyzed following methods described in Standard Methods (APHA, 2005). Samples were collected by the Khouzestan Fishery Organization, the Khouzestan Water and Power Authority (KWPA), and the Khouzestan Environmental Protection Office. Supplemental field observations were also performed to confirm some outlier and unmatched data gathered by these three organizations.

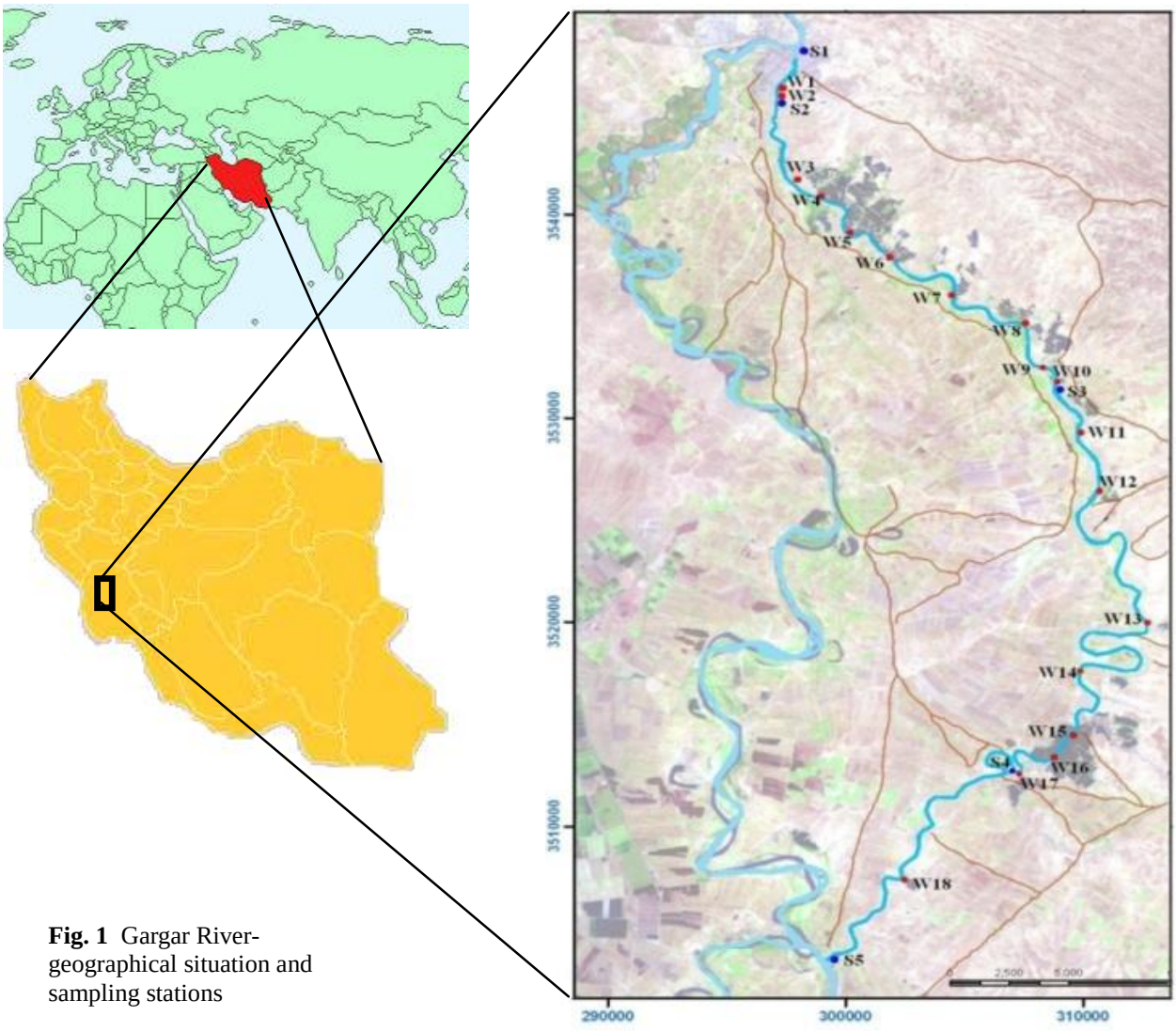


Fig. 1 Gargar River-geographical situation and sampling stations

Table 1 Water quality monitoring stations in the Gargar River

Types	Stations (abbreviations)	Distance from Downstream (Km)	Description
Stations on river	Band-e-mizan (S1)	82	North of Shoushtar
	Pol-e-Koshtargah (S2)	78	Shoushtar
	Dar Khazineh (S3)	55	South of Shoushtar
	Seyd-Hasan (S4)	24	
	Band-e-ghir (S5)	1	
Wastewaters	Shoushtar municipal wastewater (W1)	80	
	Slaughterhouse (W2)	79	
	Fish culture drainage 1 (W3)	74	
	Fish culture drainage 2 (W4)	73	
	Fish culture drainage 3 (W5)	70	
	Fish culture drainage 4 (W6)	66	Upstream of Qal'e soltan
	Fish culture drainage 5 (W7)	62	Downstraem of Qal'e soltan
	Fish culture drainage 6 (W8)	60	
	Fish culture drainage 7 (W9)	58	
	Fish culture drainage 8 (W10)	56	Downstream of Dar-Khazineh
	Fish culture drainage 9 (W11)	55	
	Fish culture drainage 10 (W12)	53	Upstraem of Shagharij-paein
	Fish culture drainage 11 (W13)	48	
	Fish culture drainage 12 (W14)	38	
	Fish culture drainage 13 (W15)	29	Upstream of Basir sofla
	Fish culture drainage 14 (W16)	24	
	Fish culture drainage 15 (W17)	19	
	Fish culture drainage 16 (W18)	7	

2.3. Modeling tool

QUAL2K has at its core a one-dimensional advection-dispersion equation as the governing equation:

$$V\frac{\partial c}{\partial t} = \frac{\partial(A_c E\frac{\partial c}{\partial x})}{\partial x}dx - \frac{\partial(A_c Uc)}{\partial x}dx + V\frac{dc}{dt} + s \quad (1)$$

in which U (LT^{-1}) is averaged velocity, A_c is cross sectional area (L^2), E equals longitudinal dispersion (L^2T^{-1}), c is concentration (ML^{-3}), V is volume (L^3), x is distance (L) and s stands for sources and sinks, which is additional inflow of water or constituent mass. QUAL2K solves this governing equation in a steady-state condition for a constituent concentration c_i in the water column (excluding hyporheic exchange) of a stream reach i (Figure 2). This gives in a general mass balance equation (the transport and loading terms for bottom algae modeling are omitted) that can be expressed as (Pelletier et al., 2006):

$$\frac{dc_i}{dt} = \frac{Q_{i-1}}{V_i}c_{i-1} - \frac{Q_i}{V_i}c_i - \frac{Q_{ab,i}}{V_i}c_i + \frac{E_{i-1}}{V_i}(c_{i-1} - c_i) + \frac{E_i}{V_i}(c_{i+1} - c_i) + \frac{W_i}{V_i} + S_i \quad (2)$$

where Q_i is the flow at reach i (L/d), $Q_{ab,i}$ is abstraction flow at reach i (L/d), V_i stands for volume of reach i (L), W_i stands for the external loading of the constituent to reach i (mg/d), S_i are sources and sinks of the constituent due to reactions and mass transfer mechanisms (mg/L/d), E_i is bulk dispersion coefficient between reaches (L/d), E_{i-1} and E_{i+1} are bulk dispersion coefficients between reaches $i-1$ and i and i and $i+1$ (L/d), respectively, c_i is concentration of water quality constituent in reach i (mg/L) and t is time (d).

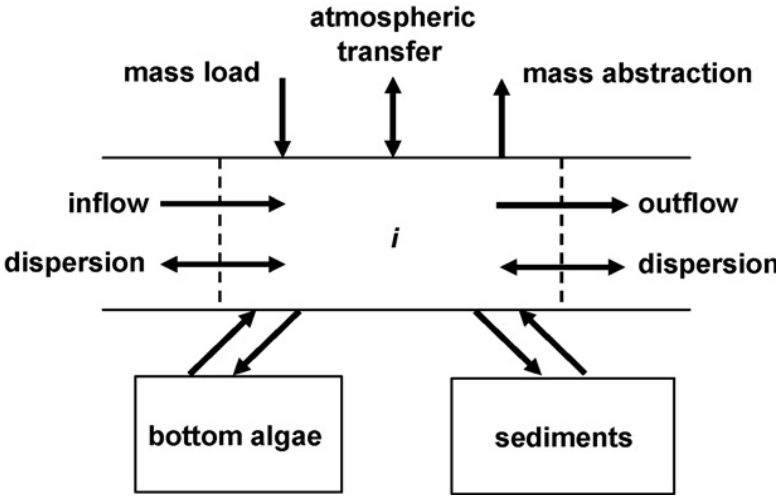


Fig. 2 Mass balance in a reach segment *i* (from Chapra et al. , 2006)

Figure 3 shows a schematic diagram of the interacting water quality state variables in the model which are considered as sources and sinks (equation 2). The complete description of processes and mathematical representations of the interacting water quality state variables, which constitute constituent specific governing equations, are available in Chapra et al. (2006).

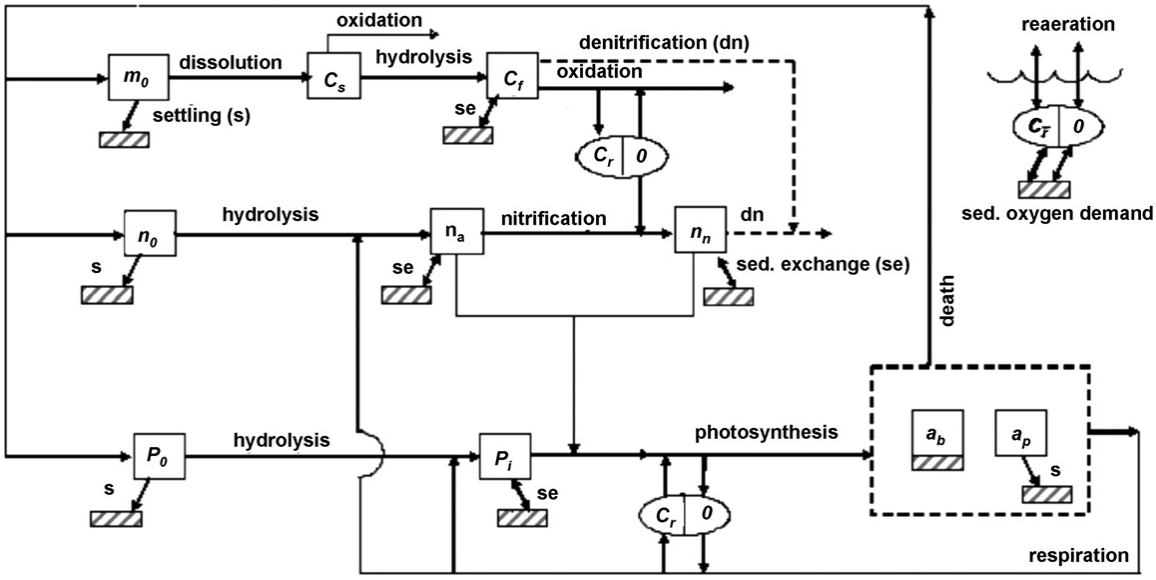


Fig. 3 Schematic diagram of interacting water quality state variables (from Chapra et al. , 2006)

To constrain the parameters of this QUAL2K mass balance equation for a given stream reach, Chapra and Canale (2002) proposed that a combination of flow, Manning's coefficient and river cross section be used (e.g., Equations 3 through 6). The method (which was adopted in this case study) can be applied iteratively from an initial depth estimate and terminated when the estimated error (equation 4) fall below a specified value 0.001%. Then, the cross-sectional area can be determined with Equation 5 and the velocity determined from the continuity equation (Equation 6).

$$H_k = \frac{(Qn)^{3/5}\left(B_0 + H_{k-1}\sqrt{s_{s1}^2+1} + H_{k-1}\sqrt{s_{s2}^2+1}\right)^{2/5}}{S^{3/10}\left[B_0 + 0.5(s_{s1}+s_{s2})H_{k-1}\right]} \quad (3)$$

$$\varepsilon_a = \left|\frac{H_{k+1}-H_k}{H_{k+1}}\right| \times 100\% \quad (4)$$

$$A_c = \left[B_0 + 0.5(s_{s1}+s_{s2})H\right]H \quad (5)$$

$$U = \frac{Q}{A_c} \quad (6)$$

2.4. Model implementation

The full 82 km length of the Gargar River was discretized into 23 reaches along with the locations of point source of identified wastewaters (Figure 4). This segmentation forms the basis for the QUAL2k modeling application. Table 2 shows the river hydraulic characteristics used as the input of the QUAL2K model. As the model simulates ultimate CBOD, it assumed 1.5 times the measured $CBOD_5$ (Kannel et al., 2006 and Chapra et al., 2006). Stream flow, temperature, pH, DO, BOD, organic nitrogen, ammonium nitrogen, nitrate nitrogen, and phosphorus data were all included in the model as input parameters. The data on phytoplankton and pathogens were not measured and, thus, these inputs were left blank. This is likely to have minimum impact on the model results as the phytoplankton concentration in the Gargar River is negligible (Rasti et al., 2007). The algae and bottom sediment oxygen demand coverage were assumed to be 50%. The

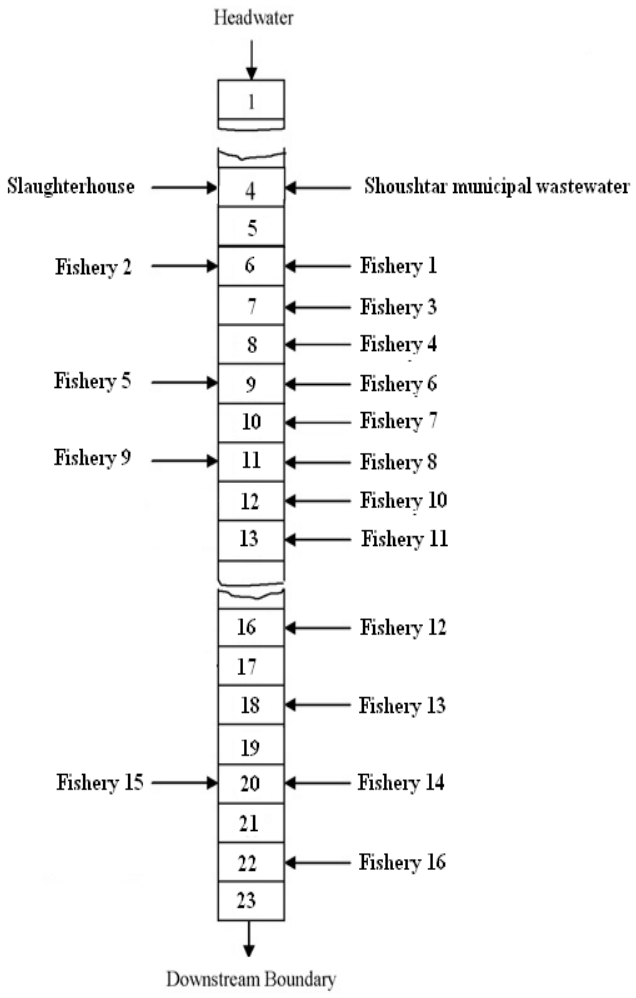


Fig. 4 System segmentation with location of pollution sources along Gargar River

sediment/hyporheic zone thickness, sediment porosity and hyporheic exchange flow were assumed as 10 cm, 0.4 and 10%, respectively, based on field observations and available operational experience. The organic nitrogen was assumed to be 35% of the total nitrogen since it was not specifically analyzed.

Fishery wastewater qualities (W3 to W18) (Figure 5) were assumed to be the same across all fisheries and set equal to the average of the quality of samples collected and analyzed by the Iranian Fishery Organization at the effluent of several fish culture farms. Fisheries water abstraction considered to be twice that of the fishery discharges located in near upstream positions. There are some different fishery wastewater data issued by the Khouzestan Environmental Protection Office, however, the office had measured these wastewater qualities just when the fisheries were appealed because of their high pollution effluents. Therefore the data from Khouzestan Environmental Protection Office could not be considered as normal data and were not used in this study. The water quality at the first monitoring station of the Gargar River, S1 (Band-e Mizan), was considered as the upstream boundary condition for the QUAL2K model.

The ranges of the model rate parameters, which are presented in Table 2, were collected from literature values including the United States Environment Protection Agency (USEPA) guidance document (USEPA, 1985) and Bowie et al. (1985). The Owens–Gibbs formula (Owens et al., 1964), which is given equation 7, was applied for calculating re-aeration rates. This equation was developed for stream depths from 0.4 to 11 ft and velocities from 0.1 to 5 ft/s (Ghosh and Mcbean, 1998).

$$K_a = 5.32\ U^{0.67} / H^{1.85} \quad (7)$$

Here, K_a is the oxygen reaeration rate coefficient (d^{-1}), U is the water velocity ($m.s^{-1}$), and H is the water depth (m).

An exponential model was applied for oxygen inhibition for CBOD oxidation, nitrification, de-nitrification, phytorespiration and bottom algae respiration. Meteorological parameters were considered equal to the data issued by the nearest meteorological station, the Shoushtar synoptic station. A Manning coefficient equal to 0.026 was used along the river consistent with sections surveyed by Khouzestan Water and Power Authority. All the other parameters were adjusted as default values in QUAL2K as there were insufficient data available to modify them.

The measured data in October 2010 were utilized for calibration of the QUAL2K model. For calibration, the model parameters such as, for example, fast CBOD oxidation rate, ammonium nitrification rate, nitrate denitrification rate, and organic N settling velocity, were changed until the differences between observed and simulated water quality parameter values were minimized. The goodness of fit was tested by a root mean squared error (RMSE), mean absolute percentage of error (MAPE), and percent bias (PBIAS) between the difference of the model predictions and the observed data for water quality constituents as presented in Equations

8, 9 and 10, respectively. These statistical error parameters are commonly used for calibration and validation of the models (Najafzadeh et al., 2013; Najafzadeh and Azamathulla, 2013; Najafzadeh and Barani, 2011; Moriasi, 2007)

$$RMSE = (\Sigma(O_{i,j} - P_{i,j})^2 / m)^{0.5} \quad (8)$$

$$MAPE = (\Sigma(|P_{i,j} - O_{i,j}|) / \Sigma(O_{i,j}) * 100/m) \quad (9)$$

$$PBIAS = (\Sigma(O_{i,j} - P_{i,j}) / \Sigma(O_{i,j}) * 100 \quad (10)$$

where $O_{i,j}$ equals to observed values, $P_{i,j}$ equals to predicted values and m is the number of pairs of predicted and observed values of the state variables (i.e. DO, CBOD and etc.). To test the ability of the calibrated model to predict water quality conditions under different conditions, the model was run to estimate water quality values observed on May without changing the calibrated parameters. Again, Equations 8, 9, and 10 were applied to assess the goodness of fit between the model predictions and the observed water quality values (i.e., validation).

3. Results and discussion

3.1. Comparing observations and model predictions

The observed data from the monitoring stations along the river conducted on 3 May 2011 and 13 October 2010 are summarized in Table 2 and Table 3, respectively. The identified wastewater quality values are provided in Table 4. The calibrated model parameters are given in Table 5. The simulation results demonstrated that the profiles of water quality upstream of 20 km have modest fitness and were well-represented in the model. Downstream of 20 km chainage, however, poor calibration was achieved using available data in the region. Unlike the simulation results, the last station (S5) was higher in CBOD and Nitrate and lower DO than the upstream station S4. This could be because of discharging wastewater into the river between S4 and S5; however, there is no detected major discharger between S4 and S5. Therefore, the profiles between S4 and S5 are not likely well-produced in the model and calculation of error statistics (RMSE, MAPE, and PBIAS) for both calibration and validation (and the subsequent sensitivity analysis) was performed without considering the data of the last station, S5.

Table 2 Water quality observed at monitoring stations along Gargar River on 3 May 2011

Station	Chain (km)	Flow (m^3/s)	Water temperature (◦C)	DO (mg/L)	BOD (mg/L)	NO_3-N (mg/L)	NH_4-N (mg/L)
S1	82	5.43	18	9.34	3.41	6.70	0.16
S2	78	-	18	8.72	3.82	7.26	0.021
S3	55	-	18	7.06	5.3	9.91	0.058
S4	24	-	19	7.97	4.8	7.87	0.068
S5	1	-	20	9.56	5.64	7.67	0.069

Table 3 Water quality observed at monitoring stations along Gargar River on 13 October 2010

Station	Chain (km)	Flow (m^3/s)	Water Temperature (◦C)	DO (mg/L)	BOD (mg/L)	NO_3-N (mg/L)	NH_4-N (mg/L)
S1	82	5.23	22	9.15	2.27	6.62	0.141
S2	78	-	23	7.27	4.16	6.92	0.470
S3	55	-	23	6.66	5.77	6.12	0.660
S4	24	-	23	8.08	3.7	5.77	0.830
S5	1	-	25	8.68	5.2	6.66	0.740

Table 4 The average measured wastewater quality discharging into Gargar River

Station	Chain (km)	Flow (L/s)	Water temperature (◦C)	pH	DO (mg/L)	BOD_5 (mg/L)	NO_3-N (mg/L)	NH_4-N (µg/L)
W1	80	81	28	6.8	0	120	2.390	22.5
W2	79	2	25	7.2	2.4	253	5.5	47
W3	74	41	28	8.9	7.1	11.9	5.5	2.4
W4	73	60	28	8.9	7.1	11.9	5.5	2.4
W5	70	195	28	8.9	7.1	11.9	5.5	2.4
W6	66	101	28	8.9	7.1	11.9	5.5	2.4
W7	62	42	28	8.9	7.1	11.9	5.5	2.4
W8	60	144	28	8.9	7.1	11.9	5.5	2.4
W9	58	80	28	8.9	7.1	11.9	5.5	2.4
W10	56	44	28	8.9	7.1	11.9	5.5	2.4
W11	55	7	28	8.9	7.1	11.9	5.5	2.4
W12	53	43	28	8.9	7.1	11.9	5.5	2.4
W13	48	31	28	8.9	7.1	11.9	5.5	2.4
W14	38	190	28	8.9	7.1	11.9	5.5	2.4
W15	29	14	28	8.9	7.1	11.9	5.5	2.4
W16	24	286	28	8.9	7.1	11.9	5.5	2.4
W17	19	32	28	8.9	7.1	11.9	5.5	2.4
W18	7	22	28	8.9	7.1	11.9	5.5	2.4

From the model results, the average velocity and water depth were 1.9 m/s and 1.4 m, respectively, along the river confirming the applicability of Owen-Gibbs equation as a re-aeration model.

The DO concentration gradually decreased along the river and remained in the standard range of values (Figure5).

However, the Gargar River water quality parameters such as BOD_5 did not meet minimum levels permissible in some stations. CBOD from municipal wastewater in the upstream parts of the river and from fisheries between chainage 70 to 20 km led to increasing CBOD along the river.

Generally, the model calibration results were in modest agreement with the measured data. The RMSE for example between the simulated and observed values for river DO, CBOD, NH_4-N and NO_3-N were 20, 18, 17 and 13%, respectively (Table 6). In the validation dataset (Figure 6), the RMSE between observed and modeled values for the river DO, CBOD, NH_4-N, and NO_3-N were 13, 32, 26, and 29%, respectively (Table 6). This indicates that the model can be calibrated in one condition and still be rather valid in another. The maximum registered levels of CBOD, NH_4-N, and NO_3-N in this study were at (or below) 8.8, 0.83 mg/L (both in October) and 9.9 mg/L (in May), respectively. The minimum observed DO was 6.7 mg/L along the river occurring in October. The modeled water quality parameters along the river in Figures 5 and 6 imply that the river, in its current condition, could largely dampen the sudden discharge of CBOD, NH_4-N, and NO_3-N. As such, the Gargar River can receive increased loading from dischargers and lessen them in some parts of the river by its self-purification capacity. However, DO decreases permanently over the entire river length. This means that oxygen used to oxidize the constituents has permanently been shifted to a level more than the re-aeration potency of the river. Apparently, DO deficit can be problematic in this system if more wastewater discharging leads to more oxygen consumption and/or

different environmental conditions (e.g., weather or climate shifts) lead to poor re-aeration.

Some errors in the modeling considered in this case study are inevitable as the field work consists of collecting a single sample in each station rather than multiple samples to assess variability. As the model predictions are based on the daily data, the observed DO may be different depending upon the time of samplings during the day. The DO levels decrease during the nighttime hours because of lower rates of photosynthesis by river plants. During the daytime, DO (and thus pH) increases because of the higher rates of photosynthesis of the plants. In spite of some incommensurability errors, the modeling results were quite acceptable to achieve goals for such a severe data shortage condition which is typical in many rivers especially in the developing countries. However, greater accuracy could likely be achieved through monitoring various input variables including algae coverage, sediment oxygen demand, and organic nitrogen over time. Further, using sophisticated 2D or 3D models may allow for a more interpretation of water quality between sites in time. Such work is outside the scope of this initial case study to explore the utility of the QUAL2K model in data-limited conditions.

Table 5 Calibrated parameters for the Gargar River water quality modeling on 3 May 2011

Parameters	Values	Units	Min. value	Max. value
ISS settling velocity	0.9209	m/d		
Fast CBOD oxidation rate	0.3	/d	0	5
Organic N settling velocity	0.84	m/d	0	2
Organic N hydrolysis	0.8	/d	0	5
Ammonium nitrification	2.0	/d	0	10
Nitrate Denitrification	0.2	/d	0	2
Sed. denitrification transfer coef.	0.9627	m/d	0	1

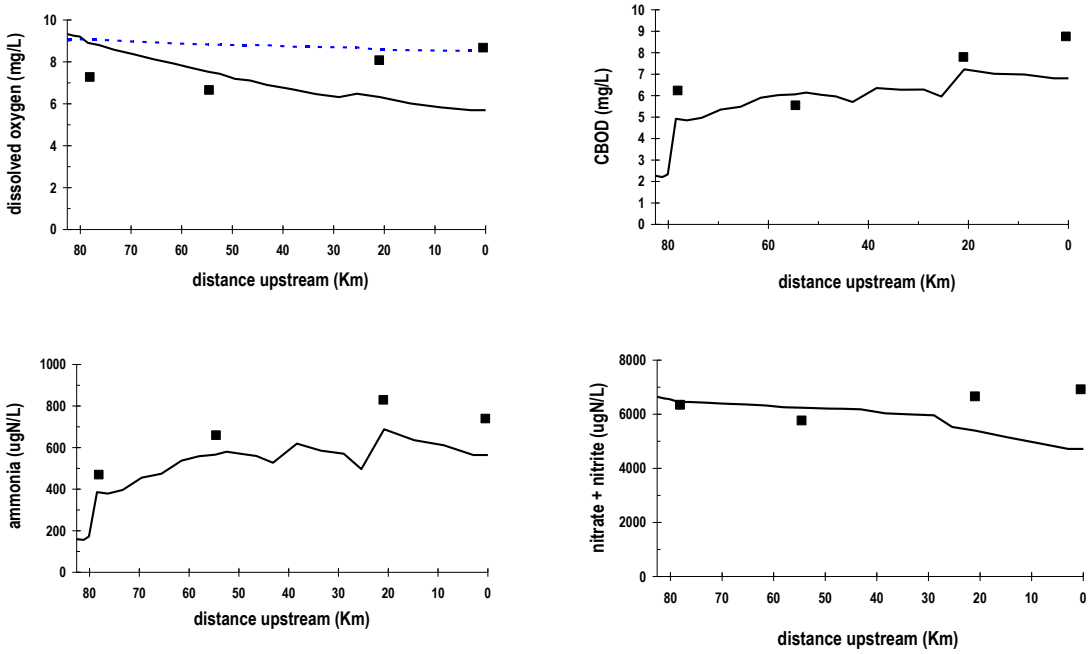


Fig. 5 Model results in Gargar River based on the data gathered on 13 October 2010

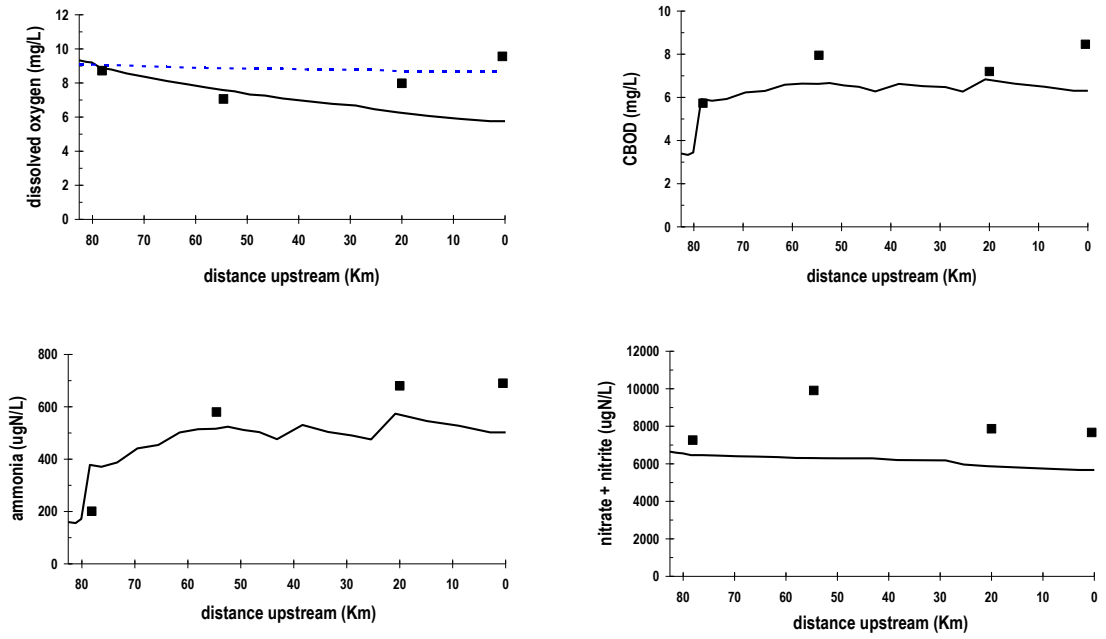


Fig. 6 Model results in Gargar River based on the data gathered on 3 May 2011.

Table 6 Root mean squared errors (RMSE), mean absolute percentage error (MAPE) and percent bias (PBIAS) for modeled versus measured water quality parameters

Parameter	RMSE		PBIAS		MAPE	
	Calibration	Validation	Calibration	Validation	Calibration	Validation
DO	1.5	1.0	-3.2	4.0	6.4	3.5
CBOD	1.2	2.2	3.2	-2.8	5.7	9.2
NH_4-N	0.108	0.124	16.1	-0.7	5.4	7.8
NO_3-N	0.817	2.415	4.0	25.4	3.4	8.5

3.2. Sensitivity analysis

To identify the parameters of the QUAL2K water quality model that have the highest influence on model predictions, a simple sensitivity analysis was performed with respect to DO estimates. The analysis was performed for the main seven model parameters and forcing functions (Table 7) by increasing and decreasing each parameter by 20% of its calibrated value and keeping the remaining parameters constant. The impacts of these changes on DO estimates were then assessed. It was found that the model was rather highly sensitive to river flow and point source discharges and moderately sensitive to fast CBOD and nitrification rate.

Table 7 Sensitivity analysis for the QUAL2K model on Gargar River based on the 3 May 2011 data

Parameters	Description	DO Change (%)	
		+20% parameter	-20% parameter
Q	River flow	3.59	-4.08
q	Point source flow	-2.34	2.54
k_{dc}	Fast CBOD oxidation rate	-0.62	1.49
k_{na}	Nitrification rate	-1.04	1.25
n	Manning coefficient	-0.43	0.83
CBOD	Point sources CBOD	-0.73	0.74
k_{dn}	Denitrification rate	0.72	-0.70

4. Conclusion

The current study characterized the quality of wastewater discharge into the Gargar River. 18 dischargers were identified along the river and their flow and water quality characteristics were analyzed. In the samples analyzed at five stations along the river, water quality parameters such as fast CBOD and DO varied between 3.47 and 5.77 mg/L and between 6.66 and 9.34 mg/L, respectively. In addition, we presented here a case study to simulate Gargar River water quality for the first time using the commonly-used, one-dimensional water quality model QUAL2K. It was possible to calibrate the model by changing various constituent rates. As such, fast CBOD oxidation, Ammonium nitrification and Nitrate denitrification rates were calibrated to be 0.3, 2.0 and 0.2 d^{-1}, respectively. While this initial study found that the model was most sensitive to river flow, point sources flow, fast CBOD oxidation rate and nitrification rate compared with the other model input parameters, QUAL2K clearly has potential for assessing water quality along the river and could be implemented as a valuable tool to inform Gargar River management strategies. For example, based on the observations provided in this study, it appears that DO may be manipulated using well-defined management strategies to keep DO concentrations above minimum allowable levels. The QUAL2K model could be used to simulate the amount of DO required and the potential impacts of such management on other water quality factors along the entire river. As such, the implementation of QUAL2K with regard to optimization techniques and accuracy assessments under various conditions warrants further consideration.

5. Acknowledgements

The present study was supported by the World Bank's RSM (Robert S. McNamara) fellowship in the form of research exchange funding for M. Rafiee. In addition, we give special thanks to Dr. Manuel Pulido-Velázquez for his advice on this work.

References

1 Ambrose, R.B., Connolly, J.P., Southerland, E., Barnwell, T.O., Schnoor, J.L., 1988. Waste allocation simulation models. J. Water Pollut. Control Fed. 6, 1646–1655.

2 APHA (American Public Health Association), 2005, Standard Methods.

3 Bowie G.L., M.B. William, Porcella D.B., Campbell C.L., Pagenkopf J.R., Rupp G.L., Johnson K.M., Chan P.W., Gherini S.A and Chamberlin C.E., 1985, Surface Water Quality Modeling. 1985, California, USA.

4 Brown, L.C., Barnwell, T.O.Jr., 1987. The Enhanced Stream Water Quality Models QUAL2E and QUAL2E-UNCAS: Documentation and User Manual. USEPA, Environmental Research Laboratory, Athens, GA, EPA/600/3-87/007.

5 Campolo M., Andreussi P., Soldati A., 2002. Water quality control in the river Arno, technical note. Water Res. 36, 2673–2680.

6 Chapra, S.C., and Canale, R., 2002. Numerical Methods for Engineers, 4th Ed. New York, McGraw-Hill.

7 Chapra, S.C., Pelletier, G.J., Tao, H., 2006. QUAL2K: A Modeling Framework for Simulating River and Stream Water Quality, Slaughterhouse2.04: Documentation and Users Manual. Civil and Environmental Engineering Dept., Tufts University, Medford, MA.

8 Cho, J. H., Sung Ryong Ha , 2010, Parameter optimization of the QUAL2K model for a multiple-reach river using an influence coefficient algorithm, Science of The Total Environment, Volume 408, Issue 8, Pages 1985-1991.

9 Cox, B.A., 2003. A review of currently available in-stream water-quality models and their applicability for simulating dissolved oxygen in lowland rivers. Sci. Total Environ. 314–316, 335–377.

10 Deksissa, T., Meirlaen, J., Ashton, P.J., Vanrolleghem, P.A., 2004. Simplifying dynamic river water quality modelling: a case study of inorganic dynamics in the Crocodile River, (South Africa). Water Air Soil Pollut. 155, 303–320.

11 Drolc, A., Konkan, J.Z.Z., 1996. Water quality modeling of the river Sava, Slovenia. Water Resources 30 (11), 2587–2592.

12 EEC, 1978. Council Directive (78/659/EEC) on the Quality of Fresh Waters Needing Protection or Improvement in order to support fish life,

retrieved 20 April 2005 from: http://europa.eu.int/comm/environment/
13 EMECS, 2001. Water Quality Conservation for Enclosed Water Bodies in Japan, International Center for the Environmental Management of Enclosed Coastal Seas (EMECS) retrieved 20 April 2005 from: http://www.emecs.or.jp/.
14 Fan, Chihhao, Chun-Han Ko, Wei-Shen Wang, 2009, An innovative modeling approach using Qual2K and HEC-RAS integration to assess the impact of tidal effect on River Water quality simulation
15 Ghosh, N.C., Mcbean, E.A., 1998. Water quality modeling of the Kali river, India. Water Air Soil Pollut. 102, 91–103.
16 ICHHTO (Iranian Cultural Heritage, Handicrafts and Tourism Organization), 2008, SHUSHTAR HISTORICAL HYDRAULIC SYSTEM, Tehran, Iran.
17 IPBO (Iranian Plan and Budget Organization),1992. Drinking Water Quality Standard (3-116), Tehran.
18 Kannel, P.R., Lee, S., Kanel, S.R., Lee, Y., Ahn, K.-H., 2007. Application of QUAL2Kw for water quality modeling and dissolved oxygen control in the river Bagmati. Environtal Monitoring Assessment 125, 201–217.
19 Moriasi, D.N., Arnold J.G., Van Liew M.W., Bingner R.L., Harmel, R. D. and Veith, T.L., 2007, Model Evaluation Guidelines for Systematic Quantification of Accuracy in Watershed Simulations Vol. 50(3): 885−900
20 Najafzadeh, M. and Azamathulla, H.M., 2013. Group method of data handling to predict scour depth around bridge piers, Neural Comput & Applic, 23:2107–2112
21 Najafzadeh, M. and Barani, G.A., 2011, Comparison of group method of data handling based genetic programming and back propagation systems to predict scour depth around bridge piers, Scientia Iranica A, 18 (6), 1207–1213
22 Najafzadeh, M., Barani, G.A., Kermani, M.R., 2013, Abutment scour in clear-water and live-bed conditions by GMDH network, Journal of Water Science Technology, 67(5):1121-8
23 Novotny, V., 2002. Water Quality: Diffusion Pollution and Watershed Management. Wiley, Hoboken, NJ. Chang, H., 2005. Spatial and temporal variations of water quality in the Han River and its tributaries, Seoul, Korea, 1993–2002. International Journal of Air and Water Pollution 161, 267–284.
24 Owens, M., Edwards, R.W., Gibbs, J.W., 1964. Some reaeration studies in streams. International Journal of Air and Water Pollution 8, 469–486.
25 Park, S.S., Na, Y., Uchrin, C.G., 2003. An oxygen equivalent model for water quality dynamics in a macrophyte dominated river. Ecological Modeling 168, 1–12.
26 Park, S.S., Lee, Y.S., 1996. A multiconstituent moving segment model for the water quality predictions in steep and shallow streams. Ecological Modeling 89, 121–131.
27 Pelletier, G.J., Chapra, C.S., Tao, H., 2006. QUAL2Kw, A framework for modeling water quality in streams and rivers using a genetic algorithm for calibration. Environmental Model. Software 21, 419–4125.
28 Rasti, M, Nabavi, S.M, Jaafarzadeh N., 2007, Investigation of Fish Farm Wastewater on Gargar River using algae as biologic indicator, 7th IREC, Ahvaz, Iran. (In Persian)
29 Tao, H, 2008. *"Calibration, Sensitivity and Uncertainty Analysis in Surface Water Quality Modelling: Dissertation for doctoral degree"*, Tufts University, MA, USA.
30 Thompson, D.H., 1925. Some observations on the oxygen requirements of fishes in the Illinois River, 111. Natural History Survey Bulletin 15, 423–437.
31 UNESCO, 2009. Shushtar Historical Hydraulic System, retrieved 24 April 2013 from: http://whc.unesco.org/en/list/1315/documents/
32 USEPA, 1985. Rates, constants and kinetics formulations in surface water quality, second ed. EPA 600/3-85-040, U.S. Environmental Protection Agency, Athens, GA, retrieved 20 October 2006 from: http://www.ecy.wa.gov/.
33 Zhang, R., Xin Qian, Huiming Li, Xingcheng Yuan, Rui Ye, 2012, selection of optimal river water quality improvement programs using QUAL2K: A case study of Taihu Lake Basin, China, Science of The Total Environment, Volume 431, Pages 278-285.

Discharge Coefficient in Vertical Intakes with Additional Plates

Vadoud Naderi[1], *Davood Farsadizadeh*[1], *Ali Hossein Zadeh Dalir*[1], *Hadi Arvanaghi*[1]
[1]Department of Water Science Engineering, Agriculture Faculty, Tabriz University, Tabriz, Iran

Abstract

One of the causes of perturbation at vertical intakes is the happening of vortices with an air core. The vortices with an air core occur whenever the submergence of the intake is less than a critical value. Anti-vortex devices and specially plates are used to avoid the negative effects of the air-core vortices. If plates are used, then the geometry of them should be studied experimentally. Accordingly, a precise set of experiments have been carried out using rectangular plates with different dimensions. The results showed that using the vertical plates can increase the critical submergence for the same discharge rates to 51%.

Keywords: Vertical Intake, Anti-Vortex Device, Submergence of Intake, Air-Core Vortices, Discharge Rate

1. Introduction

For various purposes water is taken from the reservoir by the structures called intake. An intake structure controls the flow into conveyance system with the help of the gate. When the submergence of an intake is not sufficient, air enters the intake through the air-core vortex and causes some hydraulic problems such as discharge reduction, loss of efficiency in turbines and water conveyance structures. The common solution for avoiding air entrainment is to provide the water head with greater critical submergence. The lowest vertical distance between the water level and upper level of the intake that is not associated with a vortex with air entrainment, is called critical submergence.

In all engineering projects, designing of the intakes is handled by two principles; minimizing the cost and maximizing the efficiency. Vortex occurrence in an intake structure can increase critical submergence and decrease discharge coefficient that both of them are not optimum hydraulic performances.

Several researchers have studied the relationship between vortex occurrence and intake submergence trying to find a good guidance for those of engineers designing any kinds of submerged intakes. They were mostly interested in air entraining vortices, as they are the source of biggest destroying occurrence in hydraulic machinery. Hecker (1987) shows that air entrainment takes place at vortex types V and VI of in total six stages (Figure 1) [1].

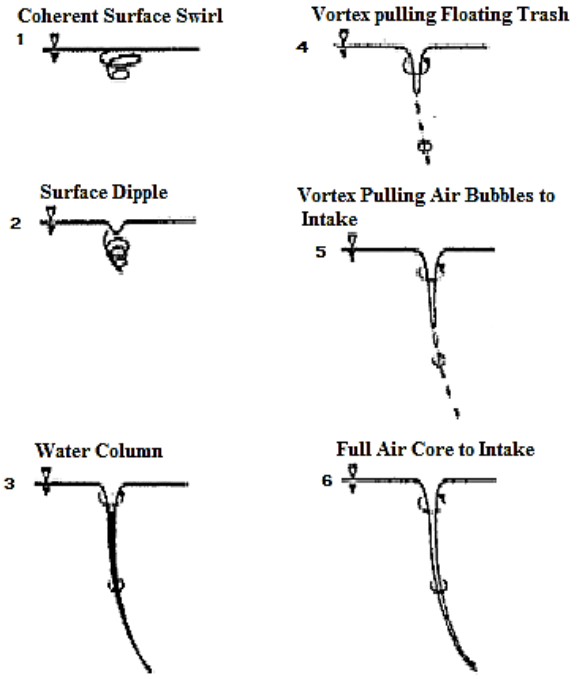


Fig .1 Vortex type classification (Hecker, 1987)

The formation of a vortex may appear at any kinds of intakes and is independent of its utilization, but the consequences and their importance differ considerably.

Rindels and Gulliver (1987) conducted studies on weak surface vortices at bell-mouth vertical intakes with headrace channel by experimental models. Guide vanes were placed to set the approach angle to the headrace, thirteen experiments were conducted with different approach angles and Froude

number ranges between 0.25 and 2.2. The variations of S_C/d with Froude number were provided [2].

Yıldırım and Kocabas (1995) concentrated their studies on critical submergence determination in the intakes with air core vortex formation. To form the flow area theoretically, a point sink was superposed with a uniform channel flow. In their study, the discharge of the point sink was equated to the discharge of the uniform flow to provide continuity in the system. In their experiment, the critical submergence level was set to the radius of the imaginary point sink [3]. They showed that the critical submergence can be predicted by means of the potential flow solution for intakes in an open channel flow, reservoirs and for rectangular intakes [4, 5]. Yildirim et al. investigated the location of the impervious boundaries on the critical submergence of an intake pipe [5]. They defined the blockage effects as the loss of surface area from a CSSS of the flow boundaries on the critical submergence [7]. Yildirim and Tastan investigated the effects of the canal bottom and the dead-end wall on the critical submergence of a single circular intake [8]. Tastan and Yildirim investigated the effects of dimensionless parameters and boundary friction on air entering vortices and the critical submergence of an intake located in still water and no-circulation imposed cross-flow [9]. Eroglu and Bahadirli obtained the critical submergence for a rectangular intake by potential flow solution [10]. Rahimzadeh et al. using experimental works defined the form of the surface flow patterns [11]. Li and Chen carried out an experimental and numerical simulation to investigate the formation and evolution of the free surface vortex [12]. Zhao et al. carried out a numerical simulation of the free surface vortex in a tank with a bottom drain port [13]. Chen et al. derived the velocity expressions of the free surface vortex using RNG k-ε turbulence model [14]. Sohn et al. used the tanks with square cross section to suppress the vortex formation [15]. Sohn et al. showed that a vane-type suppressor is effective in preventing the vortex formation [16]. A circular flat plate with a porous wall was used by Mahyari et al [17]. Sarkardeh et al. have shown that by considering factors which have an effect on vortex strength, it can be concluded that the vortex formation can also be prevented if the distance between the water surface and the intake is increased [18]. Tagvaei et al. using an experimental setup showed that the horizontal plate has a better performance in comparison with other anti-vortex devices to reduce critical submergence [19].

By increasing submergence, discharge is reduced. In the bell-mouth intakes with reducing cross sections, the flow velocity increases and pressure decreases in the centre axial of each intake. In this condition, until the pressure of the centre axial of the intake is not less than the atmospheric pressure, the air core is not formed. So the phenomenon of vortex, in effect of interaction mouth shape of intake, intake submergence and fluid properties such as viscosity and surface tension is formed. Hitherto, there are not so investigations about the discharge coefficient in tank with the vertical intake. So the aim of the present research is to study the critical submergence and discharge coefficient in a cylindrical tank with a vertical intake. In the following parts, the critical submergence is determined experimentally without any vortex suppressor and then the discharge coefficient is calculated subsequently.

2. Governing Parameters

Important dimensionless terms which should be used for experimental studies to define the discharge coefficient and the critical submergence of a vertical intake are:

$$\frac{S_C}{d}: \qquad \text{Relative Submergence (1)}$$

$$C_D = \frac{4Q}{\pi d^2 \sqrt{2g\frac{S_C}{d}}}: \qquad \text{Discharge Coefficient (2)}$$

$$Fr = \frac{4Q}{\pi d^2 \sqrt{gd^5}}: \qquad \text{Froude number (3)}$$

$$\mathrm{Re} = \frac{Q}{\upsilon d}: \qquad \text{Reynolds number (4)}$$

$$We = \frac{\rho v^2 d}{\sigma}: \qquad \text{Weber number (5)}$$

Where S_C is the critical submergence, d is the pipe intake diameter, Q is the discharge, g is the gravitational acceleration, υ is the kinematic

viscosity, ρ is the density,σ is the surface tension and v is the flow velocity in the pipe.

According to the recommended Weber number and Reynolds number ranges that is mentioned in table 1, the effects of surface tension and viscosity could be neglected.

Table1 The ranges of the Weber and Reynolds numbers for neglecting the effect of the surface tension and the viscosity

Researcher	We	Re
Daggett & Keulegan	$V^2\rho d/\sigma \geq 120$	$Q/(vD) \geq 3\times10^3$
Anwar et al.	$V^2\rho d/\sigma \geq 120$	$Q/(vS) \geq 10^4$
Jain et al.	$V^2\rho d/\sigma \geq 120$	$(gd^3)^{0.5}/v \geq 5\times10^4$

2. Materials and Methods

In this research, four different mouth shapes of vertical intake for 24 discharge rates in a cylindrical tank were tested and the corresponding critical submergences were recorded subsequently. The experiments were conducted at the hydraulic laboratory at Tabriz University in Iran. The experiments were carried out in a tank made of 2 parts. First part is a cube 1.0 meter length and 1.0 meter height and the second part is a semi-cylindrical tank, 1.0 meter in diameter and 1.0 meter in height.

Figure 2 shows the schematic diagram of the tank. The circulated water was pumped from a large sump and a triangular weir was used to measure the actual discharge of the vertical intake (at the end of experimental model). The flow enters the first part of the tank horizontally and uniformly through a sand screen diffuser. The sand screen was set in the tank to make the flow further smooth using a 0.1 meter thick rock crib, which consists of rocks coarser than 0.01 meter sieve.

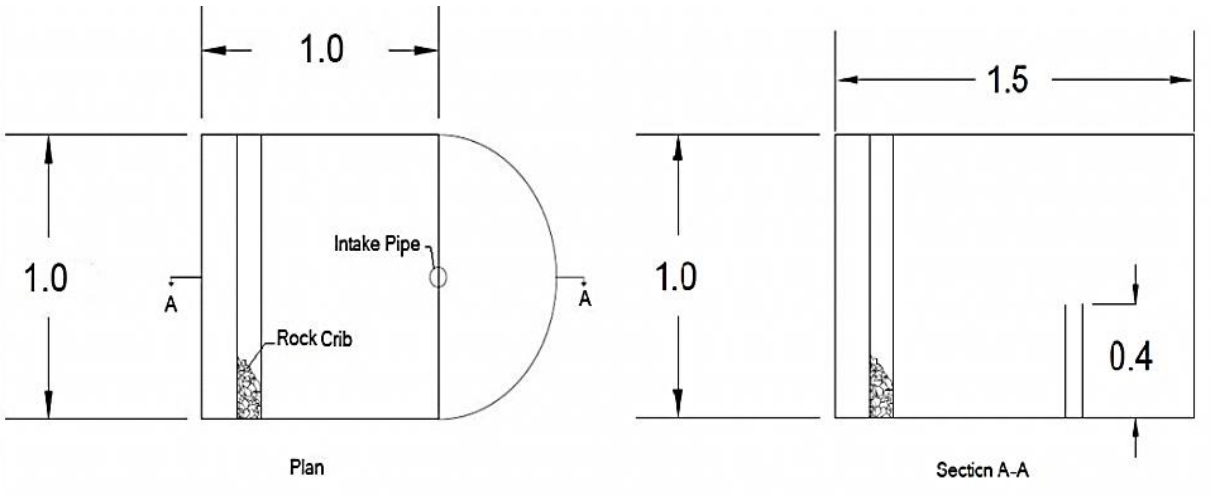


Fig. 2 Schematic diagram of the tank used in the present work

The flow discharges through a vertical pipe intake, 0.4 meter in height and 0.0704 meter in diameter at the centre of the second part of the tank. Figure 3 shows the experimental setup.

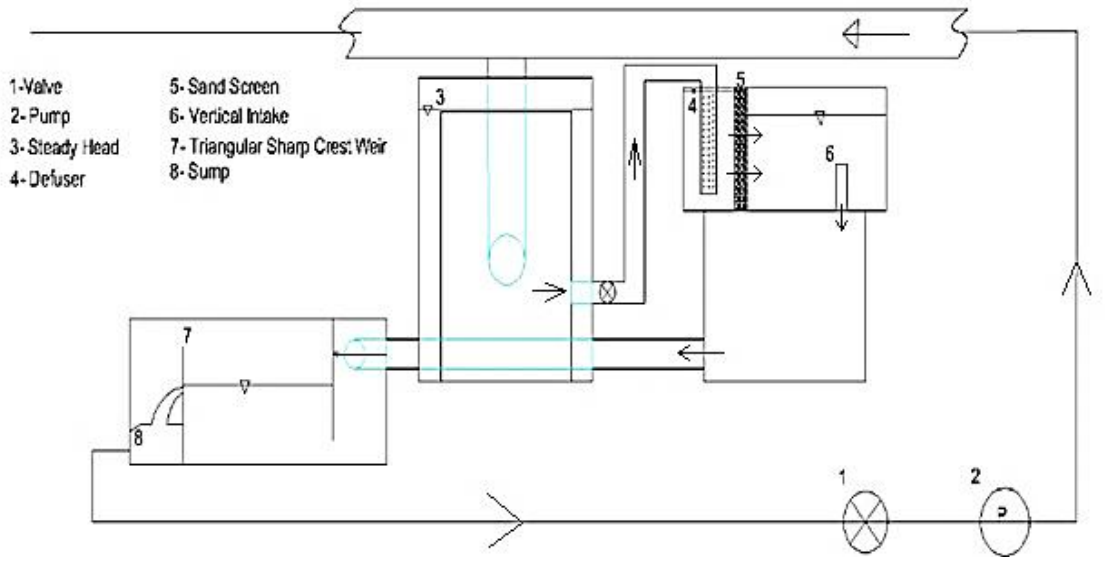


Fig. 3 Schematic diagram of the experimental setup

Two ultrasonic point gage level meters were used to measure the depth of the flow on the upper level of the intake mouth and behind of the triangular weir. The dimensions of the plates used in the present work are given in Table 2.

Table2 Variables used in present work

Dimensions of anti-vortex plates	Discharge rates (Lit/s)
2.5d×d, 2d×d, 1.5d×d, 2.5d×d/2, 2d×d/2, 1.5d×d/2, 2.5d×d/4, 2d×d/4, 1.5d×d/4	2 to 9.5 (10 different rates)

The test variables were the degree between the vertical nets and the diameter of the net orifice. The degree between the vertical plates was 90 and the diameter of the net orifice was 0.11d. Figure 4 shows the schematic diagram of three different types of vertical plates and Figure 5 shows the vertical intake used in the present work.

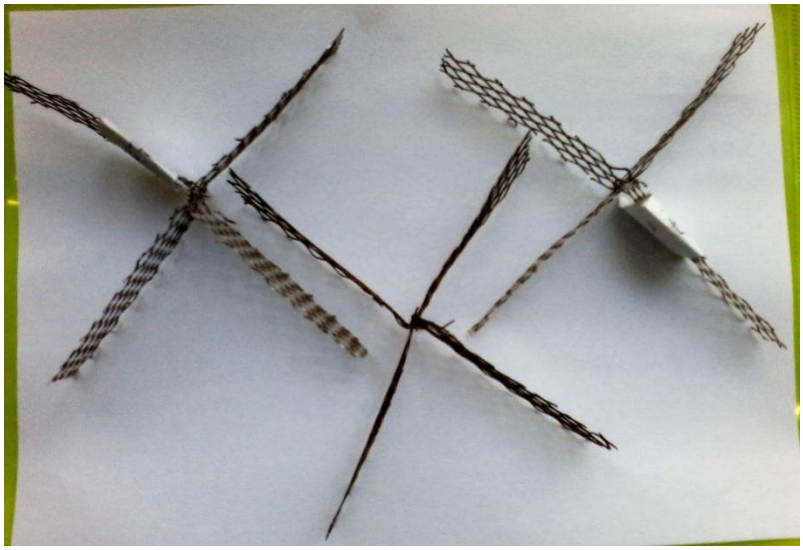


Fig. 4 Schematic model of 4 different types of vertical nets

Each test included feeding the test tank using the pump. With 15 minutes delay, the experiment was started and liquid was drained from the test tank and the flow rate and the reservoir submergence was controlled by a gate valve which was connected to the lowest level of the vertical intake. The free surface of the liquid in the tank was recorded by an ultrasonic point gage level meter. After the air entered the vertical intake, the submergence in the tank was recorded and drained flow was measured by triangular weir and then the experiment was finished.

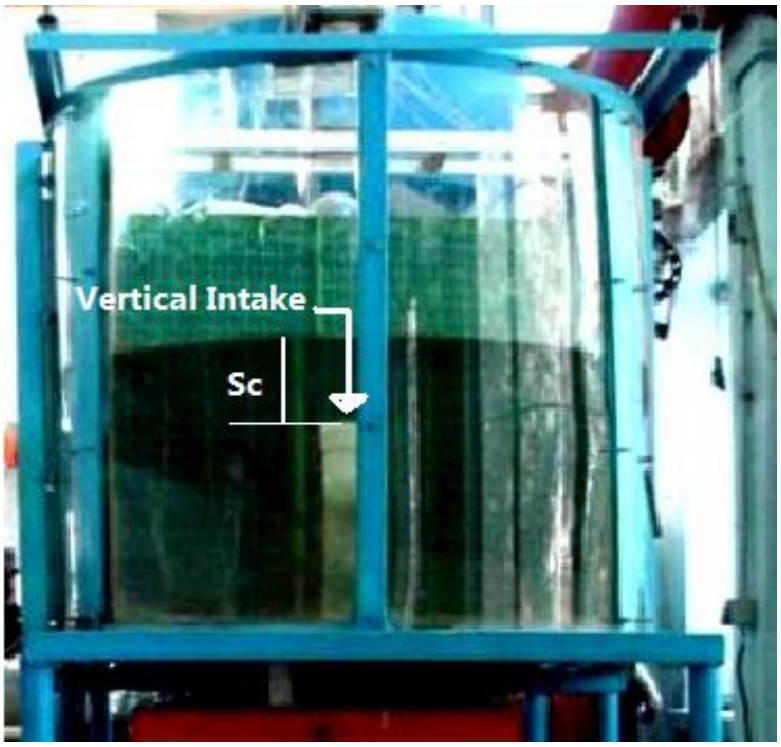


Fig. 1 The vertical intake used in the present work

3. Results and discussion

In the experimental model, the geometry was fixed and the Reynolds and Weber numbers were high enough to neglect. For a comparison of using the vertical plates on a vertical intake data with a reference, the first experiments were carried out on a simple vertical intake named intake number 1. The intake number 1 results are shown in figure 6.

By experimental findings, the critical submergence for a simple vertical intake is formulated as:

$$\frac{S_C}{d} = 3Fr^{0.248} \qquad (6)$$

Where the Froude number is limited from 0.68 to 2.86 and the R^2 from the equation 7 is 0.95.

Four different types of plates were installed on the simple vertical intake and the relevant results are shown in figures 7 to 9.

As can be seen in figures 7 to 9, the changes of the submergence ratio against the Froude number, is uptrend and with increase in submergence ratio, the discharge coefficient increases too as it is shown in figure 10.

As it is shown in figure 10, in the constant discharge coefficient, using the anti-vortex plates, the critical submergence reduces and for the same critical submergence with a simple vertical intake, the discharge coefficient increases.

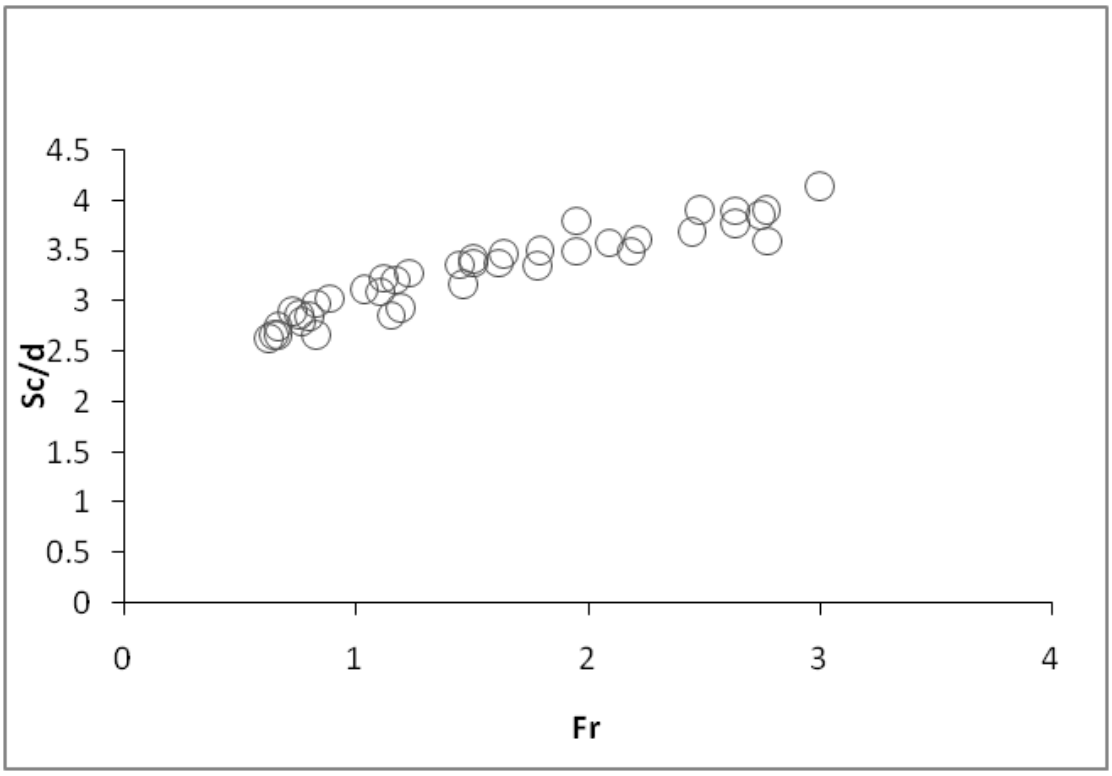


Fig. 2 The experimental results of the critical submergence at various Froude numbers (Intake No.1)

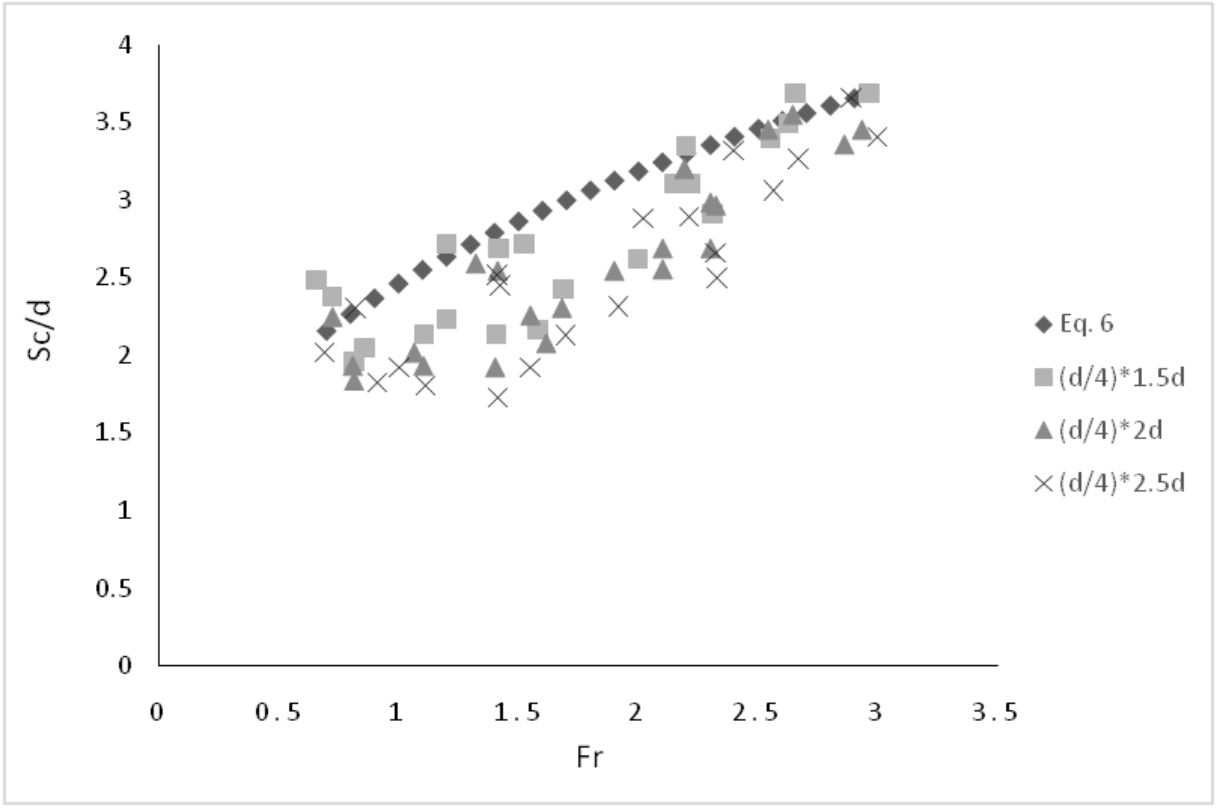


Fig. 7 The experimental results of the critical submergence at various Froude numbers.
(Plates with height of d/4)

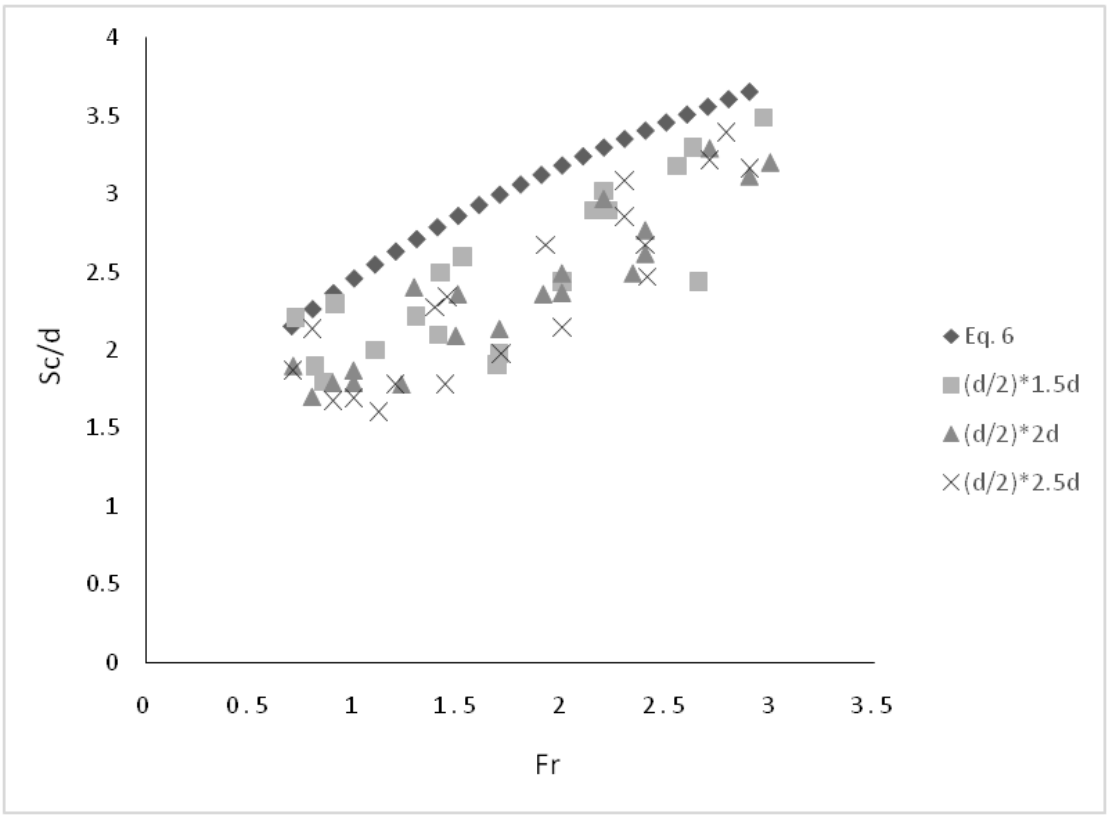


Fig. 8 The experimental results of the critical submergence at various Froude numbers. (Plates with height of d/2)

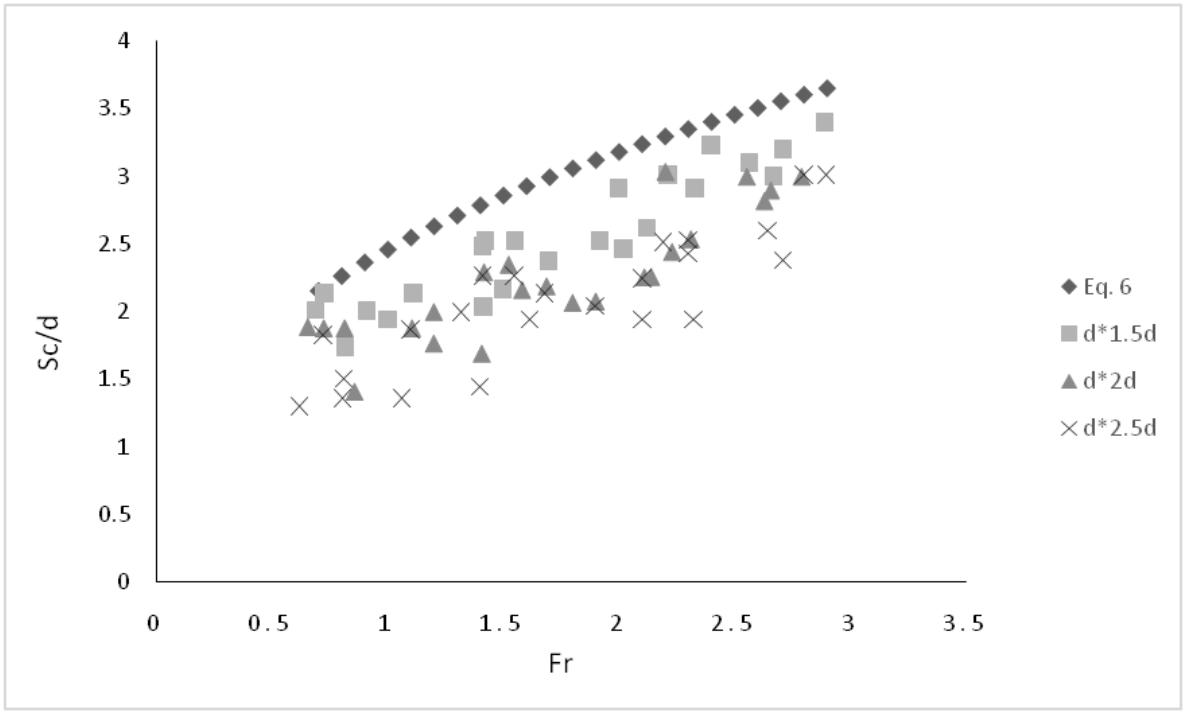


Fig. 9 The experimental results of the critical submergence at various Froude numbers. (Plates with height of d)

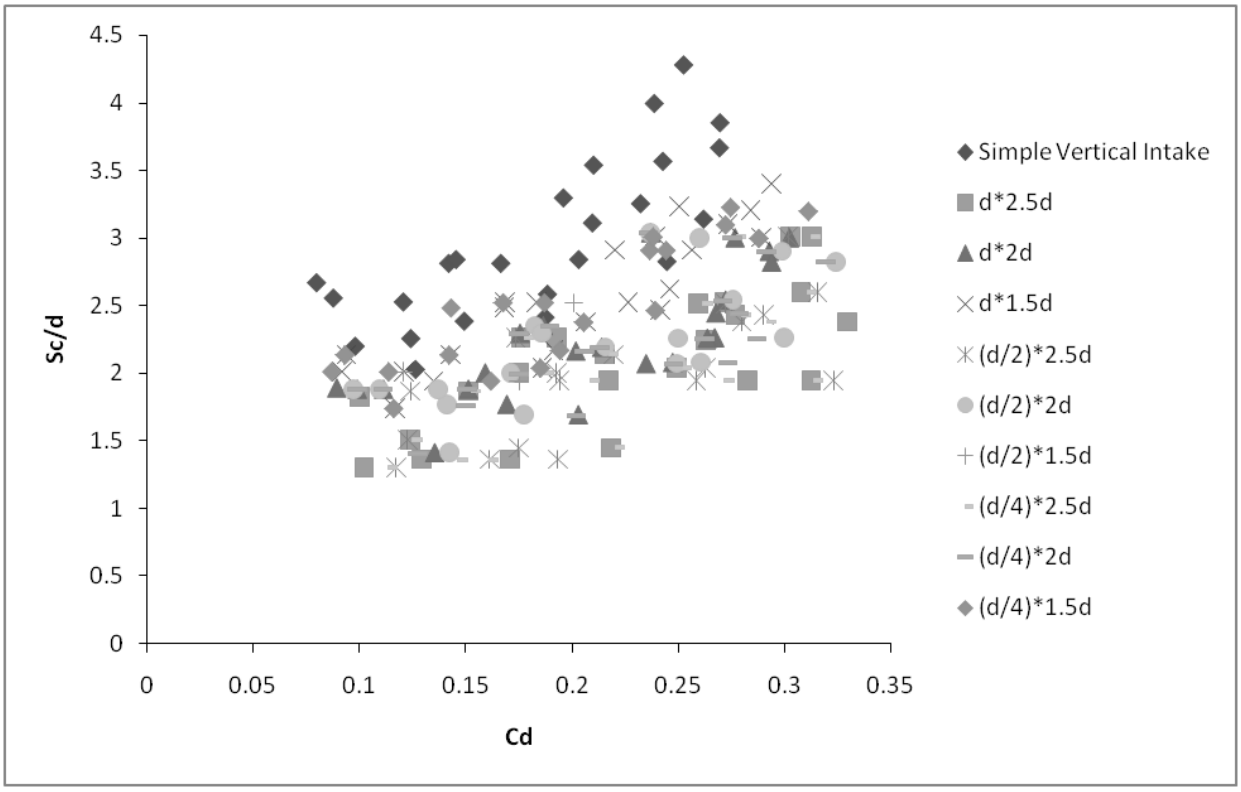


Fig. 3 Variation of discharge coefficient against the critical submergence ratio

Increasing the dimensions of the vertical meshed plates, the critical submergence rate decreases. The existence of the vertical plates on the simple shape of the intake makes the flow with lower critical submergence to reach the higher discharge coefficient. According to the results, it can be mentioned that with increasing discharge of the intake, the effect of vertical nets to reduce the critical submergence in higher discharge rates of intake will be more than the low discharge rates. This fact shows that using vertical meshed plates on the

Table 3 Sc/d values for different anti-vortex plates at the same coefficients of the discharge

	Simple	d*2.5d	d*2d	d*1.5d	d/2*2.5d	d/2*2d	d/2*1.5d	d/4*2.5d	d/4*2d	d/4*1.5d
Cd	Sc/d	Sc/d	Sc/d	Sc/d	Sc/d	Sc/d	Sc/d	Sc/d	Sc/d	Sc/d
0.07	2.029	1.193	1.45	1.589	1.077	1.415	1.461	0.99	1.401	1.651
0.09	2.243	1.347	1.604	1.781	1.234	1.57	1.651	1.158	1.556	1.832
0.11	2.431	1.484	1.739	1.95	1.375	1.706	1.82	1.313	1.691	1.99
0.13	2.599	1.609	1.86	2.103	1.504	1.828	1.974	1.457	1.813	2.133
0.15	2.752	1.724	1.97	2.244	1.625	1.94	2.116	1.593	1.924	2.263
0.17	2.893	1.831	2.071	2.375	1.739	2.043	2.249	1.723	2.027	2.383
0.19	3.025	1.932	2.166	2.498	1.847	2.139	2.374	1.847	2.123	2.495
0.21	3.148	2.028	2.255	2.614	1.949	2.23	2.492	1.966	2.213	2.601
0.23	3.265	2.119	2.339	2.724	2.047	2.316	2.605	2.081	2.298	2.701
0.25	3.375	2.206	2.419	2.828	2.141	2.397	2.713	2.192	2.38	2.796
0.27	3.481	2.289	2.495	2.929	2.232	2.474	2.816	2.3	2.457	2.886
0.29	3.582	2.37	2.567	3.025	2.32	2.549	2.915	2.405	2.531	2.973
0.31	3.679	2.447	2.637	3.118	2.405	2.62	3.012	2.508	2.602	3.056
0.33	3.772	2.522	2.704	3.207	2.488	2.689	3.104	2.608	2.671	3.136

intake mouth, effectively prevents the vortex forming and can cross flow with high efficiency. The values of ratio of the critical submergence using different dimensions of anti-vortex plates at the same discharge coefficients are given at Table 3. As can be seen from Table 3, the minimum values of the ratio of critical submergence happens when using d/4*2.5d for C_d<0.19 and d/2*2.5d for C_d>0.19.

Equation 7 is used to calculate the performance of the anti-vortex plates with respect to the simple shape of the vertical intake.

$$\text{Performance (\%)} = \frac{\frac{S_{C1}}{d} - \frac{S_{Cn}}{d}}{\frac{S_{C1}}{d}} \times 100 \qquad (7)$$

Where S_{c1}/d is the ratio of the critical submergence of the simple vertical intake at a given discharge coefficient and S_{cn}/d is the ratio of the critical submergence of the anti-vortex plates on the simple vertical intake at the same discharge coefficient. The best performance of the anti-vortex plates is shown in figure 11.

As can be seen from the Figure 11, the best performance of the anti-vortex plates happened when the d/4*2.5d anti-vortex plates were used and is 51%.

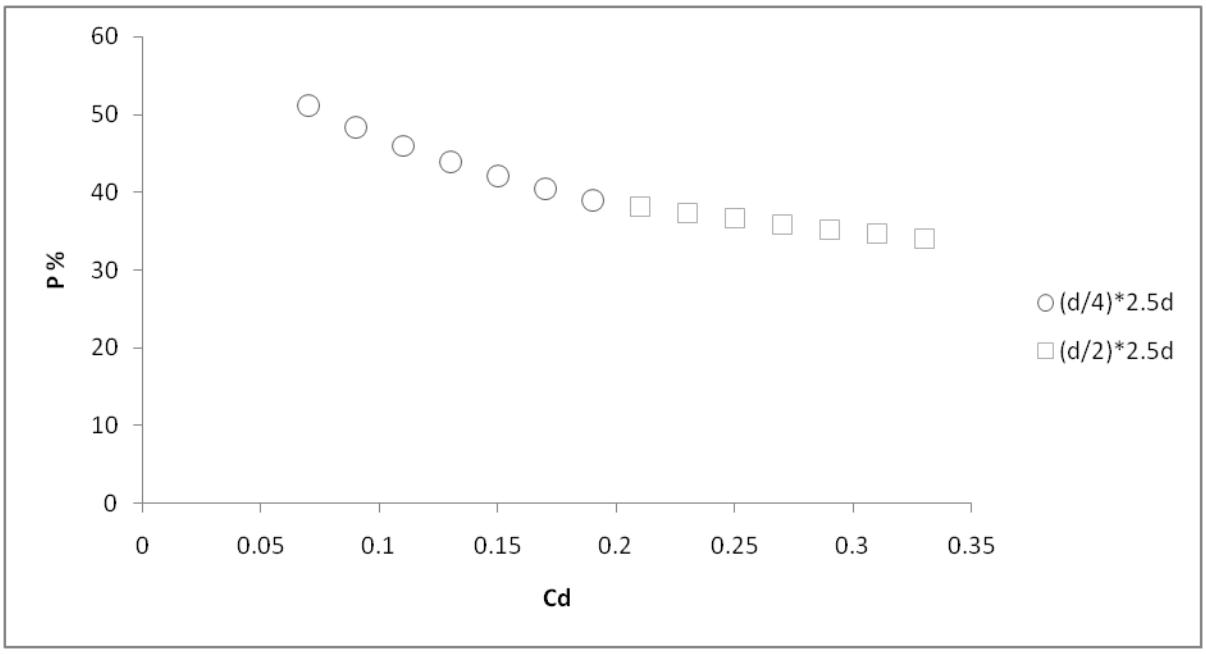


Fig. 3 The best performance of the anti-vortex plates used in present work

4. Conclusion

The vertical intake is one of the drain ports and is used in the present work. The main problem with all intakes is the development of strong vortices in their mouth. In this study, the critical submergence of the vertical intake was investigated in a reservoir tank. Developed equation can be used to predict the critical submergence ratio for a simple vertical intake while knowing hydraulic conditions. The results showed that using vertical meshed plates on the intake, the critical submergence occurs in a higher discharge rate and also the maximum discharge coefficient with a bigger dimension of the vertical meshed plates on the intake mouth is created. Analyzing the results showed that extending the length of the vertical plates is more effective than height extending to reduce the critical submergence and increase the discharge coefficient. It should be mentioned that the proposed conclusion is made with the present experimental setup and many more experimental models is needed in order to achieve a generalized sequel.

References

1 Hecker GE (1987). Fundamentals of vortex intake flow. Swirling flow problems at intakes. IHAR Hydraulic structures design manual 1, J. Knauss Ed.

Balkema, Rotterdam, The Netherlands, pp.13-38.
2 Rindels AJ and Gulliver JS (1983). An experimental study of critical submergence to avoid free-surface vortices at vertical intakes. Saint Anthony Fall Hydraulic Laboratory. Project Report No. 224.
3 Yildirim N and Kocabas F (1995). Critical submergence for intakes in open channel flow. Journal of Hydraulic Engineering, ASCE, 121(12): 900-905.
4 Yildirim, N. and Kocabas, F., Prediction of critical submergence for an intake pipe [J]. J. Hyd. Res., IHAR, 2002, 121(12): 900-905
5 Yildirim, N., Critical submergence for rectangular intake [J]. J. Engrg. Mech., ACSE, 2004, 130(10): 1195-1210
6 Yildirim, N., Kocabas, F. and Gulcan, S.C. Flow boundary effects on critical submergence of intake pipe [J]. J. Hyd. Engrg., ASCE, 2000, 126(4): 288-297.
7 Yildirim, N., Kocabas, F. and Gulcan, S.C. Errata for flow boundary effects on critical submergence of intake pipe [J]. J. Hyd. Engrg., ASCE, 2007, 133(4): 463-472.
8 Yildirim, N. and Tastan, K. Comparison of Flow-Boundary Effects on Critical Submergence of an Intake [J]. Journal of Teknik Dergi, Turkey, 2009, 20(3): 4779-4792.
9 Tastan, K. and Yildirim, N. Effect of dimensionless parameters on air-entraining vortices. [J]. J. Hyd. Res., 2010, 48(1): 57-64.
10 Eroglu, N. and Bahadirli, T., Prediction of critical submergence for a rectangular [J]. J. Energy. Engrg, ASCE, 2007, 133(2): 91-103.
11 Rahimzadeh, H., Fathi, N. and Asoodeh, M.H., An experimental model of flow surface patterns at vertical downward intake with numerical validation, Int. Conf. on water resources, Hydraulics & Hydrology. Chalkida, Greece, May 11-13, 2006, pp:111-118
12 Li, H. and Chen, H. Experimental and numerical investigation of free surface vortex [J]. Journal of Hydrodynamics, 2008, 20(4): 481-491
13 Zhao, Y. et al. Numerical analysis of structure and evolution of free water vortex [J]. Journal of Xi'an Jiaotong University, 2003, 33(3): 85-88.
14 Chen, Y., Wu, C. and Ye, M., hydraulic characteristics of vertical vortex at hydraulic intakes [J]. Journal of Hydrodynamics, 2007, 19(2): 143-149.
15 Sohn C. H., Ju N. G. and Gowda B. H. L., PIV study of vortexing during draining from square tanks [J]. Journal of mechanical science and technology, 2010, 24(4): 951-960.
16 Sohn C. H., Ju N. G. and Gowda B. H. L. Draining from cylindrical tanks with vane-type suppressors, a PIV study [J]. Journal of Visualization, 2009, 12(4): 347-360.
17 Mahyari M. N., Karimi H., Naseh H. and Mirshams M. Numerical and experimental investigation of vortex breaker effectiveness on improvement in launch vehicle ballistic parameters [J]. Journal of Mechanical Science and Technology, 2010, 24(10): 1997-2006.
18 Sarkardeh, H., Zarrati, A.R., Jabbari, E. and Roshan, R., Discussion of prediction of intake vortex risk by Nearest Neighbor Modeling [J]. Journal of Hydraulic Engineering, 2012, 137(6): 701-705.
19 Tagvaei, S.M., Roshan, R., Safavi, Kh. And Sarkardeh, H., Anti-vortex structures at hydropower dams [J]. International Journal of the Physical Science, 2012, 7(28): 5069-5077.
20 Daggett LL and Keulegan GH (1974). Similitude conditions in free-surface vortex formation. Journal of Hydraulic Engineering, ASCE, 100(11):1565-1580.
21 Anwar HO, Weller JA and Amphlett MB (1978). Similarity of free-vortex at horizontal intake. Journal of Hydraulic Research, 16(2):95-105.
22 Jain AK, Ranga Raju KG and Garde RJ (1978). Vortex formation at vertical pipe intakes. Journal of Hydraulic Engineering, ASCE, 104(10):1429-1445.
Odgaard AJ (1986). Free-surface air core vortex. Journal of Hydraulic Engineering, ASCE, 112(7): 610-620

Evaluation of Hydraulic Sensitivity Indicators for Baffle Modules (Case Study: Varamin Irrigation and Drainage Network)

Mina Sadat Seyedjavad[1]*,Mahmoud Mashaal*[1]*,Aliasghar Montazar*[1]
[1]Engineering Faculty, Collage of Abouraihan, University of Tehran,Tehran,Iran

Abstract

Measuring sensitivity of hydraulic structures is considered as an approach for evaluation of water projects performance, due to lower distribution efficiency in Irrigation and Drainage project schemes. Sensitivity analysis approach for irrigation structures is one of flow analysis methods which are developed in recent years in order to measure the behavior of flow in hydraulic structures in an irrigation network. This study examines the sensitivity of offtake structures in Varamin irrigation and drainage network project, which is one of the modern networks in Iran. The sensitivity measurement was carried out by the use of collected data from field in years of 2010, 2011 and 2012, and compared them with the water requirement for crop pattern calculated by CROPWAT model. Flow channel simulation was conducted in the project to identify the most sensitive offtake structures, due to inappropriate allocation of water particularly in downstream of network. Simulation and evaluation were carried out using SOBEK hydrodynamic model, and relationships introduced for sensitivity measures for offtake structures. Investigations and sensitive analysis on hydraulics structures in Varamin Irrigation network showed that Baffle modules have significant sensitivity. According to reviewed equations, sensitivity of Baffle modules is related to upstream depth, and opening of NEYRPIC module gates; which occurred more in terminal structures. The best way to have an optimal operation in this network is supply of required water depth in downstream of each canal. In these circumstances, the water depth in all offtakes is provided, and does not make any changes in the opening modules also.

Keywords: Sensitivity Analysis, Hydrodynamic Modeling, Turnout, Operation, Flow simulation.

1. Introduction

Measuring the sensitivity of hydraulic structures is considered as an approach for evaluation of operation of water projects performance, due to lower distribution efficiency in Irrigation and Drainage project schemes. Operation of irrigation systems, is the result of a decision making process; where the three elements of physical condition of the structures, control capacity, and hydraulic performance of the system play a key role.

Efficiency of water distribution of irrigation networks is low in some cases. Despite the modernization of irrigation and drainage networks in Iran, the overall irrigation efficiency is low due to poor network performance, resulting in very high losses of water in agriculture sector. Due to the variety of hydraulic structures and operation methods, it is manually difficult to control the behavior of various structures in an irrigation network. Since proper use and appropriate operation of these structures has made network management possible, water allocation on time and reduced losses, it seems that the identified deficiencies and structural problems in the selection, design, construction, installation and operation of networks will greatly help to prevent water loss and increase efficiency.

Flow through irrigation canals can be studied by steady or unsteady state flow relationships. The steady state flow relation is often used in the design of irrigation systems, and is realized by professional designers as well as custodian operators. Whoever, to run Irrigation schedules and operation tasks will cause unsteady flow in irrigation network schemes;

which may not be analyzed by steady states flows. Unsteady flow relations, despite particular complexities, have ability to analyze the flow and also have limited widespread use.
Hydrodynamic models are well able to simulate the flow through the network, to evaluate network performance and monitor hydraulic performance of structures. However, limited availability, complexity and the need for high expertise, caused operators of irrigation systems to have little desire to use these models [9].
Sensitivity Analysis Approach as a new intermediate method between these two methods is presented. Sensitivity analysis method for irrigation structures, is one of flow analysis methods that have been developed in recent years in order to assess the flow performance in irrigation networks, and has been used in several irrigation canal networks of the world [7].
Hydraulic Sensitivity Index of an irrigation structure is defined as the relative or absolute changes of OUTPUT hydraulic parameters of the structure to relative or absolute changes of INPUT parameters of hydraulic structures [9]. Accordingly, sensitivity analyses need to be undertaken considering a range of units, from a single structure to an irrigation system, and with regard to both delivery and conveyance.
In this method, evaluation of the system's response to input changes and disturbances, and also flow analysis are discussed by using steady flow relations and the physical structure of the network [11].
Flexibility and sensitivity of irrigation offtakes (outlets) has been considered by Mahbub and Gulhati, and Horst [4 and5]. Mahbub and Gulhati (1951) offered definition of sensitivity for channel outlet; and then they were used to evaluate the channel outlet in several canals in Indian irrigation networks. According to their definition, the sensitivity of outlets were introduced as relative changes in discharge rate, relative to changes in flow depth to normal depth [5].
Horst (1983) studied the sensitivity of irrigation structures, and extended the concept to the level of canals; and defined the flexibility index to study the propagation of changes in input discharge to canals. Horst defined the flexibility index as the ratio of relative Changes in discharge canal feeding into the relative change in current flow [4]. By his theory that was named system response theory, the response of offtakes to changes in discharge was studied by the flexibility index. Horst considered the changes in the flexibility index as a function of structure type, which depends on the type of regulating structures and flow condition, which may have a values of zero, one, and larger or smaller than one.
The sensitivity indicators used by Mahbub and Gulhati (1951), and Horst (1983) only consider the water depth as an input and the delivery as an output. Renault and Hemakumara [8].suggested a broader framework to examine offtake sensitivity which incorporated the conveyance effect (i.e. the influence of the outlet flow variation on the on-going discharge). They applied it to the study of channels in Mahavil & Kirinedoya Network in Sri Lanka and Fordova Network in Pakistan.
Albinson [1] carried out a study on the sensitivity of offtake and Cross-Regulator structures. He presented an analysis on combined effects of sensitivity of the adjacent structures to regulating structure. Instead of normal depth Shanan [10] replaced actual depth of flow in the upstream offtake in the relationship given by Mahbub and Gulhati (1951), and proposed them as sensitive indicators for offtakes.
Renault [9] presented several analytical relationships for canal reaches, and attributed the performance of distribution in system to the reach sensitivity.
Manual Flow control, in an irrigation and drainage network led to unfair distribution of water among the applicants. Hence the progress of science and the development of computer and their great impact on analysis of numerical problems has made it possible to simulate an Irrigation and Drainage network by developed hydrodynamic models for fair distribution of water for applicants in the network ; and optimal operation type to be determined.
This paper aimed to evaluate the sensitivity of the offtake structures at Varamin Irrigation and Drainage Network, which is a modern network in Iran. Due to improper water allocation, especially in downstream of the network, this paper deals with the simulation of flow in network canals and identification of more critical offtake structures. Based on these results, a new schedule of water allocation is presented to water users to manage and optimize utilization.

2. Materials and methods

Irrigation systems are made up of three main components, canal reaches to convey water, cross-regulators to control water depth within the canal and, offtakes to distribute water to dependent canals and downstream users [9]. Operating an irrigation system consists essentially of performing on specific structures (i.e. cross-regulators and offtakes), to ensure targeted change in deliveries, and to react to unexpected perturbations occurring along the system.

Measuring sensitivity of hydraulic structures is considered as an approach for evaluation of a water projects performance, due to lower distribution efficiency in Irrigation and Drainage project schemes. This study aimed to assess the sensitivity of the offtake structures found in Varamin Irrigation and Drainage Network (VIDN).

3. Study area

Varamin Irrigation Network is one of the modern irrigation networks in Iran which is located in Plains of Varamin. The Plains is located in the northern part of the southern slopes of the Alborz, which is located about 40 km southeast of Tehran at 40 ° 51 'E and between 05 ° 35 north latitude and 30 ° 35. Varamin Irrigation Network consists of 760 km of Irrigation and drainage canals; which includes approximately 500 km of third and fourth degree canals; and also includes 2,000 hydraulic structures. A view of Varamin Irrigation and Drainage Network (VIDN) is shown in Fig1.

The incoming flow and subsequently delivery flow to the farmers is varied during the different growing season and years. In other words, the network is experiencing problems with the regulation and distribution of water temporal and spatial. The local farmers' dissatisfaction has been considered as the most important challenge facing network authorities.

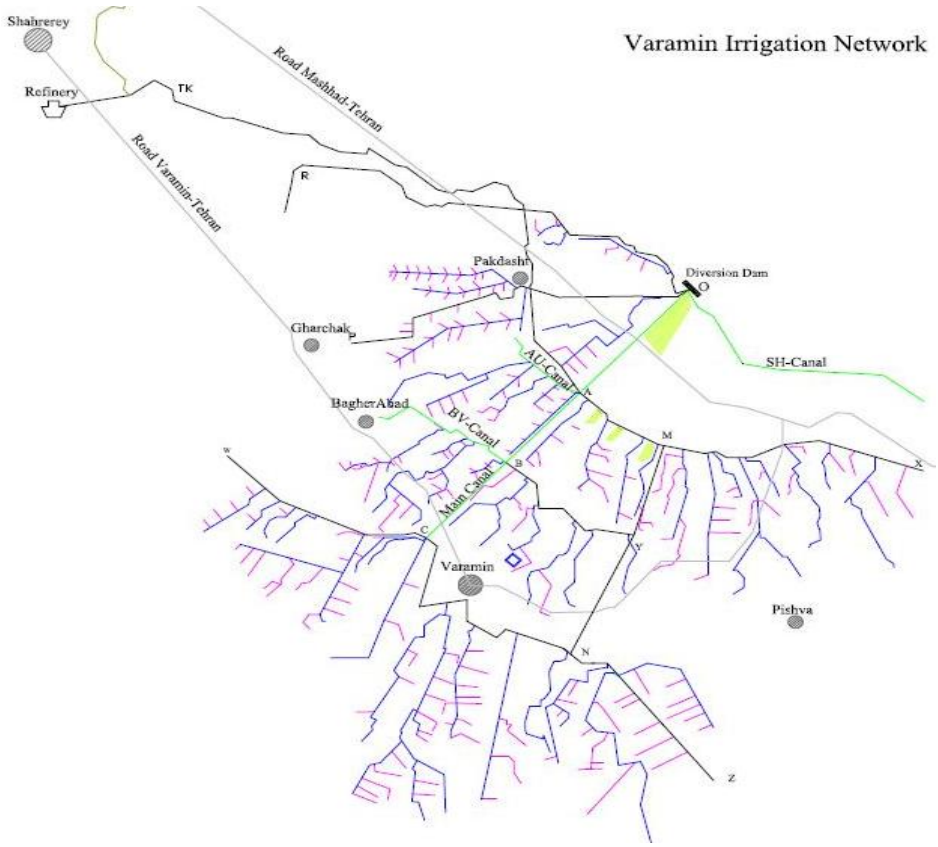


Fig. 1 A view of Varamin Irrigation Network

This paper intends to evaluate the Network performance in three secondary canals located in first, middle and end of Varamin Irrigation and Drainage Network (VIDN). Thus the work was carried out on three secondary canals namely Sharif Abad canal (SH), AU canal and BV canal, which are located within early, middle and end of Varamin Irrigation and Drainage Network respectively. Among the hydraulic structures, the baffle sluice module and Duckbill weir have a significant impact on increasing the water use efficiency. Duckbill weir (weir with fixed long length of crest) is usually used as a cross regulator, to provide proper water level for Baffle-modules; and the Baffle Modules as offtake structures are used as the most appropriate means of flow regulation and distribution at control conditions.

4. Offtake structures

A baffle sluice module (*Neyrpic orifice module*) minimizes water delivery deviation for relatively large upstream flow depth variations. The baffle modules are used as offtake structures in Varamin Irrigation Network. The module is an intake for distribution canals as well as a farm outlet or farm turnout (offtake). It is a metering device and is suitable when water is supplied on a volumetric basis. In order that the module may draw the amount of water for which it has been designed, the water level in the parent canal should be more or less constant (FAO [3]).

The module consists of a *sill*, and a downstream *glacis*, upon which is placed a fixed. metallic plate or baffle. The *sill* and the *fixed plate (*or *baffle)* is enclosed between two vertical, parallel walls, and this arrangement creates an *orifice* which can be closed by a sliding plate or shutter. The module functions only when the sliding plate is raised completely[2].

A distributor usually includes a number of modules, connected together, each one of different width and allowing the passage of a pre-determined discharge, the volume of which is indicated on the corresponding sliding plate. By combining the raising of different sliding plates, the required discharge can be obtained.

A view of Neyrpic modules is shown in Figure 2, and a sample distributor of Neyrpic orifice module in Varamin Network is presented in Figure3.The position, number and type of distributors (modules) which are located in secondary canals of Sharif Abad canal (SH), AU canal and BV canal, in Varamin irrigation network are presented in tables 1 to 3 respectively. The location of the channels and offtake structures are shown in Fig 4.

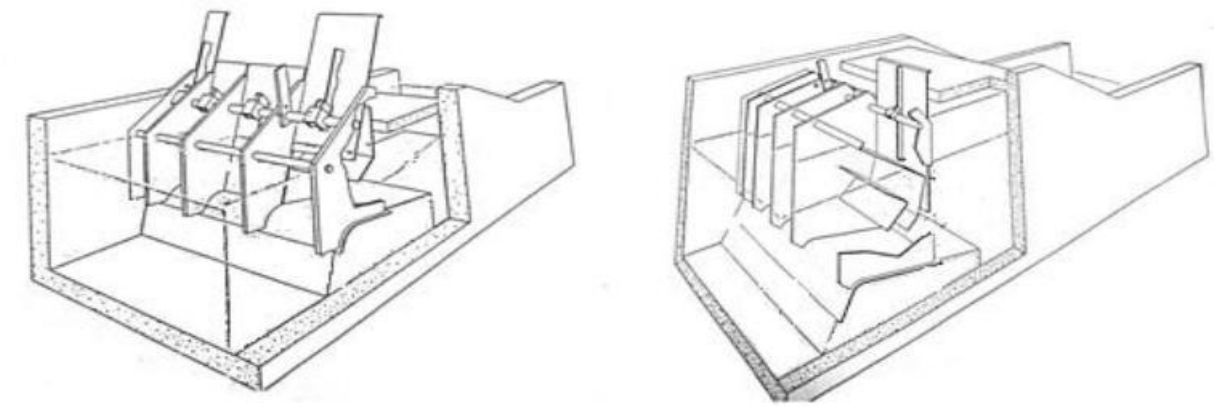


Fig. 2 View of Neyrpic modules

Table 1 Specification of Channel SH

Station (KM)	Offtake	Module	Q (lit/s)
0+800	SH1	XX2	420
1+100	SH2	XX2	180
1+700	SH3	XX2	180
2+900	SH5	XX2	180
4+300	SH7	XX2	180

Table 2 Specification of Channel AU

Station (KM)	Offtake	Module	Q (lit/s)
0+038	U1	XX2	240
1+262	U2	XX2	480
1+613	U3	XX2	300
3+124	U4	XX2	180
4+293	U5	XX2	300

Table 3 Specification of Channel BV

Station (KM)	Offtake	Module	Q (lit/s)
0+040	V1	XX2	420
2+217	V2	C1	1500
3+784	V3	XX2	300
4+678	V4	XX2	360
6+086	V5	XX2	360



Fig. 3 A sample distributor of Neyrpic orifice module in Varamin Network

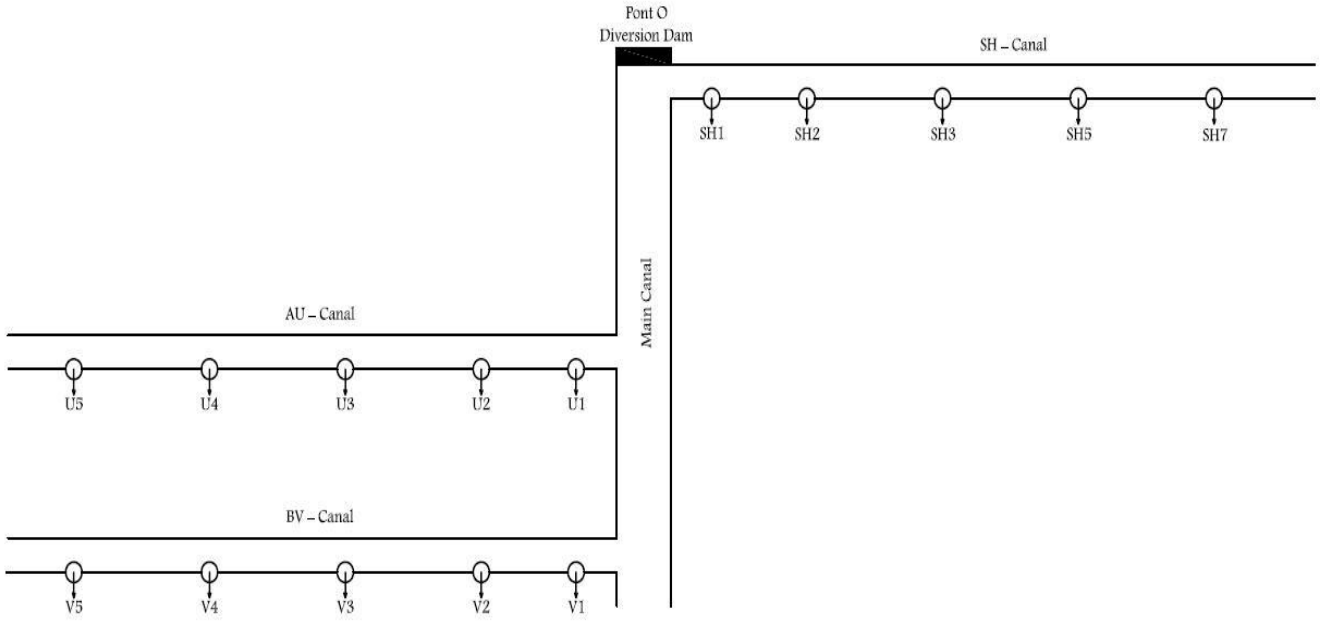


Fig. 4 A view shows the location of the channel and structures

5. Hydraulic structure sensitivity indicators

Hydraulic sensitivity Indicators can be extended in levels of structure, reach, and a set of reaches. An irrigation structure sensitivity indicator can be defined as equation one:

$$S_{IO} = \frac{\partial O}{\partial I} \quad (1)$$

Where, S_{IO}, is indicator of hydraulic sensitivity of output variable to the input variable, ∂O and ∂I are output- and input hydraulic parameters changes respectively.

In fact, hydraulic sensitivity indicator shows if the input hydraulic variable of ΔI is changed, then the output hydraulic variable to what extent will change. Renault [11] has provided the same hydraulic sensitivity Indicators as follows:

$$S_{IOa} = \frac{\partial O/O}{\partial I} \quad (2)$$

$$S_{IOr} = \frac{\partial O/O}{\partial I/I} \quad (3)$$

In the above equations S_{IOa} is absolute sensitivity indicator and SI_{Or} is relative sensitivity indicator.

6. Offtake sensitivity to the absolute change of ongoing flow

Flow through the offtake, in free-flow conditions, is a function of upstream water depth and the gate opening. So that if the gate opening is fixed and does not change the upstream depth of offtake due to flow disturbance while entering to the parent canal, flow rate passing through the offtake will change, and hydraulic performance of the network is affected. Using equation (4) can be considered the effect of variations of upstream depth on the offtake discharge.

$$S_{hq} = \frac{dq_0/q_0}{dH_{US\,(0)}} \quad (4)$$

In the above equation q is initial discharge, dq, is changes in upstream discharge, dH_{us} is changes in upstream water depth.

7. Offtake sensitivity to variation in opening of gate

the modules due to combination types of these structures. There is an option in the model as a Opening regulation of an offtake gate by hand is always with error and, this error has an impact on the discharge of intended offtake and also on the discharge of other offtakes. offtake sensitivity indicator with respect to the gate opening, S_{wq} , is presented according to equation (5).

$$S_{Wq} = \frac{dq_0/q_0}{dW_0} \quad (5)$$

where, q is offtake discharge and W is opening of the gate. The structure has, low sensitivity if the indicator is less than 1, moderate sensitivity if it is between 1 to 2 and, high sensitivity if it is greater than 2.

8. Sobek hydrodynamic model

The Sobek Hydrodynamic model was used to simulate the hydraulic performance in irrigation network in this study. This model is a powerful tool with seven different modules for the simulation of one-dimensional and two-dimensional flow, which the combination of these modules could also be used for simulation purposes. This program is an open-channel dynamic numerical modeling system, which is able to solve the equations that expresses unsteady water flow, sediment transport, water quality, morphology and salt intrusion. SOBEK simulates the flow using the St. Venant continuity equations and calculates besides discharge values, water levels and flow velocities. It uses the implicit finite difference scheme [12]. SOBEK is a powerful tool to simulate and solve problems in river management, flood protection, design of canals, irrigation systems, water quality, navigation and dredging. The SOBEK model can be used for all hydraulic adaptation measures, such as dike heightening and retention areas. As boundary conditions, the results from the coupled atmospheric - hydrologic model runs are used.

Analysis the network performance

The network has been visited, to collect the correct data required to simulate the structures in the model. A view of the structure is shown in Figure 3.The weir symbol is not used to simulate

Compound Structure, which can simulate these structures accurately. This option

requires the initial data including bed grade line, canal side slope and elevation of bed in structure location.

Given that Varamin irrigation system is not providing enough water to water users in downstream, in order to analyze the network performance, the two types of flow were simulated. To investigate the initial designing and existing conditions, simulations have been carried out for the available flow in network and, flow requirements for water users, according to water requirements for their cropping patterns.

Simulation of flow in the network was carried out for unsteady-state in steps of 5 minutes; for a period of maximum consumption (May), based on real data collected from operation stage, and data calculated from cropping pattern. For simulation in SOBEK hydrodynamic model and measuring the structure sensitivity in network, the intended scenario is simulated based on 7-day irrigation which is considered in basic network design.

9. Results and discussion

Sensitivity analyses, applied to irrigation systems, focuses primarily on the delivery and control structures (i.e., offtakes, turnouts and check structure); with the aim of appraising the system performance consequential from a perturbation in the input. So far, most of the studies on this subject have dealt with local sensitivity analyses.

Indicator of offtake sensitivity to the absolute change of upstream water depth shows the changes in discharge passing through the structure due to variations in upstream of depth.

In this study, simulations were carried out by both real and calculated data to enable us to compute the sensitivity of delivery to absolute deviation for offtake structures in Varamin irrigation network. The offtake sensitivity of delivery to absolute deviation of water depth resulted by actual and calculated data are shown in Fig 5 and Fig 6 respectively.

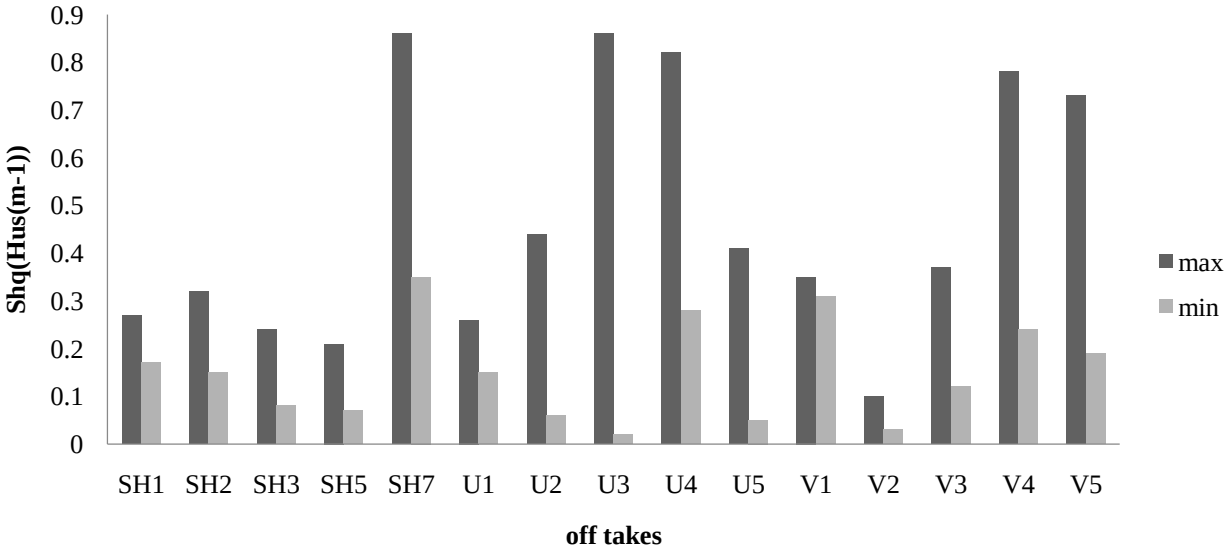


Fig. 5 Offtake sensitivity of delivery to absolute deviation of water depth Index (Real Data)

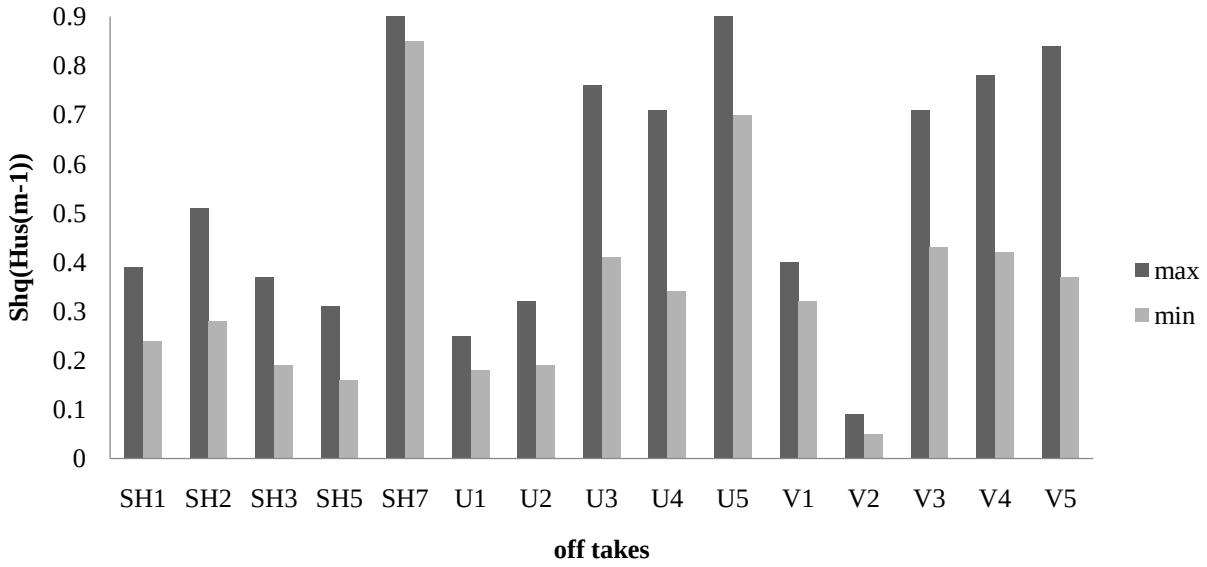


Fig. 6 Offtake sensitivity of delivery to absolute deviation of water depth Index (Calculated Data)

Baffle module as an offtake is designed so that the delivery discharge through structure has not large changes compared to variations of upstream depth of water. It is expected that this structure does not show a significant sensitivity to changes in upstream water depth (S_{hq}).In AU channel, according to diagram 5, offtake U_3 with S_{hq}= 0.20 is less sensitive compared to other structures. All of these values are in the range of low sensitivity. As the U3 offtake is in middle of the AU channel, its sensitivity is low. Because upstream cross regulator can provide the required water depth in right time, so there is not much changes in depth. But on overall results, we can say that the offtake structure U3 is the most sensitive structure in the network (with S_{hq}=0.86 when using real data).In channel BV, offtake structure V2 is the least sensitive to *absolute deviation of* upstream *water depth* (with S_{hq} =0.05) among all structures existing in channel BV. Because in baffle modules, increasing in capacity reduces the sensitivity, and offtake structure V2 which is module distributor of C1 type, among BV canal structures has the highest capacity due to high coverage lands.

According to the results for channel SH, it is observed 0.01 m increase in upstream depth of water causes *delivery* rate rises to 1.4 percent in offtake structure SH7; which indicates that the structure is located in middle range of sensitivity. This value is the highest sensitivity value among the sensitivity values obtained from the SH channel structures.

The high sensitivity of baffle module SH7 can be attributed to low water depth in the channel, which cause weir flow occur through the module. Because the depth of water in canal is not high enough to allow the blades of module to control the flow and to reduce the impact on the increasing discharge; as a result, the structure acts as a weir. This issue can be seen in Fig 7.

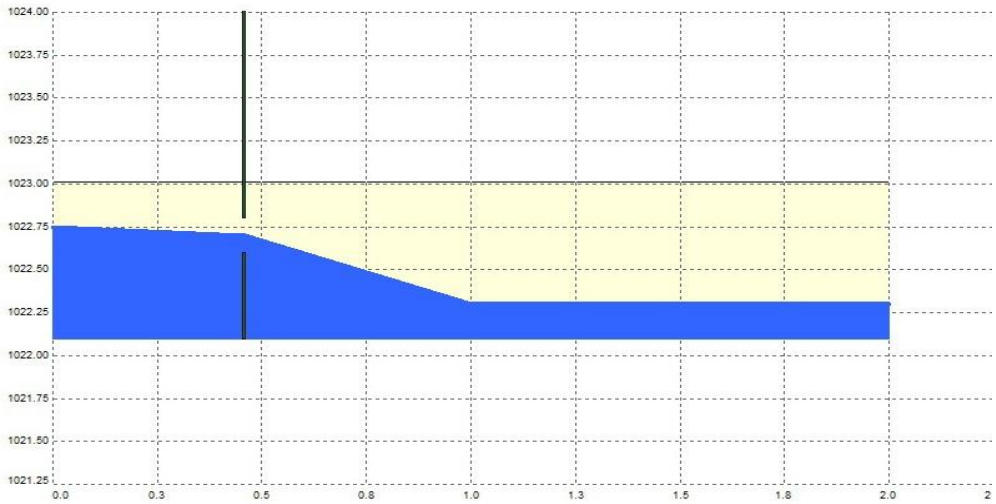


Fig. 7 Structure performance SH7 baffle module in Sobek model
(The baffle is not working due to the flow low depth)

The offtake sensitivity to variation in opening of gate resulted by actual and calculated data are presented in Fig 8 and Fig 9 respectively.

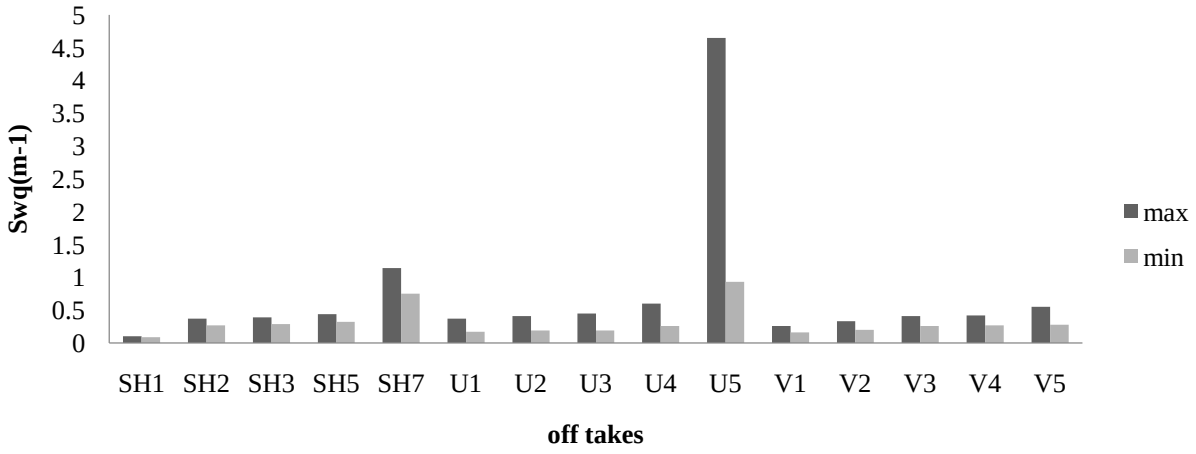


Fig. 8 Offtake sensitivity of delivery to gate opening Index (Real Data)

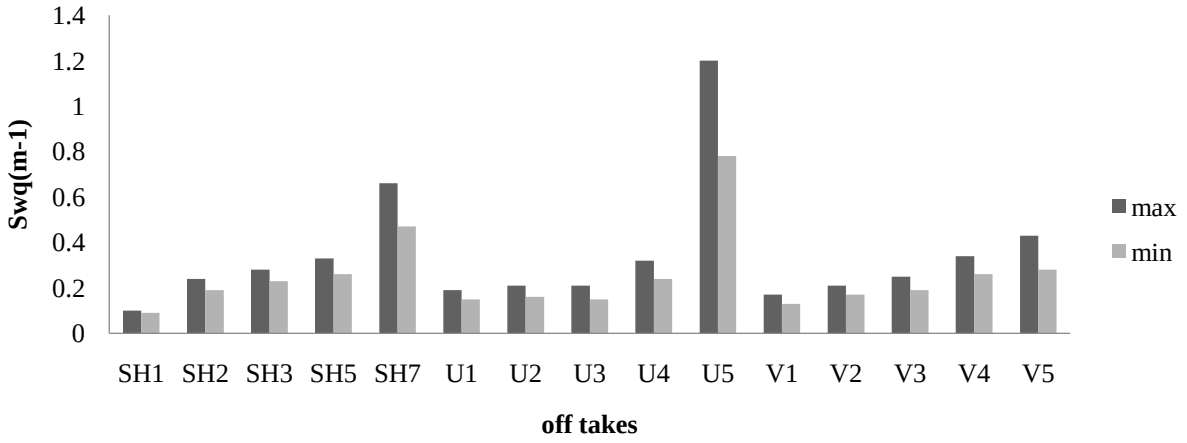


Fig. 9 Offtake sensitivity of delivery to gate opening Index (Calculated Data)

In channel AU, offtake structure U5 shows the most sensitive to variation in opening of gate (with S_{wq}=4.65 when using real data and S_{wq}=1.20 when using calculated data) among all structures existing in channel AU.
This high sensitivity indicates that the gate opening of the structure, is lowered from the upstream water level, and the results will be dramatic changes in *delivery* flow rate. Offtake structure U1 in the channel AU has lowest sensitivity to gate opening; which the values were S_{wq}=0.17 when using real data and S_{wq}=0.15 when using calculated data. The low sensitivity to variation in opening of gate for offtake structure U3 is due to locating it in the beginning of AU channel. Therefore, suitable adjustments are made by division structure in channel AU for offtake structures U1. Therefore variations on water depth only occurs in regulating structure of offtake channel AU and has no effect on offtake structure U1.In channel SH, highest and lowest offtake sensitivity to variation in opening of gate is owned to module structures of SH1and SH7, respectively. Offtake structure SH1 in the channel SH has highest sensitivity to variation in gate opening by values of S_{wq}=1.14 when using real data and S_{wq}=0.66 when using calculated data. According to sensitivity indicators values resulted from calculated data and the range between these values, we can conclude that, If the amount of water delivered to module structures is equal to the amount of water needed for structures based on cropping pattern , then there is no variation in delivery discharge even for the most sensitive structure as well. Module structure SH1 with S_{wq} = 0.09 has less sensitivity to gate opening in resulted by both actual and calculated data; and delivery discharge through the structure has not changed a lot.

Analysis of the results of the channel BV shows structure module V5 is the most sensitive offtake structure with sensitivity indicators values resulted from real and calculated data values of S_{wq} = 0.55 and S_{wq} = 0.43 respectively. According to the results, it should be stated that the highest change in delivery discharge affected by changing in gate opening is related to the calculated data. Module structure V1 with sensitivity values of 0.16 (actual data) and 0.13 (calculated data) has shown the least changes in the delivery discharge through the opening of the gate, and low sensitivity to changes in gate opening. Less sensitive to the structure changes in gate opening of Varamin irrigation network is structure module SH1. Low sensitivity of this module structure is due to the fact that it is located at the beginning of main feeder canal in the network. So, in any event, the required delivery discharge is provided. And therefore does not cause large changes in passing discharge, and consequently in the amount of the gate opening.

10. Conclusions

The studies and hydraulic sensitivity analysis on baffle modules within the Varamin irrigation and drainage network showed that these structures have significant sensitivity. According to the equations, sensitivity of baffle modules to upstream depth, occurred in structures which located further downstream of a canal reach. In this research, , module-SH7 in the SH channel, module-U3 in AU channel, and module-V5 in BV Channel showed highest sensitivity to upstream depth, according to both real and calculated data, which are located in most downstream, middle and most downstream of their reach respectively.

High sensitivity to change in upstream depth means that a modules which is located in the end and/or in the middle parts of a canal act as an weir because in these conditions water depth in the channel upstream of structure is low and discharging flow through the structure is below the baffle blade.
In other words, the depth is not completely enough to enable baffle-blades to control the passing flow, and to reduce the influence of water depth changes in the channel. In general, the studies conducted on offtake sensitivity indicator with respect to the gate opening reveal that the most sensitive structures are located at the end of each channel, and structures located in the beginning of a channel have very little sensitivity to the opening.

According to the results, we can conclude that, gate openings must be set so that the required discharge would be delivered through the entire off takes to be supplied. Furthermore, the opening of each module should be in coincidence with downstream required capacity. Because, in operation

mode, all structures in the network are opened equally. However, there is the possibility of overdose delivery in some offtakes. As a result, the required water in downstream of the network is not provided, and there is too much water loss in upstream also. Based on these results, a new schedule for the delivery of water can be suggested to Varamin irrigation network management.

For optimal operation in network, distribution of water to water users should be based on the required downstream capacity. As a result, structures which are located in further downstream, show more sensitivity; based on both equations of sensitivity to variation in upstream depth and sensitivity to variation in opening .As a result, the best way to provide suitable depth of water in downstream of each channel is by distributing and delivering water based on downstream requirements. In this situation, the required depth of water in all the off takes are provided and does not make any change in the opening of the gate, and no change occurs in the opening of the gate.

References

1 Albinson B (1986) Network Planning Criteria: Hydraulic Aspects, Guideline 5, Annex 1, in: Design and Operation Guidelines for Structured Irrigation networks. Forth Draft, South East Asia Division, World Bank, WA, DC, USA.

2 Beirami MK (2010) Water Conveyance Structure. Publication of Isfahan University of Technology.

3 FAO (1975) Small hydraulic structures models. FAO irrigation and drainage paper 26/2, Food and Agriculture Organization of the United Nations, 29-5-100161-8 Rome, Italy.

4 Ghumman AR, Khan Z and Turral H (2009) Study of feasibility of night-closure of irrigation canals for water saving. Agriculture Water Management 96(2009) 457-464.

5 Horst L (1983) Irrigation Systems Internal Report. Agricultural University Wageningen, The Netherland.

6 Mahbub SI , ND Gulhati (1951) Irrigation Outlets. Atma Ram. Delhi India.

7 Montazar A and Kouchakzadeh S (2005) Application of hydraulic sensitivity indicators in canal assessment. Journal of Irrigation and Drainage 54: 443-454.

8 Renault D, HM Hemahumara (1999) Irrigation Off takes Sensitivity .Journal Irrigation and Drainage .125(3):132-136.

9 Renault D (2000) Aggregated Sensitivity Indicators of Irrigation Systems Hydraulic Behaviour. Agriculture Water Management.43 (2), 151-171.

10 Shanan L (1992) Planning and Management of Irrigation system in Developing Countries. Agricultural Water Management, 22(1+2), the Netherlands, Elsevier.

11 Seyedjavad MS (2013) Evaluating the Operational Approaches of Varamin Irrigation Network Using SOBEK Model. Irrigation and drainage master thesis. Irrigation and drainage department Collage of Abourayhan University of Tehran.

12 WL/Delft Hydraulic (2000) Sobek Manual and Technical Reference The Netherlands.

A New Two Dimensional Model for Pollutant Transport in Ajichai River

Hassan Derakhshan[1], Mehdi Zarei Bistkonj[1]
[1]Faculty of Water Engineering, University of Zabol, Zabol, Iran

Abstract

Accurate prediction of pollution control and environmental protection need a good understanding of pollutant dynamics. Numerical model techniques are important apparatus in this research area. So a 2500 line FORTRAN 95 version code was conducted in which using approximate Riemann solver, couples the shallow water and pollution transport agents in two dimensions by the aid of unstructured meshes. A multidimensional linear reconstruction technique and multidimensional slope limiter were implemented to achieve a second-order spatial accuracy. The courant number ruled as a control parameter for stability conditions and a third order Runge-Kutta method was performed for equation discretizations. For Code verifications another author's case study was examined.
The numerical results show that the model could accurately predict the flow dynamics and pollutant transport in Ajichai River.

Keywords: FORTRAN Program, Courant Number, Pollution, Finite Volume, Ajichai River.

1. Introduction

The damage caused to the quality of water, can be regarded as an important source of pollution making it very important in Environmental Engineering Areas. The pollution concentration and distribution rate of each case helps then to control its water quality standard levels.
The numerical models have a good performance in modeling shallow water equations, besides advection- dispersion equations in pollution propagation cases. This is because of the unstructured nature and boundaries of most of Engineering problems, causing them have no direct analytical solution as a result. Among the available Numerical methods such as Finite difference, Finite element and finite volume method, the last method meets our case better, because it not only has a better accuracy in real cases, but also needs fewer memory and time for solution. Among many researchers who focused on water pollution control and flow equations are: Jawahar p and Kamath H. (2000), Zhou JG et al. (2001), Delis AI. (2003), Komatsu T. et al. (1997), Alcrudo , F. and Benkhaldoun, F.(2001), Benkhaldoun, F. and Quivy L.(2006), Benkhaldoun, F.(2002), Heniche M. (2000), James I.D. (2002), Komatsu T. et. al. (1997), Roe P.L. (1981), Vazquez M.E. (1999). For a comprehensive review of recent developments in finite volume methods for shallow water equations we refer to benkhaldoun's papers. By the aforementioned reasons, finite volume model was our choice as a research target for pollution analysis of a case study, namely Ajichai river in west of Iran (Tabriz city). To do this, in this paper we introduce a FORTRAN code whereby we can couple the flow and pollution equations to simulate finally the pollutant dispersion pattern in Ajichai river. The code was calibrated firstly by Fayssal benkhaldoun et al. model (2007) to see its robustness and finally it was used to the real Ajichai river case. According to complex and variant geometry of the river, an unstructured triangular mesh scheme was introduced to represent the river area. The Riemann solver was the discretization agent of the equations, our code may consider the advection and/or dispersion effects in pollution transmit ion besides the shallow water equations in which the continuity and momentum effects in x and y directions were considered.

2. Theory and governing equations

The procedure considered in the logic of code has been shown in the Figure 1, from which the necessary relations and governing equations are as bellows:

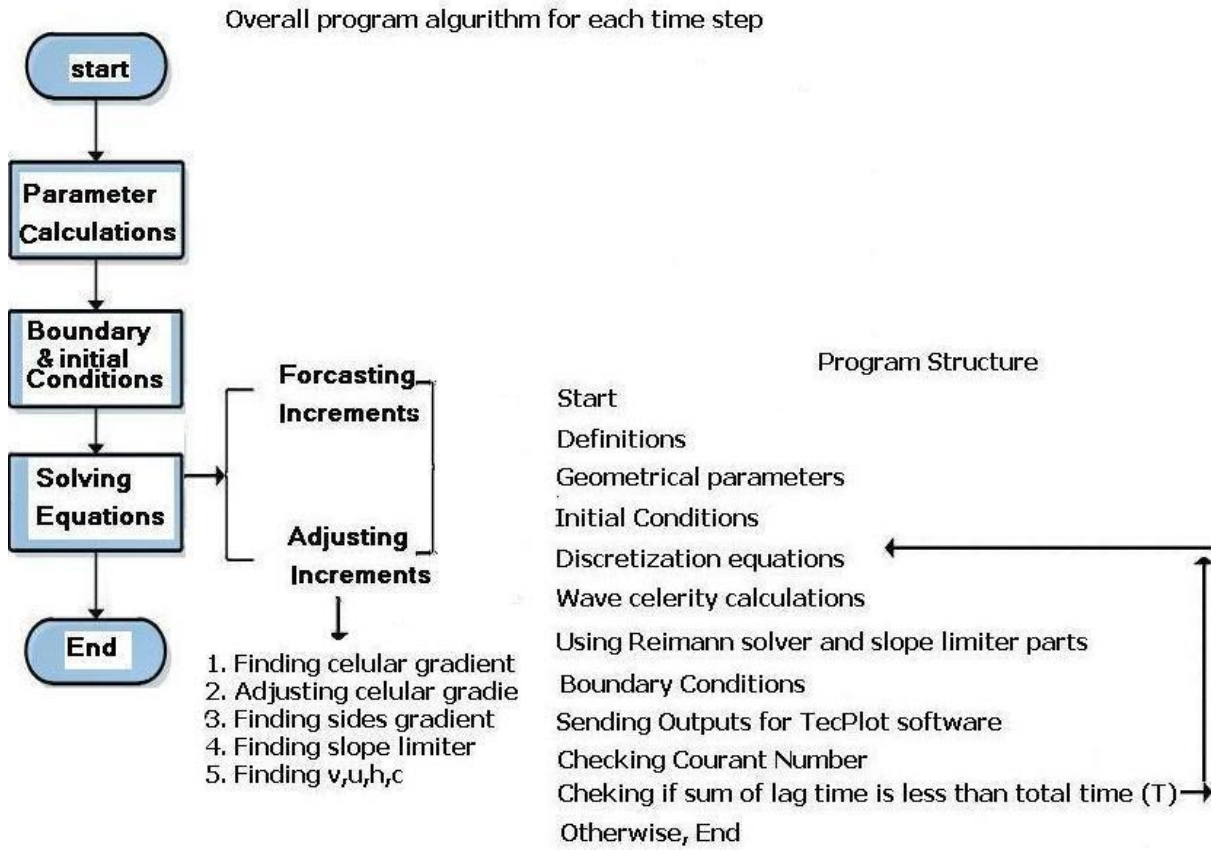


Fig. 1 Building block of Code structure for each step

General shallow depth Flow equations are:

$$\frac{\partial h}{\partial t}+\frac{\partial (hu)}{\partial x}+\frac{\partial (hv)}{\partial y}=0 \tag{1}$$

$$\frac{\partial (hu)}{\partial t}+\frac{\partial (hu^2+0.5gh^2)}{\partial x}+\frac{\partial (huv)}{\partial y}=-gh(S_{0x}-S_{fx}) \tag{2}$$

$$\frac{\partial (hv)}{\partial t}+\frac{\partial (huv)}{\partial x}+\frac{\partial (hv^2+0.5gh^2)}{\partial y}=-gh(S_{0y}-S_{fy}) \tag{3}$$

Advection –dispersion equation is presented as:

$$\frac{\partial(hc)}{\partial t}+\frac{\partial(huc)}{\partial x}+\frac{\partial(hvc)}{\partial y}=\nabla.(\nabla(\mathrm{hc}))+\mathrm{Sd} \quad (4)$$

Where t = time, x and y = horizontal coordinates, h = flow depth, u and v = depth-averaged flow velocity in x- and y-directions, C = depth-averaged volumetric pollutant concentration, The equations may be transformed to the following form:

$$\frac{\partial(U)}{\partial t}+\frac{\partial(F)}{\partial x}+\frac{\partial(G)}{\partial y}=\mathrm{S(U)} \quad (5)$$

$$\frac{\partial U}{\partial t}+\nabla.E=\mathrm{S(U)} \quad (6)$$

Where **U** is the vector of the conservative variables, **F** and **G** are the flux vectors in x- and y-direction; **S** is the vector of source terms, **E** = $(\mathbf{F},\mathbf{G}^T)$

$$U=\begin{pmatrix}h\\hu\\hv\\hc\end{pmatrix},F(U)=\begin{pmatrix}hu\\hu^2+0.5gh^2\\huv\\huc\end{pmatrix},G(U)=\begin{pmatrix}hu\\huv\\hu^2+0.5gh^2\\hvc\end{pmatrix}$$
$$S(U)=S_0+S_f+Sd=\begin{pmatrix}0\\ghS_{0x}\\ghS_{0y}\\0\end{pmatrix}+\begin{pmatrix}0\\-ghS_{fx}\\-ghS_{fy}\\0\end{pmatrix}+\begin{pmatrix}0\\0\\0\\\nabla.(\nabla(\mathrm{hc}))+Sd\end{pmatrix} \quad (7)$$

In which the dispersion matrix would be:

$$D=\begin{pmatrix}D_{xx} & D_{xy}\\D_{yx} & D_{yy}\end{pmatrix} \quad (8)$$

The bottom slope is:

$$S_{0x}=\frac{\partial z}{\partial x},S_{oy}=\frac{\partial z}{\partial y} \quad (9)$$

Manning equation for friction slope calculation is:

$$S_{fx}=\frac{n^2u\sqrt{(u^2+v^2)}}{h^{4/3}},S_{fy}=\frac{n^2v\sqrt{(u^2+v^2)}}{h^{4/3}} \quad (10)$$

Bed slope, friction slope and diffusion equation terms are:

$$S_0=\begin{pmatrix}0 & -ghS_{0x} & -ghS_{0y} & 0\end{pmatrix}^T$$
$$S_f=\begin{pmatrix}0 & -ghS_{fx} & -ghS_{fy} & 0\end{pmatrix}^T \quad (11)$$
$$Sd=\begin{pmatrix}0 & 0 & 0 & \nabla.(D\nabla(hc))+Sc\end{pmatrix}^T$$

g = gravitational acceleration, S_{0x} *and* S_{0y}= bed slopes in x-and y-directions, S_{fx} and S_{fy} = friction slopes in x-and y-directions, D_{xx}, D_{xy}, D_{yx}, and D_{yy} = empirical dispersion coefficients accounting for turbulent diffusion and shear flow dispersion (L2/T), Sd= the additional source/sink for the pollutant.

For decomposition of domain we have:

$$\int \frac{\partial U}{\partial t} dA + \int \nabla . E dA = \int \mathrm{S(U)} dA \qquad (12)$$

Considering Gauss theorem makes this equation form to:

$$\int \frac{\partial U}{\partial t} dA + \oint E.n dL = \int \mathrm{S(U)} dA \qquad (13)$$

In which a Delaunay-type triangle-shaped control volume is considered during a cell-centered finite volume method and can be converted to a new form by mid-point rule as:

$$\frac{\partial U_i}{\partial t} = -\frac{1}{\mathrm{A_i}} \sum_{j=1}^{3} (E_{ij}.n_{ij}) L_j + S_i \qquad (14)$$

Here we used cell center as data saving place instead of joints.

U_i has a mean value over the control volume A_i, and E_{ij} is the numerical flux vector through the edge j, and is calculated by a HLL approximate Riemann solver as:

$$\mathrm{E.n_{ij}} = \begin{cases} E_L.n_{ij} & if \quad S_L \geq 0 \\ \dfrac{S_R(E_L.n_{ij}) - S_L(E_{R.}n_{ij}) + S_L S_R(U_R - U_L)}{S_R - S_L} & if \quad S_L < 0 < S_R \\ E_{R.}n_{ij} & if \quad S_R \leq 0 \end{cases} \qquad (15)$$

In which U_L and U_R are value on cell I and the adjacent cell to side j respectively, and S_R and S_L are the related wave celerity estimates.

$$\mathrm{S_L} = \begin{cases} \min(q_L.n - \sqrt{gh_L}, u_* - \sqrt{gh_*}) & if \quad h_L > 0, h_R > 0 \\ q_L.n - \sqrt{gh_L} & if \quad h_L > 0, h_R = 0 \\ q_R.n - 2\sqrt{gh_R} & if \quad h_L = 0, h_R > 0 \end{cases}$$

$$\mathrm{S_R} = \begin{cases} \max(q_R.n + \sqrt{gh_R}, u_* + \sqrt{gh_*}) & if \quad h_L > 0, h_R > 0 \\ q_L.n + 2\sqrt{gh_L} & if \quad h_L > 0, h_R = 0 \\ q_R.n + \sqrt{gh_R} & if \quad h_L = 0, h_R > 0 \end{cases} \qquad (16)$$

$q=(u\ v)^T$ and $\sqrt{gh_*}$ and u_* have a form as (Toro, 2001):

$$u_* = 0.5(q_L + q_R) + \sqrt{gh_L} - \sqrt{gh_R} \qquad (17)$$

$$\sqrt{gh_*} = 0.25(q_L - q_R).n + 0.5(\sqrt{gh_L} + \sqrt{gh_R}) \qquad (18)$$

In which h_L, h_R are the related depths and the q_L, q_R are the corresponding water velocities. To avoid the oscillations around the discontinuities, a linear reconstruction was made by slope limiter provided by Jawahar and kamath (2000).

The modified Gausian diffusion term is :

$$\int \nabla.(Dh\nabla c)dA = \oint_i (Dh\nabla c).ndL \qquad (19)$$

Or it can be rewritten in the form of:

$$\oint_i (Dh\nabla c).ndL = \sum_{j=1}^{3} (Dh\nabla c)ij.\eta_{ij} L_j \qquad (20)$$

For time integration, the equation 15 is decomposed to these two equations to be solved in a semi implicitly manner.

$$\frac{\partial U_i}{\partial t} = -\frac{1}{A_i}\sum_{j=1}^{3}(E_{ij}.n_{ij})L_j + S_{0i} \qquad (21)$$

In which The right hand side term consists of advection and bed slope source term while the right hand side term of the second equation (Equation 22) includes friction slope and pollutant diffusion source terms.

$$\frac{\partial U_i}{\partial t} = S_{fi} + S_{di} \qquad (22)$$

These equations must be solved in conjunction with the equation 23 by a third order Runge - Kutta method:

$$u_1 = u^n + \Delta t f(u^n)$$
$$u_2 = \frac{3}{4}u^n + \frac{1}{4}u_1 + \frac{1}{4}\Delta t f(u_1) \qquad (23)$$
$$u^{n+1} = \frac{1}{4}u^n + \frac{1}{3}u_2 + \frac{2}{3}\Delta t f(u_2)$$

In the first step, Equation 23 is solved by an explicit method, then using the values obtained from the first step as the initial conditions, Equation 22 is solved using an implicit method and the same run continues for the next steps.

The boundary conditions are described in the result part.

3. Results

A test example is selected to check the performance of the proposed scheme (Fig. 2). The example solves a pollutant transport in a squared cavity with smooth bottom. All the results presented in this section are computed with variable time step sizes Δt adjusted at each step according to courant Number constraint for stability conditions:

$$\Delta t \le \frac{\min(d_i)}{2\max\left(\left(\sqrt{u^2+v^2}+c\right)_i\right)} \qquad (24)$$

where d_i is the distance between the centroid of two adjacent triangle meshes and Δt is less than 1 as a constraint.

As for code verification example, we have a pure advection (D ≡ 0) of a pollutant transport in a squared cavity with smooth topography. The flow domain is a 9000 m × 9000 m squared channel with bottom slopes $S_{0x} = S_{0y} = -0.001$. The Manning resistance coefficient is set to n = 0.025 $s/m^{1/3}$. Uniform flow velocities u = v = 0.5 m/s and the uniform flow water depth are considered as initial condition. The initial condition for the pollutant concentration is given by the superposition of two Gaussian pulses centered in (x_1 = 1400 m, y_1 = 1400 m) and (x_2 = 2400 m, y_2 = 2400 m), respectively, where the pollution initial condition is:

$$c(0,x,y) = 10*\exp\left(-\frac{(x-1400)^2+(y-1400)^2}{264^2}\right) + 6.5*\exp\left(-\frac{(x-2400)^2+(y-2400)^2}{264^2}\right) \qquad (25)$$

As boundary conditions, we use transparent flow conditions at all cavity boundaries. It is easy to check that the pollutant concentration is a wave that moves along the diagonal cross-section x = y preserving its shape with the constant speed u=v=0.5 m/s.

Figure 2 shows the results of this code for the example used by the mentioned specification.

The results for advection in three discrete times, namely t= 1628 s, t= 5235 s and t= 9600 s are also shown.

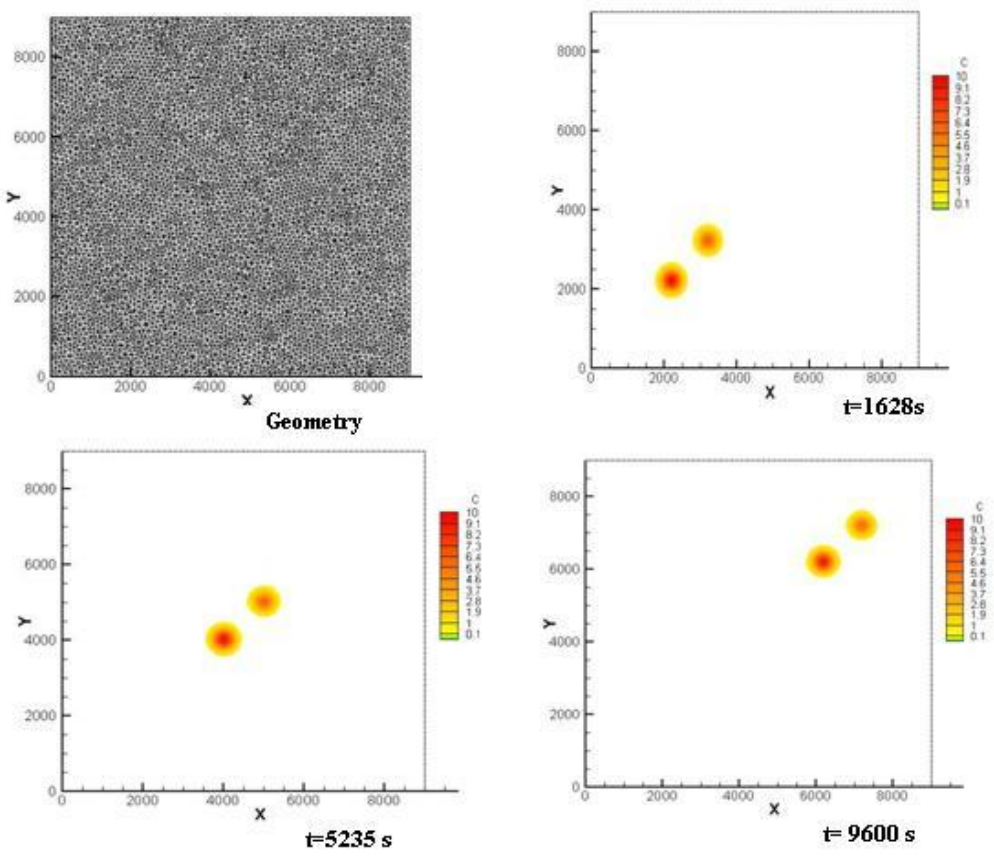


Fig. 2 adopted cavity meshes and the advection results throughout 3 different times. Which are comparable to the results given in Benkhaldoun's paper (2007) as in figure 3

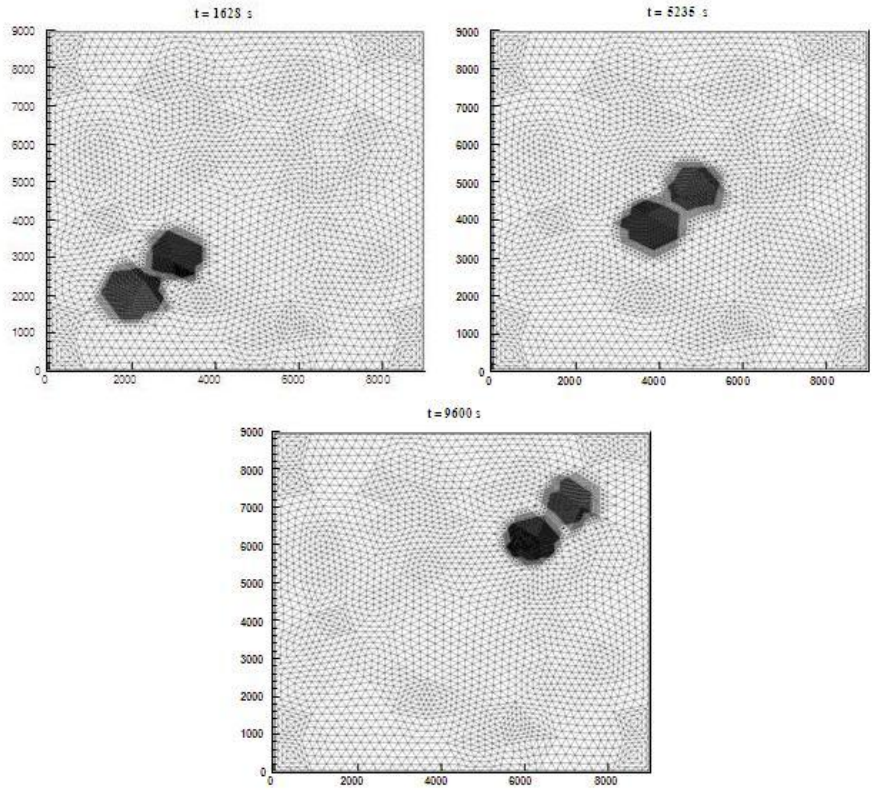


Fig. 3 contours of pollutant concentration at 3 simulation times: t = 1628 s, 5235 s and 9600 s

The real case study specifications:

The Ajichai river (figure 4) is a 147 km river in west of Iran (Tabriz), from which a 25 km; in-between two existent hydrometric stations; was chosen as our target to simulate its pollution concentration distribution.

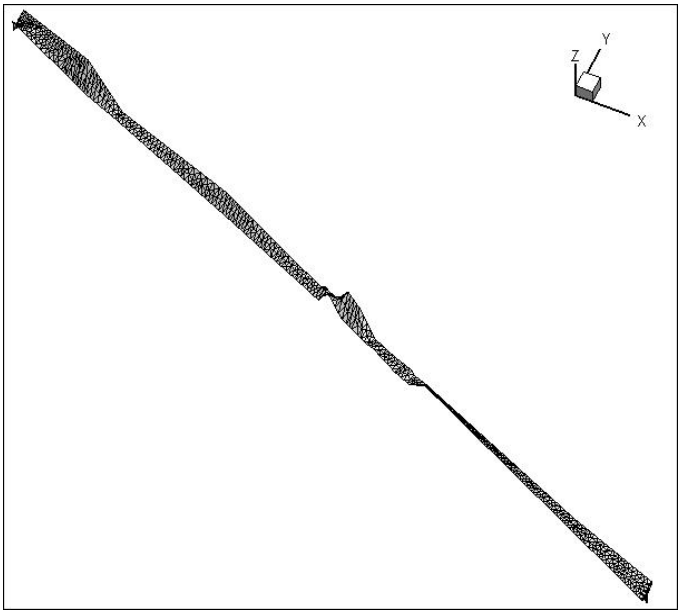


Fig. 4 Ajichai river layout in Iran (Tabriz) in specified river reach part

The related initial conditions are:

$$c(0,x,y) = 4.65*10\text{^}{-5}*(x\text{^}2 + y\text{^}2)\text{^}0.5 - 32.2743 \quad (26)$$

This is taken from logged data spreadsheet.
The entrance flow boundary condition is:
U=2.6 m/s, V=0
And for concentrations we have:

$$c(t,x,y) = \left((j-1)/(nstep-1)\right)*0.496 + 1.0185 \quad (27)$$

According to the data, the entrance B. C. depth variation is also as the following:

$$h(t,x,y) = 1646.24 - levelv(i) \quad (28)$$

The exit flow boundary condition is:
U=2.36 m/s, V=0
And for concentrations we have:
C=0
According the data, the exit B. C. depth variation is also as the following:

$$h(t,x,y) = 1604.87 - levelv(i) \quad (29)$$

The level is the height of points from the datum.
The figure 5 reveals the 6 hr simulated pollutant concentration distribution along the river reach, while D=1.

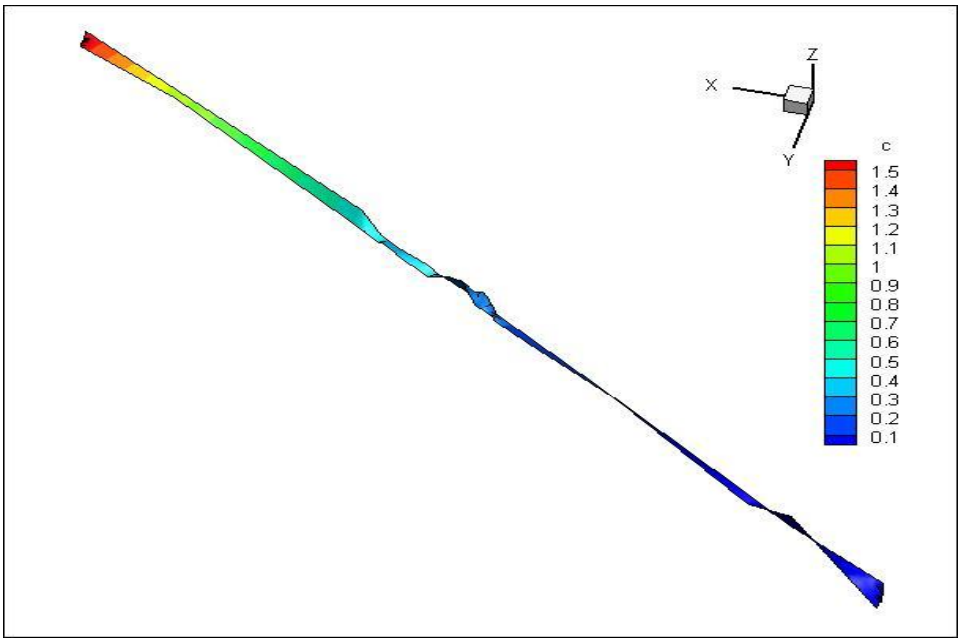


Fig. 5 simulated pollutant concentration in the Ajichai river reach

4. Conclusion

1. Numerical results of FORTRAN 95 code demonstrate the accuracy and robustness of the scheme to simulate the concentrations along the cavity, compared to reference example and its applicability in predicting pollutant transport under shallow water flow conditions.
2. The developed Fortran 95 code could handle the simulation of concentrations along the Ajichai river reach.
3. It is possible to monitor the concentrations according to standard levels in any point of the reach.

4. It could be extendable to other rivers to find their pollution map in case of mapping necessities.
5. The implementation on unstructured meshes allowing for local mesh refinement during the simulation process helps us predict in more real cases.
6. The courant stability condition was satisfied as a constraint throughout all the simulation process.

References

1 Alcrudo F., F. Benkhaldoun, "Exact Solutions to the Riemann Problem of the Shallow Water Equations with a Bottom Step", Comput. Fluids. 30, 643–671 (2001).

2 Benkhaldoun, F. "Analysis and Validation of a new Finite Volume Scheme for Nonhomoge- neous Systems", Finite Volumes for Complex Applications IV: Problems & Perspectives, Hermes Science Publications, R. Herbin, D. Kroner Eds. 269–276 (2002).

3 Benkhaldoun F., L. Quivy, "A Non Homogeous Riemann Solver for Shallow Water and Two Phase Flows", Flow Turbulence Combustion. 76 391–402 (2006).

4 Benkhaldoun F. , Elmahi I. , Seaid M. , 2007, Well-balanced finite volume schemes for pollutant transport on unstructured meshes, pp 180-203. Journal of Computational Physics 226, 1 (2007) 180–203

5 Delis AI. Improved application of the HLLE Riemann solver for the shallow water equations with source terms. Commun. Numer. Meth. Eng. 2003; **19**:59-83.

6 Heniche M., Y. Secretan, P. Boudreau, M. Leclerc, "A Two-Dimensional Finite Element Drying-Wetting Shallow Water Model for Rivers and Estuaries", Advances in Water Resources.23, 359–372 (2000).

7 James I.D. , "Modelling Pollution Dispersion, the Ecosystem and Water Quality in Coastal Waters: A Review", Environ. Model Software. 17, 363–385 (2002).

8 Jawahar P, Kamath H. A high-resolution procedure for Euler and Navier-Stokes computations on unstructured grids. Journal of Computational Physics 2000; 164: 165-203.

9 Komatsu T, Ohgushi K, Asai K. Refined numerical scheme for advective transport in diffusion simulation. J. Hydraulic Eng. 1997; 123: 41–50.

10 Komatsu T., K. Ohgushi, K. Asai, "Refined numerical scheme for advective transport in diffusion simulation", J. Hydraulic Eng. 123, 41–50 (1997).

11 Lin B., R.A. Falconer, "Tidal flow and transport modeling using ultimate quickest scheme", J. Hydraulic Eng. 123, 303–314 (1997).

12 Roe P.L. , "Approximate Riemann Solvers, Parameter Vectors and Difference Schemes", J. Comp. Physics. 43, 357-372 (1981).

13 Toro E.F. , "Shock-Capturing Methods for Free-Surface Shallow Waters", Wiley Chichester2001

14 [V´azquez M.E., "Improved Treatment of Source Terms in Upwind Schemes for the Shallow Water Equations in Channels with Irregular Geometry", J. Comp. Physics. 148, 497–526 (1999).

15 Zhou JG, Causon DM, Mingham CG, Ingram DM.The Surface Gradient Method for the Treatment of Source Terms in the Shallow-Water Equations. J Comput Phys 2001; 168: 1-25.

Theoretical Criterion for Stability of Free Hydraulic Jump on Adverse Stilling Basins

Hossein Khalili Shayan[1] *, Javad Farhoudi* [1]
[1]Irrigation and Reclamation Engineering Dept. , University of Tehran, Tehran, Iran

Abstract

Hydraulic jump on adverse stilling basin is an unstable phenomenon which causes some complexities in controlling of the jump. This paper considers the stability of free hydraulic jump on adverse stilling basins from a theoretical point of view. A minimum value of upstream Froude number is needed to produce the free hydraulic jump on adverse stilling basins which was presented by a theoretical equation. Also, the effects of an end sill and divergence in section on the minimum Froude number were investigated. Moreover, it is required that the bed has a minimum friction for making the jump stable which is obtained as a function of upstream Froude number and bed slope. This condition was compared with the criterion proposed by previous researchers and showed the considerable deviations at larger bed slopes. The result showed that it is impossible to establish the hydraulic jump on concrete adverse stilling basins without any appurtenances. However, diverging in section can improve the stability of hydraulic jump on adverse stilling basins.

Keywords: Hydraulic Jump, Adverse Basin, Stability, End Sill, Diverging Stilling Basin.

1. Introduction

Stilling basin is a common tool being used as an economic device to dissipate excess energy at the downstream of hydraulic structures. It is understood that any alterations in channel geometry, such as adverse slope of stilling basin, would change the characteristics of hydraulic jump and therefore its influences on downstream of such structures. It could be noted that the effect of water weight in adverse basins, as shown in Fig. a. 1, would alter the characteristics of hydraulic jump compared with the classical hydraulic jump. Hydraulic jump on an adverse slope is an interesting phenomenon which affects the sequent depths, energy loss and length of stilling basin. This phenomenon can shorten the stilling basin and the height of the side walls; hence optimize the costs of construction.

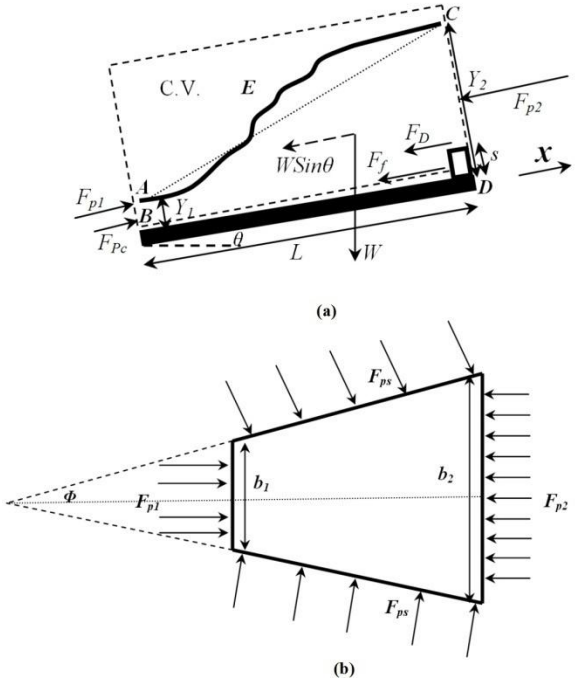


Fig. 1 (a) Acting forces on hydraulic jump on an adverse slope, (b) Plan view of acting forces on diverging hydraulic jump

Hydraulic jump on an adverse slope is an unstable phenomenon which causes some complexities in controlling of the jump which is the core of many reports published by different investigators in past decades. Okada and Aki (1959) carried several experiments of a stabilized hydraulic jump on an adverse sloping bed and finished on a reverse one. The experiments of Okada and Aki (1959) were carried out for approaching Froude numbers in the range of 9 to 13 which was outside the normal design range of conventional stilling basins. Rajaratnam (1966) classified the hydraulic jump on an adverse slope as F-type and concluded that ''it is almost impossible to establish a complete jump on the reverse slope,''. Hartung and Csallner (1967) indicated that an adverse transitional section at the downstream of a bucket spillway could be used to stabilize the hydraulic jump at low Froude numbers. They used a roughened bed in their experiments. Ohashi et al. (1973) studied the hydraulic jump which was located entirely on the adverse basin and confirmed its instability. McCorquodale and Mohamed (1994) carried out a set of experiments where both the toe and end of the hydraulic jump were located inside the adverse bed. They reported that the jump would be established at Froude numbers larger than 9 and would require continuous adjustment of tailwater to maintain a stationary position at Froude numbers less than about 4. Pagliara and Peruginelli (2000) concluded from their experiments that the presence of an end sill at the end of adverse stilling basins would stabilize the position of the hydraulic jump only for Froude numbers greater than 7.5. Baines and Whitehead (2003) reported that the jump was stable at downslope and was unstable in adverse basins regardless of Froude number and slope quantities. According to studies conducted by Defina et al. (2008) on the hydraulic jump at an adverse prismatic basin, the existence of a stable hydraulic jump is related to the presence of friction at large flow boundaries.

This paper reports the derivation of a theoretical equation, using momentum equation, to achieve the minimum Froude number of incoming flow in an adverse stilling basin where a stable hydraulic jump could be attained. The effects of end sill, divergence of side walls, boundary friction and water weight on adverse basin were also considered to develop partial required conditions for a stable hydraulic jump.

2. Estimation of minimum upstream Froude number for establishing hydraulic jump on an adverse slope

Establishing a hydraulic jump on an adverse slope requires overcoming the water weight on stilling basin which needs a minimum hydrodynamic force induced by incoming supercritical flow.

a) Hydraulic jump on prismatic channels: For free hydraulic jump on adverse basins, forces influencing the control volume, as shown in Figs. a. 1 and b. 1 are:

- ✓ Forces due to hydrostatic pressure distribution at the beginning and the end of a hydraulic jump are F_{p1}, F_{p2}, respectively,
- ✓ Force due to deviation from hydrostatic pressure distribution at the beginning of the hydraulic jump is F_{Pc},
- ✓ Weight of the water enclosed between the approach and sequent depths is W,
- ✓ The drag force exerted by end sill is F_D,
- ✓ The lateral forces resulted from side walls are F_{ps}, and,
- ✓ Friction force is F_f.

Assuming the hydrostatic pressure distribution at the toe and end of a hydraulic jump ($F_{Pc}=0$), overlooking from the normal acceleration, the air entrainment, and the effect of friction force on the hydraulic jump ($F_f=0$), the momentum equation in an adverse sloping prismatic rectangular channel can be written as:

$$\sum F_x = F_{p1} - \left(F_{p2} + W\sin\theta\right) = \rho bq\left(\beta_2 V_2 - \beta_1 V_1\right) \quad (1)$$

in which, $F_{p1} = \gamma b\frac{Y_1^2}{2}\cos\theta$, $F_{p2} = \gamma b\frac{Y_2^2}{2}\cos\theta, W = \gamma kbL\left(\frac{Y_1+Y_2}{2}\right)$, b is

the width of the basin, ρ is the density of water, γ is the specific weight of water, Y_1, Y_2 are the flow depths, V_1, V_2 are the flow velocities, θ is the angle of the bed slope, L is the length of stilling basin, q is the flow discharge per unit width of the rectangular basin, β_1, β_2 are the momentum correction coefficients at the beginning and the end of hydraulic jump, respectively. k is a coefficient for determining the weight of water in the control volume (W_{ABCDE}) to the weight of the water considering linear profile for the hydraulic jump (W_{ABCD}), (see Fig. a. 1). McCorquodale and Mohamed (1994) measured the velocity profile in the jet near supercritical section and approximated β_1 with 1.03. Okada and Aki (1959) proposed $k = 1.29 - 1.49$ for slopes of $-\frac{1}{4}, -\frac{1}{5}, -\frac{1}{6}$ while McCorquodale and Mohamed (1994) $k = 0.78 - 1.38$ for $0, -\frac{1}{5}, -\frac{1}{6}, -\frac{1}{10}$. However, Pagliara and Peruginelli (2000) concluded that the k values do not depend on the bed slope or the approaching Froude number and found a constant value of $k = 1.06$ from their experimental data. They proposed $\beta_2 = 1$ for the velocity distribution at the end of a hydraulic jump. Substituting the above relationships in Eq. (1) results:

$$\frac{q^2}{g} = \left(\frac{4Y_1Y_2}{4Y_1 - (4\beta_1)Y_2}\right)\left(\left(\frac{Y_1^2}{2} - \frac{Y_2^2}{2}\right)\cos\theta - kL\left(\frac{Y_1 + Y_2}{2}\right)\sin\theta\right) \quad (2)$$

Introducing $m = \frac{Y_2}{Y_1}$, the upstream Froude number for hydraulic jump on the sloping prismatic rectangular channel $Fr_1 = \frac{q}{\sqrt{gY_1^3\cos\theta}}$, and assuming $\beta_1 = 1$, $k = 1$, one obtains:

$$Fr_1^2 = \frac{m\left(1 - m^2 - \frac{L\tan\theta}{Y_1}(1+m)\right)}{2(1-m)} \quad (3)$$

where, $m = \frac{Y_2}{Y_1}$ which could be equal or less than the sequent depth ratio depending on the length of the stilling basin. Equation (3) is a general estimation of a complete free jump in the basin where upstream Froude numbers can take any values.

Figure 2 depicts the variation of the upstream Froude number with flow characteristics and bed dimensions from which the following results can be drawn:

1- The ratio of flow depth decreases with the length or bed slope, for a certain value of upstream Froude number,

2- Figure 2 indicates that a minimum value of upstream Froude number ($Fr_{1\min}$) is required to establish the free hydraulic jump on an adverse bed despite of classical hydraulic jump on a horizontal bed.

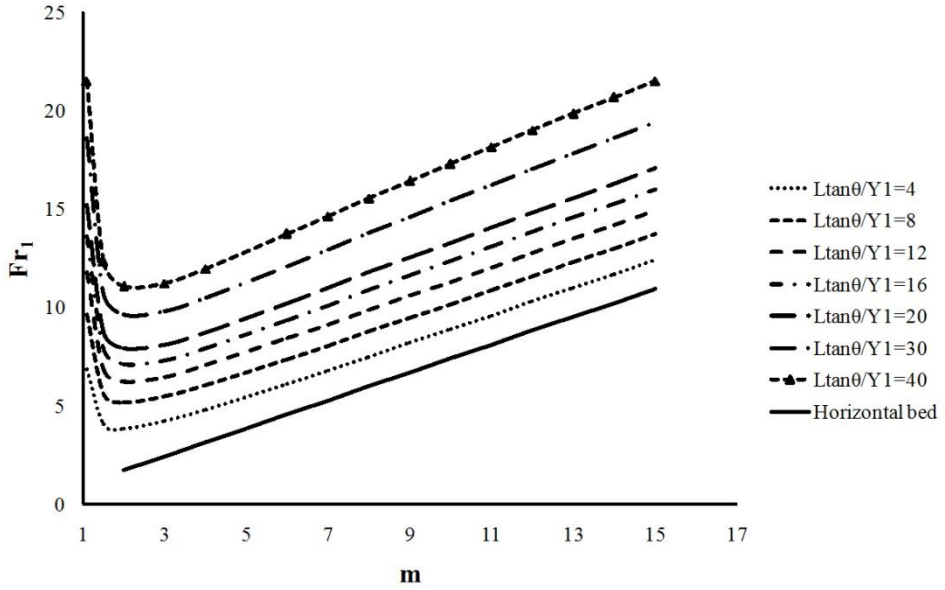


Fig. **2** Determination of sequent depths in hydraulic jump on an adverse slope

Figure 3 compares the minimum Froude numbers determined from Fig. 2 which is based on experimental data from several researchers. It is found that the hydraulic jump at the lesser Froude number is more submerged.

Using an end sill, drag force (F_D) will influence the control volume, as shown in Fig. a. 1. The drag force exerted by end sill is defined as:

$$F_D = \frac{1}{2}\rho C_D b s V_1^2 \qquad (4)$$

where, $V_1 = \frac{q}{Y_1}$, s is the sill height, and C_D is the drag coefficient. Ohatsu et al. (1991) proposed the following relationship for estimating the drag coefficient due to an end sill at the distance x_s from the toe of a classical hydraulic jump which is assumed valid for hydraulic jump on an adverse slope:

$$C_D = 0.71 - 0.85\left(\frac{x_s}{5.5Y_2}\right) \qquad (5)$$

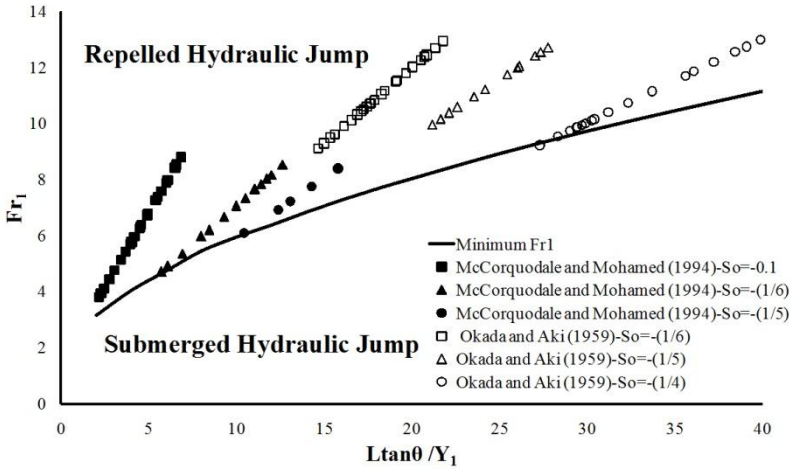


Fig. **3** The minimum values of upstream Froude numbers for developing free hydraulic jump on adverse bed

Substituting the drag force in Eq. (1) and following a similar procedure, we could obtain the following relationship for estimating the upstream Froude number required to stabilize the hydraulic jump on an adverse basin with an end sill:

$$Fr_1^2 = \frac{m\left(1-m^2-\frac{L\tan\theta}{Y_1}(1+m)\right)}{2(1-m)+C_D Sm} \qquad (6)$$

where $S=\frac{s}{Y_1}$. Figure 4 shows the effect of end sill height on developing hydraulic jump on an adverse slope for $\frac{L\tan\theta}{Y_1}=15$. It could be observed that the required upstream Froude number increases with the height of the end sill. Moreover, the ratio of flow depths decrease with the sill height, for certain values of upstream Froude number, length and bed slope, respective

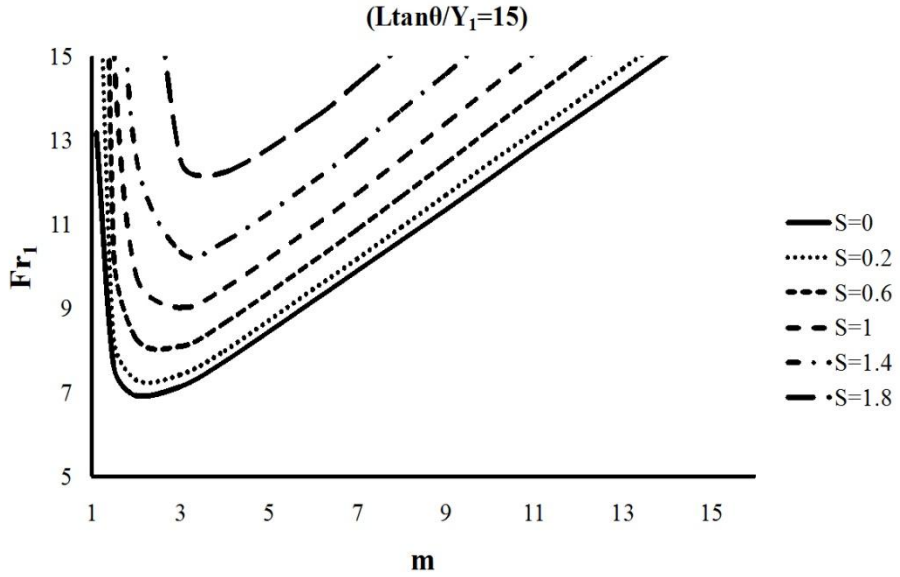


Fig. 4 Effects of end sill height on minimum values of upstream Froude numbers and sequent depths $(\frac{L\tan\theta}{Y_1}=15)$

b) Hydraulic jump on nonprismatic channels: For nonprismatic stilling basins with diverging walls, the lateral forces resulting from side walls (F_{ps}), influence the control volume, which are the reactions of pressure distribution in the *x*-direction (F_{psx}) (see Fig. b. 1). Kasi et al. (2011) investigated the diverging hydraulic jump with adverse bed. They compared linear, parabolic and elliptic profiles and recommended that the parabolic profile is more accordant with the experimental data. They have suggested the following relationship for the profile of hydraulic jump on an adverse slope in diverging rectangular basins:

$$Y(x)=Y_1+(Y_2-Y_1)\left[2\left(\frac{x}{L}\right)-\left(\frac{x}{L}\right)^2\right] \qquad (7)$$

Integration of Eq. (7) result:

$$WSin\theta = \gamma \sin\theta \int_{x=0}^{x=L} b(x).Ydx = \gamma \sin\theta \left[Lb_1\left(\frac{1}{3}Y_1 + \frac{2}{3}Y_2\right) + (b_2 - b_1)L\left(\frac{1}{12}Y_1 + \frac{5}{12}Y_2\right)\right] \quad (8)$$

where ϕ is the diverging angle of the basin section. Substituting the lateral pressure force into Eq. (1), gives the following equation for

Assuming hydrostatic pressure distribution yields:

$$F_{psx} = 2F_{ps}\sin\phi = 2\gamma \sin\phi \int_{x=0}^{x=L} \frac{Y^2}{2} dx = 2\gamma L \sin\phi\left(\frac{1}{10}Y_1^2 + \frac{4}{15}Y_2^2 + \frac{2}{15}Y_1Y_2\right) \quad (9)$$

estimating the required upstream Froude number in this case:

$$Fr_1^2 = \frac{m}{B\left(1-\frac{m}{B}\right)}\left[\frac{1}{2} + \frac{2\kappa L\sin\phi}{Y_1\cos\theta}\left(\frac{1}{10} + \frac{4}{15}m^2 + \frac{2}{15}m\right) - \frac{m^2}{2B} - \frac{L\tan\theta}{Y_1}\left(\frac{1}{3} + \frac{2}{3}m + \left(\frac{1-B}{B}\right)\left(\frac{1}{12} + \frac{5}{12}m\right)\right)\right] \quad (10)$$

in which $\kappa = \frac{Y_1}{b_1}$, $B = \frac{b_1}{b_2} = \frac{1}{1 + 2\kappa\frac{L\tan\theta}{Y_1}}$ ..

The effects of diverging section on flow depths ratios and upstream Froude number for $\frac{L\tan\theta}{Y_1} = 15$, $\kappa = 0.072$ is shown in Fig. 5.

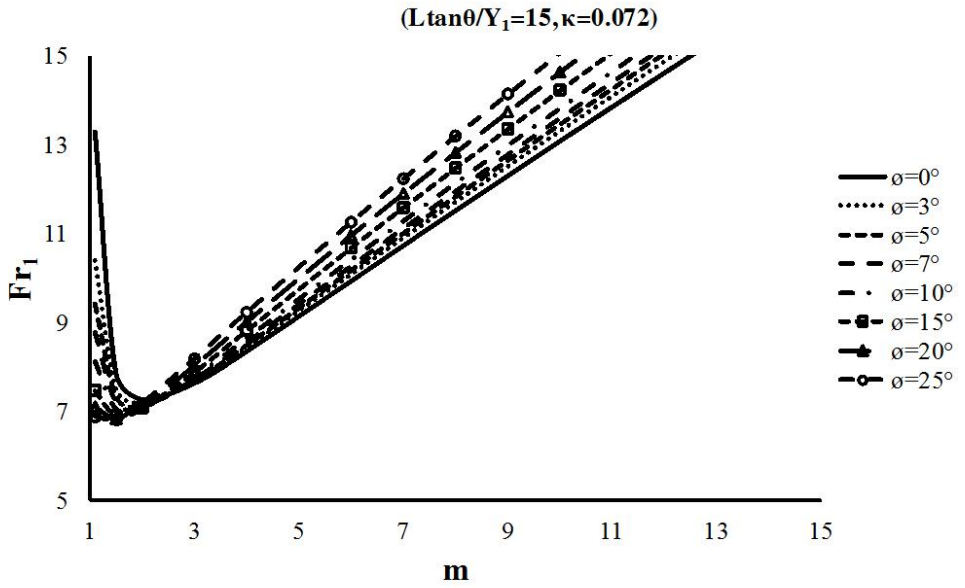


Fig. 5 Effects of divergence basin angle on minimum values of upstream Froude numbers and sequent depths $(\frac{L\tan\theta}{Y_1} = 15, \kappa = 0.072)$

It can be seen that the threshold value of Froude number for free hydraulic jump will decrease as the angle of divergence increases. This is the result of increased lateral pressure forces on decreasing the contribution of hydrostatic pressure force at the end of the stilling basin. It is evident that the depth ratio from the end to the toe will decrease in the diverging section. Interpolating the minimum threshold values from Eq. (10), gives the following regression relationship for estimating the minimum values of upstream Froude numbers related to the geometry of basin:

$$Fr_{1(\min)} = 1.564\left(\frac{L\tan\theta}{Y_1}\right)^{0.522} + 0.878e^{-0.026\phi} \tag{11}$$

It is noted that the Eq. (11) only represents the requirements to establish a free hydraulic jump on an adverse slope.

3. Theoretical criterion for establishing a hydraulic jump on an adverse slope

The stability criterion defined by Defina et al. (2008) was presented for adverse slopes with bed slopes less than -4%. They have overlooked the effects of water weight on sequent depths and its role on jump instability. This negligence doubts the reliability of their recommendations for larger slopes. By referring to Fig. a. 6 and using the momentum equation for a control volume enclosed between sequent depths at steady state conditions, one can obtain:

$$M_1 = M_2 + \frac{W\sin\theta}{\gamma b} + \frac{F_f}{\gamma b} \tag{12}$$

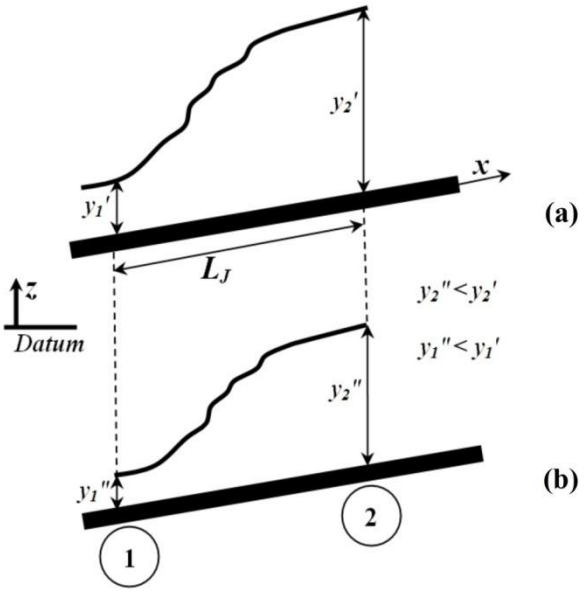
where M_1, M_2 are the specific forces at sections (1) and (2), respectively. In Fig. b. 6 the hydraulic jump dispositions and hence sequent depths in sections (1) and (2) are decreased to y_1'', y_2''.. Considering a unit control volume in both cases, the momentum equation is rewritten as:

$$M_1' = M_2' + \frac{W'\sin\theta}{\gamma b} + \frac{F_f'}{\gamma b} + f' \tag{13}$$

where $f' = \frac{F'}{\gamma b}$, and F' is the stabilizing force to restore the jump to its primary state. Differentiating Eqs. (12) and (13) on a small decrement, gives:

$$\frac{dM_1}{dx} = \frac{dM_2}{dx} + \frac{\sin\theta}{\gamma b}\left(\frac{dW}{dx}\right)_{|2} + f' \tag{14}$$

Fig. **6** Sketch of hydraulic jump on an adverse slope in a) stable stationary state, b) unstable stationary state



The hydraulic jump is defined stable if it slightly displaces from its equilibrium location and returns to its initial position (Baines and Whitehead, 2003). Therefore, a stabilizing force is required to achieve the stability of a hydraulic jump, (i.e. $f' > 0$):

$$f' = \frac{dM_1}{dx} - \frac{dM_2}{dx} - \frac{\sin\theta}{\gamma b}\left(\frac{dW}{dx}\right)_{|2} > 0 \rightarrow \frac{dM_1}{dx} > \frac{dM_2}{dx} + \frac{\sin\theta}{\gamma b}\left(\frac{dW}{dx}\right)_{|2} \quad (15)$$

The specific force on a sloping bed can be defined as:

$$M = \frac{y'^2}{2}\cos^3\theta + \frac{q^2}{gy'\cos\theta} \quad (16)$$

Differentiating Eq. (16) and using the chain role gives:

$$\frac{dM}{dx} = \frac{dM}{dy'} \times \frac{dy'}{dx}, \frac{dM}{dy'} = \frac{d}{dy'}\left(\frac{y'^2}{2}\cos^3\theta + \frac{q^2}{gy'\cos\theta}\right) = y'\cos^3\theta - \frac{q^2}{gy'^2\cos\theta} \quad (17)$$

On the other hand, differentiation of Bernoulli's equation at the x direction, results in the following

$$H = z + y'\cos\theta + \frac{q^2}{2gy'^2\cos^2\theta} \rightarrow \frac{dH}{dx} = \frac{dz}{dx} + \frac{dy'}{dx}\left(\cos\theta - \frac{q^2}{gy'^3\cos^2\theta}\right) \quad (18)$$

where, $\frac{dz}{dx} = -\sin\theta$, $\frac{dH}{dx} = -S_f$. Byintroducing the friction slope from the Chézy formula $S_f = \frac{q^2}{C^2y^3} = \frac{q^2}{C^2y'^3\cos^3\theta}$, the Froude number on the sloping bed $Fr = \frac{q}{\sqrt{gy'^3\cos^4\theta}}$ and assuming a wide channel ($R \approx y$), yields that:

$$\frac{dy'}{dx} = -\frac{c^2\tan\theta + Fr^2}{c^2\left(1 - Fr^2\right)}, \frac{dM}{dx} = -y'\cos^3\theta\left(\frac{c^2\tan\theta + Fr^2}{c^2}\right) \quad (19)$$

where, $c = \frac{C}{\sqrt{g}}$ and C is the Chézy coefficient. Despite recommendations by Kasi et al. (2011), and to achieve a simplified relationship, the linear profile for a hydraulic jump on an adverse slope is assumed by the following formulas:

$$y = y_1 + \left(\frac{y_2 - y_1}{L_J}\right)x, W(x) = k\gamma b\int_0^x y dx \rightarrow \frac{1}{\gamma b}\left(\frac{dW}{dx}\right)_{|2} = -ky_2 = -ky_2' \cos\theta \qquad (20)$$

It should be noted that the weight of water in the control volume decreases when moving to a new state and $\frac{dW}{dx} < 0$. Introducing the above relationships in Eq. (15) and using $Fr_2^2 = Fr_1^2\left(\frac{y_1}{y_2}\right)^3$, yields:

$$c^2 < \frac{\left(\left(\frac{y_2}{y_1}\right)^{-2} - 1\right)Fr_1^2 \cos^3\theta}{-k\left(\frac{y_2}{y_1}\right)\sin\theta + \left(1 - \frac{y_2}{y_1}\right)\cos^2\theta.\sin\theta} \qquad (21)$$

On the other hand, Pagliara and Peruginelli (2000) proposed the following relationship for estimating sequent depths of a hydraulic jump on an adverse slope at $0 \prec \tan\theta \prec 0.25$:

$$\frac{y_2}{y_1} = \frac{1}{2}\left(\sqrt{1+8G_1^{\,2}} - 1\right), G = 3.317^{-1.518\tan\theta} Fr_1 \qquad (22)$$

Combining the above equations will result in the required conditions to establish a stable hydraulic jump on adverse beds:

$$C = c\sqrt{g} \rightarrow C^2 < g\frac{\left(4\left(\sqrt{1+8G_1^2} - 1\right)^{-2} - 1\right)Fr_1^2 \cos^3\theta}{-\frac{k\sin\theta}{2}\left(\sqrt{1+8G_1^2} - 1\right) + \left(1 - \frac{1}{2}\left(\sqrt{1+8G_1^2} - 1\right)\right)\cos^2\theta.\sin\theta} \qquad (23)$$

Equation (23) indicates the role of bed friction on the stability of an upward hydraulic jump, previously mentioned by Defina et al. (2008). The equation dictates that the stability of a hydraulic jump on an adverse slope requires a maximum value of Chézy coefficient as a function of upstream Froude numbers and bed slopes. Figure 7 demonstrates the variation of threshold values of Chézy coefficient with the upstream Froude number and bed slope. It can be concluded that:

- ✓ The jump would return to its stationary position as the friction force becomes larger than its threshold values,
- ✓ As the bed slope decreases, the range of the Chézy coefficient for jump stability grows.
- ✓ For a given value of bed slope, hydraulic jump on an adverse slope at higher upstream Froude numbers will be more stable if the boundary roughness is lesser. This is verified by reports from McCorquodale and Mohamed (1994) and Pagliara and Peruginelli (2000).

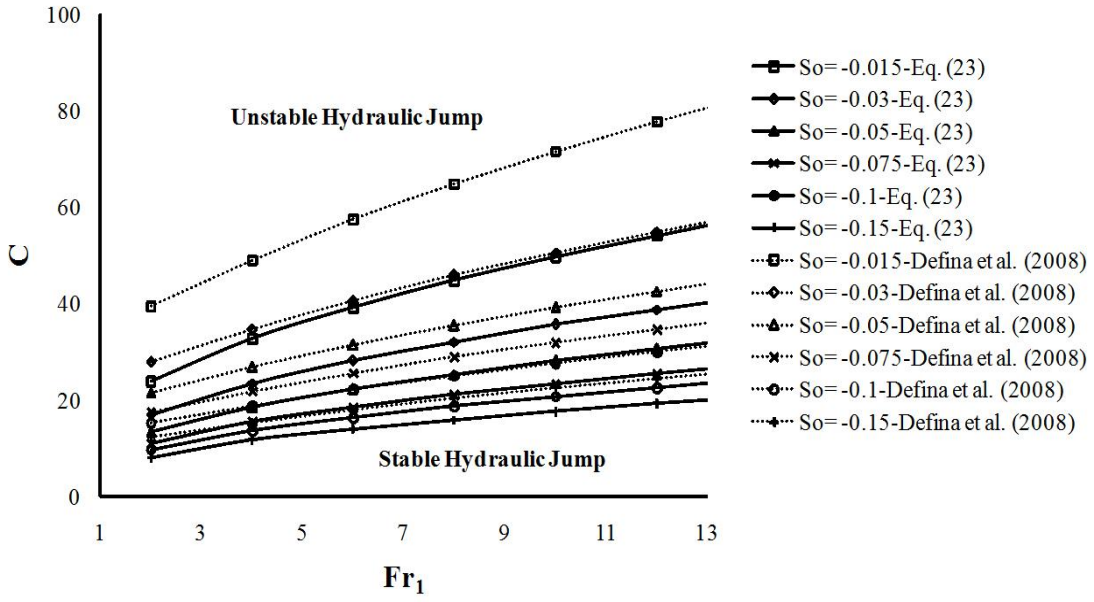


Fig. 7 Comparison between Eq. (23) and Defina et al. (2008) in estimating the maximum values of Chézy coefficient for stability of hydraulic jump on an adverse slope

Figure 7 compares the proposed criterion based on Eq. (23) and that of Defina et al. (2008). It can be seen that maximum values of the Chézy coefficient determined from Defina et al. (2008), would be greater than those calculated by Eq. (23). This can be attributed to overlooking of water weight on adverse basin.

Using Manning's equation, the minimum required roughness for stability of a hydraulic jump on an adverse slope downstream of a sluice gate, will be:

$$\xrightarrow{C=\frac{1}{n}y_1^{1/6}} n \geq \left[(C_c w)^{1/3} \frac{\cos^2\theta.\sin\theta\left(1-\frac{1}{2}\left(\sqrt{1+8G^2}-1\right)\right)-\frac{k\sin\theta}{2}\left(\sqrt{1+8G^2}-1\right)}{\left(2^{7/3}\left(\sqrt{1+8G^2}-1\right)^{-7/3}-1\right)Fr_1^2 g\cos^{8/3}\theta} \right]^{1/2} \quad (24)$$

where $C_c = \frac{y_1}{w}$ is the contraction coefficient. Figure 8 illustrates the variation of Manning's factor at the threshold state with the upstream Froude number and bed slope, assuming $C_c = 0.61$, and $w = 1.5cm$.

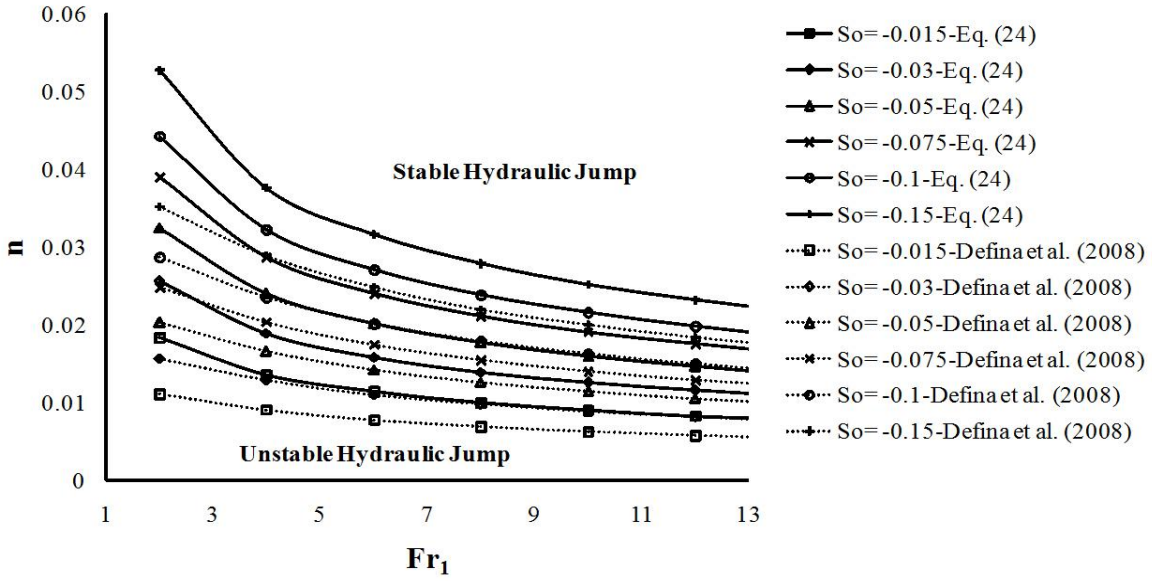


Fig. 8 Comparison between Eq. (24) and Defina et al. (2008) in estimating the minimum values of Manning's factor for stability of hydraulic jump on an adverse slope

These values were assumed for evaluating the minimum required bed roughness in a laboratory scale. Considering Manning's factor for concrete stilling basin (i.e. 0.014) and gate openings in a practical range, it is impossible to establish the free hydraulic jump on adverse bed in absence of any appurtenances. For this reason, presence of artificial roughness, sills or baffle blocks is required to stabilize the hydraulic jump on an adverse slope. The bed friction would be responsible for stability of a hydraulic jump on an adverse slope at a minimum upstream Froude number as shown in Eq. (11). Consequently, the minimum Froude number is not enough for stability of a hydraulic jump on an adverse slope. It should be noted that as the bed slope increases, the discrepancy among the values obtained from Defina et al. (2008)'s equation and Eq. (23) become larger. For example in slope -0.15 and initial Froude number of 9 for a hydraulic jump, Defina et al. (2008)'s equation, attains the minimum Manning coefficient needed for a stable jump about 21 percent less than recommended method.

From Fig. 8, it can be concluded that neglecting the influence of water weight on adverse bed in Defina et al. (2008)'s equation, will mislead in recognition of the stability limits of a hydraulic jump on an adverse slope. However, Eq. (23) can resolve this defect.

In case of a diverging hydraulic jump on an adverse slope, if induced lateral pressure force by side walls is introduced into Eq. (15), the following relationship will be obtained:

$$C^2 < g\frac{\left(\frac{b_2}{b_1}.\frac{y_2}{y_1}Fr_2^2 - Fr_1^2\right)\cos^4\theta}{\left[\cos^3\theta.\tan\phi\left(\left(\frac{y_2}{y_1}\right)^2\left(\frac{y_1}{b_1}\right)\left(1-2Fr_2^2\right)-\frac{y_1}{b_1}\left(1-2Fr_1^2\right)\right)+\cos^3\theta.\sin\theta\left(1-\frac{b_2}{b_1}\frac{y_2}{y_1}\right)+\sin\phi\left(\frac{y_2}{y_1}\right)^2\left(\frac{y_1}{b_1}\right)-\frac{b_2}{b_1}\frac{y_2}{y_1}\cos\theta.\sin\theta\right]} \quad (25)$$

in which, $\frac{b_2}{b_1} = 1 + 2\frac{L_J}{y_1}\frac{y_1}{b_1}\tan\phi$ and $Fr_2^2 = Fr_1^2\left(\frac{y_1}{y_2}\right)^3\left(\frac{b_1}{b_2}\right)^2$. Kasi et al. [9] proposed the following relationships for estimating the sequent depths and the length of a diverging hydraulic jump on adverse bed from experimental data:

$$\frac{y_2}{y_1} = 0.309(1-\tan\theta)^{3.542}.(1+\phi)^{-0.1197}.(Fr_1)^{0.5175}.\left(\frac{L_J}{y_1}\right)^{.5444} + 1.4396$$
$$\frac{L_J}{y_1} = 2.9607(1-\tan\theta)^{3.7214}.(1+\phi)^{-0.0774}.(Fr_1)^{1.4997} \quad (26)$$

Figure 9 shows the effect of the divergence angle on the stability of a hydraulic jump for two different bed slopes and $\frac{y_1}{b_1} = 0.072$. It can be observed that the minimum required bed friction to stabilize the hydraulic jump on an adverse slope will decrease as the divergence angle increases. For example at a slope equal to -0.05, it can be observed from Fig. 9 that an increase of the divergence angle of the basin from 0 to 1.5 degrees at a initial hydraulic jump Froude number of 0.9 causes an approximate 37% rise in the maximum possible Chezy coefficient for a stable hydraulic jump. Therefore, the establishment of a stable hydraulic jump on an adverse slope can be achieved in nonprismatic basins. Figure 9 was depicted for a certain condition where the length of the adverse basin equals to the length of the hydraulic jump. One can employ Eq. (26) to observe any adverse basins with different arbitrary dimensions. It should be noted that the minimum friction necessary for stability of a hydraulic jump from Figs. 7,8 and 9 for specific values of gate opening and initial diversion basin width is depicted and lacks practical purposes. Despite this proposed Eqs. (23), (24) and (25) due to their theoretical bases, can be used in general design of adverse basins and for reliability of the stability of a hydraulic jump.

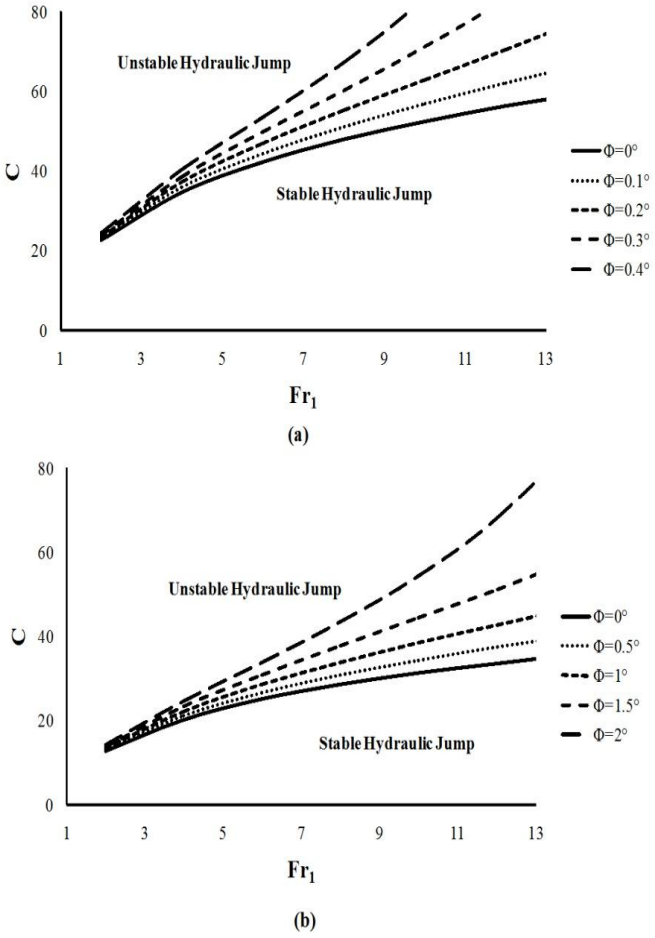


Fig. 9 Effect of divergence angle and bed slope on stability of hydraulic jump on an adverse slope a) $S_o = -0.015$, b) $S_o = -0.05$

4. Conclusions

In this research, a theoretical equation for estimating the minimum upstream Froude number to establish the free hydraulic jump on an adverse bed was presented. The following conclusions may be drawn:

- ✓ The required upstream Froude number increases when the height of end sill increases. Also, the threshold value of Froude number for free hydraulic jump would be decreased as the angle of divergence increases.
- ✓ A theoretical relation was developed to estimate the minimum values of upstream Froude numbers related to basin geometries.
- ✓ Considering the Manning's factor for concrete stilling basin and gate opening in practical range, it is impossible to establish the free hydraulic jump on an adverse bed in the absence of any appurtenances.
- ✓ Some deviations were observed in estimating the stability criterions from both proposed method and Defina et al. (2008), especially in large bed slopes.
- ✓ The minimum required bed friction to stabilize the hydraulic jump on an adverse slope decreases when the divergence angle increases.
- ✓ The establishment of stable hydraulic jump on an adverse slope could be achieved in the nonprismatic basins.
- ✓

References

1 Baines PG, Whitehead JA (2005) On multiple states in single-layer flows. Physics Fluids 15: 298.

2 Defina A, Susin FM, Viero DP (2008) Bed friction effects on the stability of a stationary

3 hydraulic jump in a rectangular upward sloping channel. Physics Fluids 20: 1-7.

4 Hartung F, Csallner K (1967) Zur Frage der Tosbecken bei Flusswehren. Wasserwortschaft 57(2): 100-101 (in Germany).

5 Kasi A, Farhoudi J, Esmaeili Varaki M (2011) Theoretical and Experimental investigation of diverging hydraulic jump on adverse slope. Iranian Water Research Journal 5(9): 121-130 (in Persian).

6 McCorquodale JA, Mohamed MS (1994) Hydraulic jumps on adverse slopes. Journal of Hydraulic Research, 32(1): 119–130.

7 Ohashi K, Sakabe I, Aki S (1973) Design of combined hydraulic jump and ski-jump energy dissipaters of flood spillway. Proc., 13th ICOLD Congress, Madrid, Spanish: 311-333.

8 Ohtsu I, Yasuda Y, Yamanaka Y (1991) Drag on vertical sill of forced jump. Journal of Hydraulic Research 29(1): 29-47.

9 Okada A, Aki S (1959) Hydraulic studies of hydraulic jump on reversed slope channel. Journal of Electrical Technology Institute 5(6): 161-174 (in Japanese).

10 Pagliara S, Peruginelli A (2000) Limiting and sill-controlled adverse-slope hydraulic jump. [10] Journal of Hydraulic Engineering, ASCE 126(11): 847-851.

11 Rajaratnam N (1966) The hydraulic jump in sloping channels. Irrigation and Power 23 (2): 137–149.

Notation

The following symbols are used in this paper:

F_{p1} Force due to hydrostatic pressure distribution at the beginning of hydraulic jump

F_{p2} Force due to hydrostatic pressure distribution at the end of hydraulic jump

F_{Pc} Force due to deviation from hydrostatic pressure distribution at the beginning of hydraulic jump

W Weight of the water enclosed between the approach and sequent depths

F_f Friction force

θ Angle of the basin slope

ρ Density of water

b Width of basin

q Flow discharge per unit width of the rectangular basin

β_2 Momentum correction coefficients at the end of hydraulic jump

β_1 Momentum correction coefficients at the beginning of hydraulic jump

γ Specific weight of water

Y_1 Flow depth at the beginning of hydraulic jump

Y_2 Flow depth at the end of stilling basin

k Shape factor for hydraulic jump on an adverse slope

L Length of basin

m Ratio of flow depths at the beginning and the end of hydraulic jump

g Acceleration due to the gravity

Fr_1 Upstream Froude number

$Fr_{1\min}$ Minimum value of upstream Froude number for establishing the free hydraulic jump on adverse bed

F_D Drag force

C_D Drag coefficient

s Sill height

F_{ps} Lateral pressure force

ϕ Expending angle of basin in degree

M_1 Specific force at the beginning of hydraulic jump

M_2 Specific force at the end of hydraulic jump

F' Stabilizing force of moved jump to the primal state

y_1' Orthogonal depth at the beginning of hydraulic jump

y_2' Orthogonal depth at the end of hydraulic jump

H Total head

z Bed elevation

S_f Friction slope

C Chézy coefficient

R Hydraulic radius

n Manning's factor

C_c Contraction coefficient of sluice gate

w Gate opening

L_J Length of hydraulic jump

S_o Basin slope

Journal of
Hydraulic Structures
Scientific Professional Quarterly

Contents **Volume 1 - Issue 2 - 2013**

A Discrete Singular Convolution Method for the Seepage Analysis in Porous Media with Irregular Geometry(1-9)
A.Zayeri Baghlani Nejad , M. Shokrollahi

A Case Study of Water Quality Modeling of the Gargar River, Iran(10-22)
M. Rafiee , A. M. Akhond Ali , H. Moazed; S. W. Lyon , N. Jaafarzadeh , B. Zahraie

Discharge Coefficient in Vertical Intakes with Additional Plates(23-32)
V. Naderi , D. Farsadizadeh , A. Hossein Zadeh Dalir , H. Arvanaghi

Evaluation of Hydraulic Sensitivity Indicators for Baffle Modules (33-43)
M. Seyedjavad , M. Mashaal , A. Montazar

A New Two Dimensional Model for Pollutant Transport in Ajichai River (44-52)
H. Derakhshan , M. Zarei Bistkonj

Theoretical Criterion for Stability of Free Hydraulic Jump on Adverse Stilling Basins(53-66)
J. Farhoudi , H. Khalili Shayan

Address :
Engineering Faculty, Shahid Chamran University of Ahwaz
Phone: +986113330011 , +986113337010
Website: jhs.scu.ac.ir
Email: jhs@scu.ac.ir
Ahwaz, Khouzestan Province, Iran